Landscape influences on downstream concentrations of mercury, methylmercury, and dissolved organic carbon in permafrost peatland catchments

by

Renae Shewan

A thesis submitted in partial fulfillment of the requirements for the degree of

Master of Science

in

Water and Land Resources

Department of Renewable Resources

University of Alberta

© Renae Shewan, 2024

Abstract:

Thawing permafrost in northern regions threatens to increase the downstream delivery of mercury (Hg) and its organic form, methylmercury (MeHg). Permafrost thaw may mobilize large Hg and dissolved organic carbon (DOC) stores from permafrost soils. Once mobilized, inorganic Hg (Hg(II)) can be transformed (methylated) by microbes into MeHg, a neurotoxin that bioaccumulates up aquatic food webs. Permafrost thaw may increase methylation in peatland complexes as elevated and dry permafrost peat plateaus thaw into peatland ecosystems, which can be favorable environments for microbes responsible for methylation. Transport of Hg and MeHg is often facilitated by binding to DOC and as peatlands become increasingly hydrologically connected with continued thaw, increased export of allochthonous DOC, Hg, and MeHg to downstream inland waters may occur. It remains uncertain how these changes will influence downstream concentrations of Hg, MeHg, and DOC as well as the composition of dissolved organic matter (DOM) at a catchment scale within the Taiga Plains of western Canada.

In this study, I completed three sampling campaigns of 93 streams throughout the Northwest Territories and northern Alberta located within the Taiga Plains of western Canada (summer 2021 and 2022). The study area was characterized by extensive peatlands and represented a permafrost gradient with more southern catchments characterized by no permafrost or sporadic permafrost to the more northern catchments which were underlain by extensive discontinuous permafrost. Streams were sampled for Hg, MeHg, and DOC concentrations and DOM composition indices to: 1) Investigate the role of catchment characteristics, including landcover, size, climate, and seasonality (June vs July vs August) as it relates to flow conditions on downstream concentrations; 2) use a developed statistical model to estimate concentrations of unsampled streams in the study region under current and future climate conditions; and 3) understand how the composition of DOM in streams relates to downstream concentrations of Hg and MeHg.

Random forest models were used to investigate the role of catchment characteristics in driving downstream concentrations. Mean annual temperature (MAT) and pH were established as the two most important variables for predicting MeHg and DOC concentrations, demonstrating the influence of peatlands and permafrost extent on these parameters. Turbidity was the most important variable for predicting Hg concentrations, indicating the importance of colloidal or particulate bound Hg in regulating concentrations. Using these models to predict unsampled

streams within the region resulted in an overall trend of higher concentrations of Hg, MeHg, and DOC in more southern permafrost regions compared to more northern streams underlain by more extensive permafrost.

More aromatic DOM was associated with higher flow and low electrical conductivity likely highlighting the influence of organic surface and shallow subsurface flow paths in contributing aromatic DOM in these catchments. Bulk DOC concentrations were highly correlated with MeHg concentrations while Hg preferentially associated with DOM of high aromatic composition.

As northern regions continue to warm, our findings suggest that concentrations of Hg, MeHg, and DOC will increase within the more northern catchments of the study region. Understanding factors that influence Hg export in northern rivers is important to anticipate and monitor the influence of climate change on northern aquatic ecosystems for the local communities which rely on them.

Preface

This thesis has been divided into three chapters. Chapter one provides a general introduction on the topic matter and study objective. While the final chapter provides conclusions and recommendations for the future. The second chapter is a collaborative project which has been written as a stand-alone manuscript, intended for eventual publication. For the work presented in this chapter, D.O. was responsible for conceptualization of the project, and study design was the work of R.S. and D.O., although both were with input from co-authors. R.S. completed most field and laboratory work with contributions from L.M.T., M.M., C.C., K.M. and H.K.S. for the fieldwork and additional support of L.M.T and K.M. for laboratory work. R.S. led the data analysis and manuscript writing with guidance from D.O., L.M.T., C.A.E., and S.E.T. All listed co-authors will contribute to writing and review before being submitted for publication.

Chapter 2:

R. Shewan, L.M. Thompson, M. Munson, C.A. Emmerton, S.E. Tank, C. Cunada, K. Marouelli, H.K. Swanson, R.F. Connon, D. Olefeldt. Strong influence of climate on riverine methylmercury and dissolved organic carbon across peatland - rich northwestern Canada. In preparation for publication.

Acknowledgments

I am extremely grateful to my supervisor, Dr. David Olefeldt, for his continued belief and support in me and the many opportunities he has given me throughout the past four years, both before and throughout my masters. I have grown and learned so much with his guidance and knowledge. Thank you also to my supervisor committee, Dr. Craig Emmerton and Dr. Suzanne Tank for their continued valuable insights and support. I am also very grateful to the collaborators that I have had the chance to meet and work with including Dr. Heidi Swanson, Chris Cunada, Dr. Ryan Connon, and Matthew Munson.

Field work for this project took place on Treaty 8 and 11 lands, with additional research activities on Treaty 6. These areas are the traditional lands of a number of Indigenous Nations and groups. A huge thank you to Dene Tha' First Nation's Lands Department, and Kátł'odeeche Fırst Nation Lands Department; Nahendeh Kehotsendı Program, for their support and contributions to this or other projects. A particular thank you also goes out to Matthew Munson who facilitated many of the opportunities I had to meet and learn from community members of Dene Tha' First Nation, a valuable learning experience for which I am so grateful.

I feel very fortunate to have had a number of mentors both before and throughout grad school who have inspired and supported me. The list is extensive, but in particular, this thanks goes out to Dr. Lauren Thompson and Dr. Laureen Echiverri who have both taught me so much along the way and have played a role in how I got to where I am today.

The support and friendship of my fellow lab mates in the Catchment and Wetland Sciences lab have been invaluable throughout the last few years and have very much made this project possible and much more enjoyable. Thank you to Dr. Lorna Harris, Dr. Mckenzie Khun, Dr. Julia Orlova, Dr. Rebecca Frei, Dr. Lauren Thompson, Chris Schulze, Jessica Lagroix, Matthew Munson, Fares Mandour, Kasha Kempton, and Fiona Kurylowicz. Many of you filled the long days in the field and lab with humor and fun and these are memories I'll never forget. A special thanks also goes out to the undergraduate assistants who gave up many weeks away from home to make this project possible, thank you so much to Kate Marouelli and Robbie Potts.

Most of all I want to thank my family and friends who have been there for me every step of the way. Thank you to my parents and brothers for believing in me and encouraging me always. I am also so grateful for the support that I find with my friends, who were always there to listen and put grad school into perspective.

Thank you to all the funders of this project including, the NWT Cumulative Impact Monitoring Program, the Alberta – NWT Transboundary Water Agreement, the Natural Sciences and Engineering Research Council of Canada (NSERC) Discovery Grant and Northern Supplement, the Northern Scientific Training Program and UAlberta North. Additional financial support was provided by NSERC CGS-M, and the University of Alberta.

Table of Contents

List of Tables

List of Figures

Chapter 1: General introduction

Streams and rivers act as the link between their contributing terrestrial landscape (catchment) and downstream aquatic environments, transporting carbon, nutrients, and contaminants, such as mercury (Hg), to downstream waters (Petrone et al. 2006; Zolkos et al. 2020; Liu et al. 2021; Chupakov et al. 2023). The concentration and export of constituents in streams and rivers are therefore sensitive to disturbances that occur in their catchment (Zampella, 1994; St. Pierre et al. 2018; Emmerton et al. 2020). As the climate continues to warm, northern environments are currently undergoing unprecedented rates of change and disturbance, including the rapid thawing of permafrost. There is growing concern that permafrost thaw will mobilize large stores of inorganic Hg bound to the organic matter in frozen soils and consequently result in an increased export of carbon, Hg, and its organic form, methylmercury (MeHg), to downstream waters (Rydberg et al. 2010; Gordon et al. 2016; Schuster et al. 2018, St. Pierre et al. 2018; Schaefer et al. 2020). However, there have been limited studies which investigate the influence of permafrost thaw on downstream concentrations of Hg and MeHg in mid-sized rivers from a catchment perspective.

1.1 Hg as an element of concern in aquatic systems

Hg is a toxic element which is of particular concern within aquatic environments. The organic form, MeHg, is a potent neurotoxin that can bioaccumulate within organisms and bio magnify up aquatic food webs; higher trophic-level organisms, such as predatory fish, can accumulate high and potentially toxic concentrations of MeHg (Kidd et al. 2011). Consumption of contaminated fish is the primary pathway of human Hg exposure (Clarkson et al. 2003; Mergler et al. 2007). Hg detrimentally affects the neurological and nervous systems in humans (Clarkson et al. 2003; Mergler et al. 2007; Rice et al. 2014) and can result in effects including memory loss, dysarthis, and an impact to motor and behavioral function (Rice et al. 2014; Takoka et al. 2014). Additionally, Hg poisoning can impact the cardiovascular, digestive, reproductive, and immune systems (Clarkson et al. 2003; Mergler et al. 2007; Rice et al. 2014). Northern Indigenous communities are disproportionately exposed to foodborne Hg through consumption of traditional foods, yet these traditional foods are associated with numerous nutritional benefits and are important culturally (Houde et al. 2022).

The fraction in which Hg is found in aquatic systems influences the bioavailability of Hg and the subsequent risk of it entering aquatic food webs. Dissolved forms of Hg and MeHg have typically been considered more bioavailable than particulate bound forms (Jonnson et al. 2012; Le Faucheur et al. 2014), although recent studies show that particulate bound Hg may be more bioavailable for methylation than previously thought (Zhao et al. 2019; Xiang et al. 2022). The concentrations and fractions of Hg and MeHg which end up downstream are the result of a variety of processes which occur within aquatic systems and the surrounding landscape.

1.2 Landscape sources and sinks of Hg and MeHg.

Hg in relatively remote regions, such as the Canadian North, arises primarily through atmospheric deposition from far-off Hg sources (Dastoor et al. 2015; Obrist et al. 2017). Gaseous elemental Hg (Hg(0)) is the most common form of atmospheric Hg (Steffen et al. 2015) and remains in the atmosphere for up to 6 to 24 months (Schroeder and Munthe, 1998; Holmes et al. 2006). During this time, it can undergo long range transport, allowing it to travel long distances from its emission source (Schroeder and Munthe, 1998). For example, models estimate that a large proportion of anthropogenic Hg currently being deposited to the Canadian Artic originates from outside North America (Dastoor et al. 2015). Hg can be released to the atmosphere naturally, through processes such as rock weathering and volcanic eruptions, as a result of anthropogenic activities, including coal combustion and artisanal gold mining, or through re-emission of previously deposited Hg (Sundseth et al. 2017; UN Environment, 2019). Present atmospheric Hg levels have been estimated to be approximately 390% (Streets et al. 2011) - 450% (UN Environment, 2019) higher than natural background levels due to anthropogenic inputs. Preventative measures to limit anthropogenic releases of Hg have been agreed to by a number of countries in the form of the 2013 Minamata Convention on Mercury. However, Hg levels in many environments have the potential to remain high even with changing atmospheric concentrations due to inputs of legacy Hg from accumulated stores in natural reserves such as permafrost (Rydberg et al. 2010; Schuster et al. 2018; Mu et al. 2020; Rutkowski et al. 2021).

Hg in the atmosphere is deposited onto terrestrial and aquatic environments through wet or dry deposition either in a gaseous form or bound to particulates (Gustin, 2011). Once on the landscape, a variety of processes make up much of the Hg cycle, including evasion back into the atmosphere, sequestering into soils and sediments, and transformations between the prevailing forms of Hg

(Hg(0), inorganic divalent Hg(II), MeHg). Certain landscape compartments are particularly influential within this cycle. Upland forests can contain large stores of Hg within soils and vegetation (Giesler et al. 2017; Wang et al. 2020). As Hg is flushed from the forest soil and transported (mobilized), or deposited directly, to different portions of the landscape including wetlands and lakes, Hg is likely to undergo transformations dependent on the surrounding environmental conditions (Tjerngren et al. 2012; Paranjape and Hall, 2017; Klapstein and O'Driscoll, 2018; Poulin et al. 2019, Branfireun et al. 2020), which subsequently may influence downstream concentrations.

Wetland environments are important for the production and subsequent transport of MeHg to streams (St. Louis et al. 1994; Brigham et al. 2009; Fink-Mercier, Lapierre, et al. 2022). The saturated, anoxic conditions of wetlands are favorable for many of the microbes responsible for methylation (Paranjape & Hall, 2017; Bravo & Cosio, 2020), characterized by presence of the hgcA and hgcB gene cluster (Parks et al. 2013). Methylation is additionally mediated by environmental and geochemical characteristics (Paranjape & Hall, 2017; Bravo & Cosio, 2020; Thompson, 2023). Wetlands often have high quantities of dissolved organic matter (DOM), which can facilitate methylation by acting as an electron donor and stimulating microbial activity (Paranjape and Hall, 2017, Jiang et al. 2018). However, the role of DOM on the bioavailability of Hg is complex (Ma et al. 2019). Studies have indicated that DOM may increase or decrease bioavailability of Hg, depending on sulfur dynamics and DOM composition (i.e., lability or aromaticity) (Graham et al. 2012; Jonsson et al. 2012; Ma et al. 2019; Poulin et al. 2019; Thompson, 2023). Oxidized forms of iron and sulfur can act as electron acceptors for some methylating bacteria; intermediate or high trophic status fen wetlands can receive electron acceptors through groundwater connectivity, resulting in higher MeHg production compared to bogs or peat plateaus, which have lower groundwater connectivity (Tjerngren et al. 2012; Poulin et al. 2019; Thompson, 2023). However, rich fens can have lower methylation rates than intermediate fens (Tjerngren et al 2012; Poulin et al. 2019). This could be attributed to high sulphate or trophic conditions additionally stimulating higher rates of demethylation resulting in an overall lower net methylation rate (Mitchell et al. 2008; Tjerngren et al. 2012). Higher concentrations of sulfur may also inhibit methylation by forming HgS precipitates and limiting bioavailability of Hg(II) (Zhang et al. 2011). Net MeHg production occurs in many wetlands, representing an important source to downstream environments.

The influence of lakes on concentrations of Hg and MeHg can be highly variable depending on characteristics of both the lake and the surrounding landscape (Branfireun et al. 2020). The potential for MeHg production within anoxic zones of lake sediments and the water column has long been established (Pak and Bartha, 1998; Eckley and Hintelmann, 2006; Paranjape and Hall, 2017). Additionally, locations in lakes associated with primary producers and on particles within the oxic water column have been recognized as methylation sites (Mauro et al. 2002; Hamelin et al. 2015; Gascón Díez et al. 2016; Paranjape and Hall 2017; Branfireun et al. 2020). In some cases, lakes can be a Hg and MeHg sink within the landscape (St. Pierre et al. 2019; Fink-Mercier, Lapierre, et al. 2022; Thompson, Khun, et al. 2023). Sedimentation can promote the storage of Hg and MeHg in lake sediments while sunlight mediated processes including the photodemethylation of MeHg, and the photo reduction of Hg (II) can volatize Hg forms into the atmosphere, contributing to a reduction of transport of Hg and MeHg downstream (Hammerschmidt and Fitzgerald, 2006; Hines and Brezonik, 2007; Jeremiason et al. 2009; Klapstein and O'Driscoll, 2018; St. Pierre et al. 2019; Schütze et al. 2021). DOM concentration and composition are an important influence on many of these processes. As noted above, DOM may increase or decrease the bioavailability of Hg, where Hg associated with autochthonous DOM can better facilitate methylation than allochthonous landscape derived DOM (Bravo et al. 2017; Bravo et al. 2018; Jiang et al. 2018). High quantities of DOM can also limit photochemical reactions by attenuating solar radiation, although a small amount of DOM may be necessary for facilitating these reactions in the first place (Klapstein and O'Driscoll, 2018). Branfireun et al. (2020) highlights some of the complexity of Hg cycling within lakes and the interactions between lake characteristics and their surrounding catchment. When MeHg, DOM, and Hg are predominantly terrestrially sourced, the contribution of in-lake production of DOM and MeHg tends to be limited (Branfireun et al. 2020), which likely aligns with cases where lakes can be net sinks within the landscape.

In addition to the influence of surrounding catchment landcover, conditions within streams themselves may play a role in Hg dynamics. Like wetlands and lakes, Hg transformations and cycling can occur within streams, including photo demethylation (Tsui et al. 2012) and MeHg production in stream sediments (Marvin-DiPasquale et al. 2009; Huang and Mitchell, 2023), which may constitute an important MeHg source in some systems (Huang and Mitchell, 2023).

1.3 Mobilization of DOC, Hg, and MeHg in riverine environments

Mobilization of Hg and MeHg to downstream environments is generally facilitated by particulate matter and DOM (Dittman et al. 2010; Bravo et al. 2018). Hg concentrations in streams are often associated with aromatic or coloured DOM, indicative of transport from terrestrial sources (Dittman et al. 2010; Bravo et al. 2018; Lescord et al. 2018; Fink-Mercier, del Giorgio, et al. 2022). Land cover and hydrology can also influence the partitioning between dissolved and particulate fractions of Hg and MeHg. Landscapes with steeper slopes that favor erosion, or which have limited sources of DOM tend to have more particulate-bound Hg and MeHg (St. Pierre et al. 2018; Campeau et al. 2022; Emmerton et al. 2022). In these systems Hg concentrations tend to correlate with suspended sediments or turbidity and, in some cases, with stream flow (Ricassi et al. 2011; Campeau et al. 2022; Emmerton et al. 2022). Precipitation and high flows may increase the amount of suspended sediment in streams, particularly in steeper catchments, by facilitating erosion or remobilization of sediments (Vercruysse et al. 2017) and any associated Hg (Ricassi et al. 2011). Catchments with lower relief and influenced by wetlands tend to have most Hg and MeHg in the dissolved fraction (Emmerton et al. 2022; Campeau et al. 2022; Thompson, Khun, et al. 2023; Thompson, Low, et al. 2023).

Flow paths and hydrologic connectivity play an important role in driving downstream concentrations (Laudon et al. 2011; Rose et al. 2018). In catchments of forested or mixed landcover, low flows are mainly associated with mineral groundwater inputs (Burd et al. 2018). Under high flow conditions as the hydrologic connectivity of the catchment increases and the water table rises, contributions from more organic subsurface flow of uplands and riparian areas are expected (Burd et al. 2018; Laudon et al 2011). In these catchments summer high flows are often, but not always, associated with an increase in concentrations of dissolved organic carbon (DOC) and Hg as organic layers with high DOC and Hg become connected (Brigham et al. 2009; Dittman et al. 2010; Ducharme et al. 2021; Gandois et al. 2021; Shrogen et al. 2021; Thompson, Low, et al. 2023). In peatland catchments, during low flow conditions peatlands may contribute water in addition to groundwater inputs, but flow contribution may be dependent on their hydrologic condition (Laudon et al. 2011; Goodbrand et al. 2019). At higher flows, increased contributions of precipitation may dilute the carbon rich peatland water resulting in dilution of organic rich sources and consequently DOC (Laudon et al. 2011). Concentrations of MeHg have been shown to increase, decrease, or have little relationship with flow conditions (Brigham et al. 2009; Dittman

et al. 2010; Wasiuta et al. 2019; Thompson, Low, et al. 2023), likely highlighting the importance of factors relating to production within catchments (Wasiuta et al. 2019; Thompson, Low, et al. 2023). Additional factors such as antecedent moisture conditions, lake influence, and position of landscape features may play important additional roles in how different flow levels influence downstream water chemistry (Oswald and Branfireun, 2014; Herndon et al. 2015; Shrogen et al. 2021).

1.4 Permafrost thaw and other disturbances in the Taiga Plains

As the climate warms, northern environments are undergoing rapid change including the thawing of permafrost. Permafrost thaw can alter the land cover and hydrology (Connon et al. 2014; Wright et al. 2022) of the surrounding landscape and consequently may impact downstream water chemistry (Rydberg et al. 2010; Olefeldt et al. 2014; Gordon et al. 2016). Permafrost in northern environments is estimated to contain large stores of legacy Hg, DOC, and nutrients (Schuster et al. 2018; Hugelius et al. 2020). With ongoing thaw, the production of MeHg on the landscape, and downstream transport of Hg, MeHg, and DOC may increase (Rydberg et al. 2010; Olefeldt et al. 2014; Gordon et al. 2016; Fahnestock et al. 2019; Thompson, 2023).

Within the more southern regions of the Taiga Plains of western Canada, permafrost is primarily in peat plateaus, where the heat conductivity properties of peat provide insulation for underlying permafrost (Ecosystem Classification Group, 2007; Shur and Jorgenson, 2007; Holloway & Lewkowicz, 2020). Peat plateaus are found within peatland complexes which also include bogs and fens (Quinton et al. 2003; Wright et al. 2022). As permafrost thaws, ice-rich permafrost peat plateaus are converted into thawed, waterlogged, nutrient-poor bogs or nutrient-rich fens (Gordon et al. 2016; Fahnestock et al. 2019). As wetlands are preferential areas of MeHg production (Paranjape & Hall, 2017; Bravo & Cosio, 2020) this transformation is likely to elevate the potential for production on the landscape (Fahnestock et al. 2019; Thompson, 2023). Thaw further influences Hg transport by increasing the hydrological connectivity of previously isolated peatlands to downstream waters (Connon et al. 2014; Wright et al. 2022).

Additional impacts of climate change including rising temperatures, an increase in the frequency of wildfires, and a possible increase in precipitation (Bush and Lemmon, 2019), may further influence or expediate changes to the Hg cycle. Increased wildfires may result in more rapid

degradation of permafrost than otherwise expected (Gibson et al. 2018; Wright et al. 2022) and can additionally alter the ecosystem functioning and hydrology of an area, potentially influencing downstream water chemistry (Ackley et al. 2021; Hutchins et al. 2023). In addition to the increase in temperature facilitating permafrost thaw, warmer temperatures in soil and water may stimulate microbial activity and the subsequent methylation of Hg (Paranjape & Hall 2017; Bravo and Cosio, 2020; Sun et al. 2023; Thompson, Low, et al. 2023). Finally, changing patterns of precipitation may alter the hydrologic processes of a landscape and subsequent transport of Hg, MeHg, and DOC to downstream waters.

1.5 Objectives

The potential increase of MeHg production and transport to inland waters could pose a health risk to local communities who incorporate local fish as a part of their traditional diet. Despite the potential health risk it presents, the influence of permafrost thaw on MeHg and Hg concentrations at the catchment scale remains uncertain (Wright et al. 2022). Here we investigate the influence of permafrost thaw and focus on a region where thaw is rapidly occurring at the permafrost boundary. Understanding how catchment characteristics and permafrost extent jointly influence downstream Hg dynamics is necessary for a better assessment and prediction of the risk that future permafrost thaw poses to downstream aquatic ecosystems.

This thesis seeks to identify the catchment scale predictors of concentrations of Hg, MeHg, and DOC in streams and rivers in the Taiga Plains of western Canada. We sampled 93 streams with catchments of varying size, land cover, climate, and permafrost extent for a suite of water chemistry parameters including Hg, MeHg, and DOC concentrations, DOM composition, and major ions and metals. The specific goals of this research were to:

1) Determine how land cover and climate associate with downstream Hg, MeHg, and DOC concentrations.
2) Assess the relationship of DOC concentrations and DOM composition with concentrations of Hg and MeHg.
3) Predict concentrations of MeHg, Hg, and DOC in un-sampled streams within the study region in order to inform on important areas for future land management, monitoring, and research.

Chapter 2: Strong influence of climate on riverine methylmercury and dissolved organic carbon across peatland - rich northwestern Canada

Abstract:

Permafrost thaw in northern peatland catchments threatens to mobilize mercury (Hg) attached to the organic matter in frozen soils and increase the production of the neurotoxin methylmercury (MeHg). As landscape hydrologic connectivity increases with thaw, increased downstream transport of Hg and MeHg attached to organic carbon (OC) may occur, but the impact at a catchment scale remains unclear. Here we sampled stream water for concentrations of Hg, MeHg, and dissolved organic carbon (DOC) in 93 streams on three separate occasions throughout the summers of 2021 and 2022 in the peatland-rich Taiga Plains of western Canada. Catchments were selected to represent a range of size, permafrost extent, land cover, and climate. The most important landscape predictors for total MeHg (TMeHg) and DOC concentrations were mean annual air temperature and stream pH. TMeHg and DOC concentrations increased approximately 0.2 ng L^{-1} and 9 mg L^{-1} respectively once temperatures were above the threshold of -2°C. Turbidity was the most important predictor for total Hg (THg) concentrations indicating the importance of colloidal or particulate bound Hg in regulating concentrations. Hg had a stronger association with aromatic DOM while aromaticity did not appear to influence the association of MeHg with DOC. Overall, higher concentrations of TMeHg, DOC, and THg were found in the warmer, more southern region of our study area, and observed concentrations were well below water quality guidelines for the protection of aquatic health. While more research is needed to understand the processes responsible for the observed -2ºC threshold increase in MeHg and DOC occurring at the boundary of peatland permafrost, our study suggests that continued warming may increase MeHg and Hg in aquatic ecosystems of current permafrost regions, which may have implications for the accumulation of MeHg in aquatic food webs.

2.1 Introduction

Mercury (Hg) is a metal of high concern in aquatic environments as its organic form, methylmercury (MeHg), biomagnifies and bioaccumulates in aquatic food webs (Kidd et al. 2011). Consumption of MeHg contaminated fish may present a human health risk and can cause a variety of neurological, cardiovascular, and reproductive health effects (Mergler et al. 2007; Clarkson et al. 2003; Rice et al. 2014; Takoka et al. 2014). MeHg represents a particular risk for northern Indigenous communities through the consumption of locally caught food, which is very important both culturally and nutritionally (Houde et al. 2022). In these northern regions, atmospheric deposition is the primary source of Hg, which has generally been transported from distant sources as gaseous elemental Hg (Hg(0)) (Dastoor et al. 2015; Obrist et al. 2017). Once deposited, inorganic Hg (Hg(II)) in northern regions can be sequestered and stored in frozen permafrost soils, where it has been accumulating over millennia (Obrist et al. 2017). With ongoing climate change, northern Canadian environments are warming at three times the global rate (Bush and Lemmen, 2019). As a result, permafrost degradation and thaw are occurring and threaten to mobilize stored Hg bound to the organic matter in soils and may increase the transport of Hg and MeHg to inland waters (Rydberg et al. 2010; Gordon et al. 2016; Shuster et al. 2018; St. Pierre et al. 2018; Schaefer et al. 2020).

Streams and rivers are closely connected to their surrounding catchment and as such Hg and MeHg concentrations often represent the processes occurring upstream in the catchment. Wetlands are generally an important landscape source of MeHg to downstream waters (St. Louis et al. 1994; Brigham et al. 2009; Fink-Mercier, Lapierre, et al. 2022), as they can provide the environmental conditions required for microbe facilitated methylation. This includes anoxic conditions, labile organic matter inputs, and presence of electron acceptors such as oxidized forms of iron and sulfur (Paranjape and Hall, 2017; Bravo and Cosio, 2020). Lake systems can be a net source or sink of MeHg and Hg on the landscape, as they have numerous potential sites of MeHg production (Branfireun et al. 2020) but are also environments where sedimentation and sunlight mediated processes may decrease the Hg and MeHg in the water column (Hammerschmidt and Fitzgerald, 2006; Hines and Brezonik, 2007; Jeremiason et al. 2009; Klapstein and O'Driscoll, 2018; St. Pierre et al. 2019; Schütze et al. 2021). In catchments with extensive peatlands, terrestrial inputs generally dominate the MeHg lake pool (Branfireun et al. 2020), and lakes are likely to act as a Hg sink

(Fink-Mercier, Lapierre, et al. 2022; Thompson, Khun, et al. 2023). In addition, disturbances such as wildfire can alter the land cover and hydrologic conditions of a landscape and may subsequently also influence the Hg and MeHg dynamics (Ackley et al. 2021).

The transport of Hg and MeHg from the surrounding landscape to stream systems is primarily facilitated by dissolved organic matter (DOM) or particulate matter (Dittman et al. 2010; Bravo et al. 2018). In catchments containing extensive peatlands, Hg and MeHg in streams are often in the dissolved fraction and associated with more aromatic or coloured DOM (Dittman et al. 2010; Bravo et al. 2018; Lescord et al. 2018; Fink-Mercier, del Giorgio, et al. 2022; Thompson, Khun et al. 2023; Thompson, Low, et al. 2023). In contrast steeper catchments with low peatland cover tend to have more particulate bound Hg and MeHg (St. Pierre et al. 2018; Campeau et al. 2022; Emmerton et al. 2022).

Hydrologic connectivity further regulates the transport of DOC, Hg, and MeHg to downstream environments. DOC and Hg commonly show a transport limited response, where concentrations increase with flow (Brigham et al. 2009; Dittman et al. 2010; Ducharme et al. 2021; Gandois et al. 2021; Shrogen et al. 2021; Thompson, Low, et al. 2023). However, this effect is not necessarily consistent across all catchments or seasons (Laudon et al. 2011; Herndon et al. 2015; Gandois et al. 2021; Thompson, Low et al. 2023). Likewise, MeHg shows varying responses to changing flow (Brigham et al. 2009; Dittman et al. 2010; Wasiuta et al. 2019; Thompson, Low, et al. 2023). The position of different landcovers within the catchment (Herndon et al. 2015), antecedent moisture conditions (Oswald and Branfireun, 2014), and factors relating to the production of MeHg on the landscape such as ground or water temperature (Sun et al. 2023; Thompson, Low, et al. 2023) likely influence the responses of THg, DOC, and MeHg concentrations to changes in flow. However, catchment size may also regulate concentration dynamics, as larger catchments tend to be less influenced by differences in flow or land cover (Creed et al. 2015; Emmerton et al. 2022) and in – channel stream erosion, and deposition dynamics are also likely to play a role, especially during high flow periods (Emmerton et al. 2022).

Permafrost thaw alters landcover and hydrology (Wright et al. 2022), both of which influence the production of MeHg and transport of Hg and MeHg downstream. Approximately 35% of the discontinuous permafrost region of the Taiga Plains is composed of peatland complexes consisting

of bogs, fens, and elevated peat plateaus underlain by permafrost (Carpino et al. 2021). As permafrost thaws, plateaus transform into thaw wetlands, consequently increasing the potential for production of MeHg within the system (Gordon et al. 2016; Fahnestock et al. 2019; Tarbier et al. 2021; Thompson, 2023). Permafrost thaw throughout the discontinuous permafrost region of the Taiga Plains also increases the hydrologic connectivity of a landscape (Connon et al 2014; Wright et al. 2022) and therefore the potential transport of Hg and MeHg downstream. However, at the catchment scale, the influence of permafrost thaw features on downstream concentrations remains uncertain. Within the Taiga Plains, a study by Thompson, Khun, et al. (2023) sampled streams over a 1700 km latitudinal transect and found higher concentrations of THg in more northern regions but no latitudinal trend for concentrations of MeHg or DOC in streams. However, within parts of the same study region Olefeldt et al. (2014) showed that DOC concentrations and aromaticity increase south of the permafrost boundary, and may indicate the potential for elevated Hg and MeHg transported along with the DOC.

As ongoing climate change alters northern landscapes it is increasingly important to understand how climate associated disturbances will impact the concentrations of Hg, MeHg, and DOC in downstream waters, as they may alter the health and functioning of aquatic systems. There are many processes on the landscape which mediate the production and subsequent transport of MeHg and Hg downstream. By investigating the drivers of Hg and MeHg at a catchment scale, we can better evaluate the influence of permafrost extent on downstream concentrations in the context of other landscape processes and drivers. Here we sampled 93 streams throughout the sporadic and discontinuous permafrost zone in the Taiga Plains of Northwestern Canada. Streams were sampled a total of three times, once in July 2021 and once in June and August 2022 to capture some of the hydrologic variability throughout the summer season. Streams were selected to represent a range of land cover, size, and climate to assess which characteristics influenced concentrations of Hg and MeHg downstream. Statistical models were used to estimate concentrations of Hg, MeHg, and DOC in unsampled streams of the region in order to assess the risk of elevated Hg and MeHg across the region.

2.2 Methods

2.2.1 Study area

Samples were collected from streams and rivers in northern Alberta and the South Slave and Dehcho regions (Northwest Territories). The study area ranged a transect of roughly 730 km from the most southern to most northern catchments and had an area of approximately 250000 km^2 (Figure 2.1). Samples were collected primarily within the Taiga Plains ecozone of Canada with a few of the most southern sites located in the Boreal Plains ecozone. Long-term (1991-2020) mean annual precipitation (MAP) varies between 320 and 370 mm within the study region, while mean annual average temperature (MAT) varies between -0.6 and -4.8°C (ECCC, 2023).

The Taiga Plains are underlain by sedimentary rock primarily from the Devonian and Cretaceous periods (Garrity & Soller, 2009). The Devonian rock is commonly limestone, with some highly calcareous limestone close to the southern border of NWT, in addition, Devonian geology in the area also include some dolomite, shale, and sandstone. Cretaceous period rock within the area likely consists of mainly shale and sandstone (Ecosystem Classification Group 2007; Stantec Consulting Ltd. 2016). Surficial geology includes widespread lacustrine and till deposits from the last glaciation and the influence of the post glacial lake McConnell (Ecosystem Classification Group, 2007). Peatland ecosystems are widespread within the area (Ecosystem Classification Group, 2007) and Carpino et al. (2021) estimated that approximately 35% of the landscape within the discontinuous permafrost region are made up of peatland complexes consisting of elevated peat plateaus, bogs, and channel fens. Freshwater lakes and ponds make up around 18% of the landscape in the northern areas of our study region (Ecosystem Classification Group, 2007) compared to around 1% in the Hay River Basin (Stantec Consulting Ltd. 2016). The rest of the landscape is generally forested upland areas ranging between deciduous, mixed, and coniferous with common species including aspen, black and white spruce, and Jack pine (Ecosystem Classification Group, 2007; Stantec Consulting Ltd. 2016). Within the study area, permafrost extent ranges from isolated or sporadic in the southern regions to extensive discontinuous in the more northern regions (Brown et al. 2002). Most permafrost within our study area occurs in areas with thick organic layers including peatlands and some forests (Ecosystem Classification Group, 2007; Holloway & Lewkowicz, 2020; Wright et al. 2022) and is likely enabled by the heat conductivity properties of these organic layers (Shur and Jorgenson, 2007; Holloway &

Lewkowicz, 2020; Wright et al. 2022). Permafrost in these regions is undergoing warming and thaw due to climate warming (Bush and Lemmen, 2019; Biskaborn et al. 2019). Northern Canada is warming at around three times the global average and has warmed by approximately 2.3°C since 1948 (Bush and Lemmen, 2019). In the more southern areas of our study region, the mean annual temperature has increased by about 2°C since 1962 (Holloway & Lewkowicz, 2020).

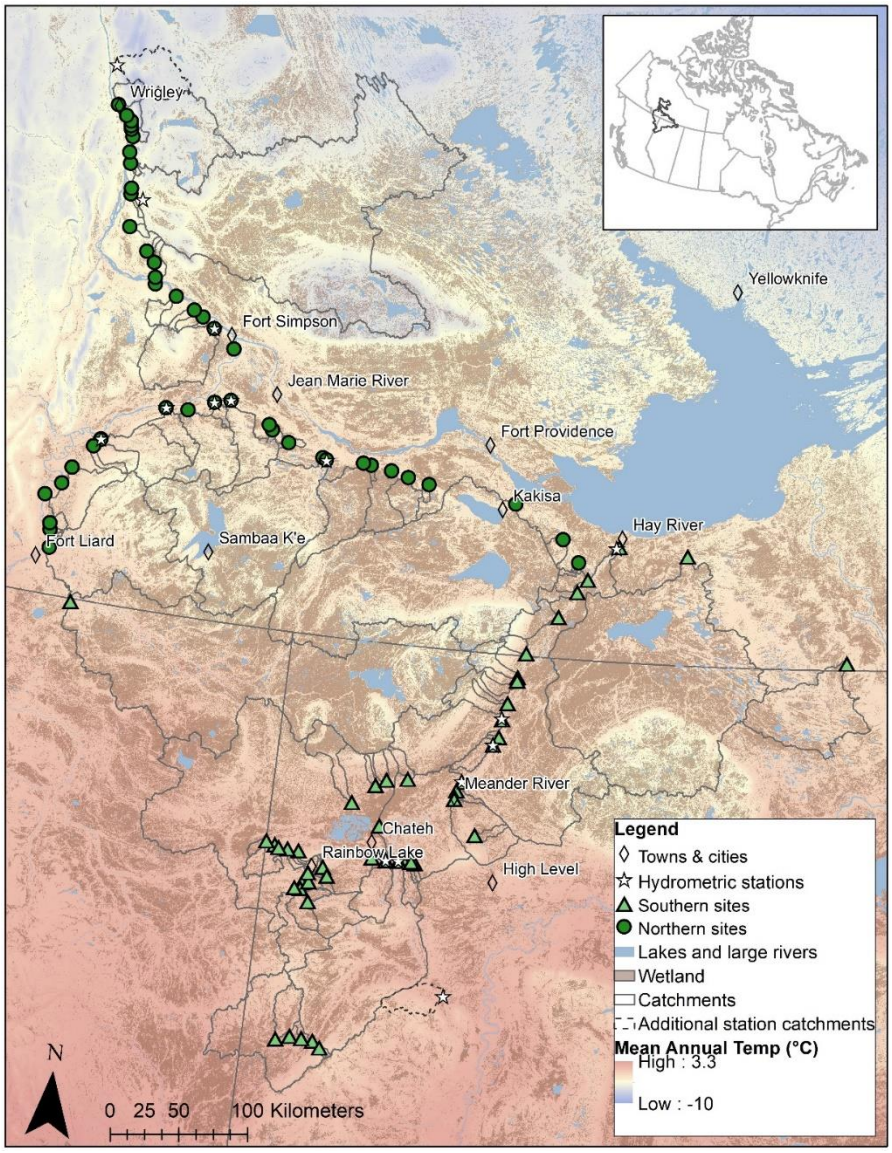

Figure 2.1. Map of the study area in Northern Alberta and the Northwest Territories, Canada. Green circles (northern catchments) and triangles (southern catchments) show the sampling location on each river. Additionally shown are the hydrometric stations used for flow percentile calculations (ECCC, 2022). Catchment delineation is shown for all sampled rivers and for additional rivers used for their hydrometric station data. Mean annual temperature is the average for the period of 1991 to 2020 and was accessed from Wang et al. (2016). The wetland cover is modified from Hermosilla et al. (2018, 2022). Where available, catchment delineation was based on delineations from the National Hydrometric Network Basin Polygons (Natural Resources Canada, 2022).

2.2.2 Sample collection

Water samples were collected during three sampling trips, in each of July 2021, June 2022, and August 2022. Streams were selected using hydrographic maps and were selected along the limited highways and industry access roads in the region. Most large rivers were sampled, and additional smaller rivers and streams were selected to include a number of streams which have previously been studied (Olefeldt et al. 2014; Thompson, Khun et al. 2023; Thompson, Low, et al. 2023) and to ensure a range of catchment characteristics including catchment area, land cover, and expected differences in permafrost extent. Several sites of interest were included based on discussion with knowledgeable community members in a meeting facilitated by Dene Tha' First Nation's Lands Department.

We sampled 93 streams and rivers. In total 72 streams were sampled during all three sampling trips, 17 were sampled during two of the three sampling trips and four streams were sampled only once (Table A.2.1). The discrepancy in the number of samples per stream is attributed to several factors, including an expanded sampling in 2022, several sites being dry or stagnant during the August sampling, and limited access to some of the sites due to natural events (flooding, fire, wildlife) or construction.

We collected total (unfiltered) Hg (THg) and total (unfiltered) MeHg (TMeHg) samples using certified 125 mL (THg) and 250 mL (TMeHg) precleaned glass amber bottles. Samples were collected from the bank of each stream, using the clean hands-dirty hands protocol (St. Louis et al. 1994; U.S. EPA, 1996). In July 2021 and June 2022, in addition to the unfiltered samples, we collected and filtered samples for the analysis of dissolved Hg (DHg) and dissolved MeHg (DMeHg) at each site. This consisted of collecting an extra 125 ml and 250 ml bottle of water which were filtered through acid cleaned 0.45 µm cellulose nitrate filter towers and transferred into a new bottle within 24 hours. We used 0.2% and 0.4% trace-metal grade hydrochloric acid to preserve Hg and MeHg samples, respectively. Samples were kept cool during transit and then refrigerated until analysis. Analysis of 96% of THg and DHg samples occurred within three and a half months of sampling. Analysis of TMeHg and DMeHg in 2022 occurred within 194 days of collection while analysis of TMeHg and DMeHg were delayed by lab limitations for the July 2021 samples due to coronavirus (SARS-CoV-2) and were therefore run within a maximum of 262 days of sampling.

In addition, we collected grab samples for analysis of DOC, additional nutrients, and major ions, and for absorbance and fluorescence spectroscopy of DOM. We collected two bottles of filtered water using 60 ml acid washed amber glass bottles and 0.7 µm GF/F, Whatman filters. One of the bottles was preserved using 0.6 mL of 3M hydrochloric acid and run for DOC/TN and ICP-OES analysis while the other was left unpreserved for absorbance and fluorescence spectroscopy. These bottles were kept cool in transit and then refrigerated. In addition, we collected an extra 60 mL bottle of filtered water for colorimetric ion analysis using Thermo Scientific Nalgene Narrow-Mouth LDPE bottles and 0.7 µm GF/F Whatman filters. This bottle was left unpreserved, kept cool in transit, and then frozen in our laboratory until it was submitted for analysis. In situ measurements of pH, electrical conductivity (EC), water temperature, and turbidity (only 2022) were measured at each stream. Turbidity was measured using a calibrated LaMotte 2020i Turbidity Meter (LaMotte, 2020). pH, EC, and water temperature were measured using a calibrated Elite PCTS pH / Conductivity / TDS / Salinity Pocket Tester (Thermo Scientific).

2.2.3 Sample analysis

Hg and MeHg concentrations (both total and dissolved) were analyzed in the Biogeochemical Analytical Service Laboratory (BASL) at the University of Alberta. THg and DHg were analysed using EPA Method 1631 (U.S. EPA, 2002). Samples were first oxidized to HgII with the addition of bromine monochloride for at least 12 hours and then neutralized. Once neutralized, HgII is reduced to Hg0 with the addition of stannous chloride. Cold vapour atomic fluorescence spectrometry was then used to determine the concentrations of Hg within a sample (BASL, 2023). The detection limit is 0.06 ng L^{-1} for total and 0.08 ng L^{-1} for dissolved Hg. Quality control (QC) standards and blanks were run every 10 or 20 samples, and a 9-point calibration curve was run at the beginning of each day that samples were analyzed. One sample spiked with a known amount of $HgCl_2$ was run for each group of 20 samples to ensure there was accurate recovery. A duplicate was also run in every batch of 20 samples.

TMeHg and DMeHg samples were analyzed using EPA Method 1630 (U.S. EPA 1998) with isotope dilution (Hintelmann & Ogrinc, 2002). Samples were first distilled and then measured using ICP-Mass Spectrometry. Before distillation all samples are spiked with a known amount of MeHg isotope $Me^{201}Hg$ and then distilled at 127 °C by a Tekran 2750 Methyl Mercury Distillation

system (BASL, 2023). After distillation, sodium tetraethyl borate is added to the distilled samples to ethylate MeHg to the volatile MeHgEt. Samples were then analyzed using a 2700 Methyl Mercury Analyzer coupled to Agilent 7900 ICP Mass Spectrometer (BASL, 2023). The detection limit for MeHg samples was 0.01 ng L^{-1}. Distillation and method blanks, QC standards containing a known amount of MeHg, samples spiked with an additional amount of MeHg, and duplicates were run in each round of 40 samples to ensure the reliability of the analysis.

The Natural Resources Analytical Laboratory (NRAL) at the University of Alberta completed the remaining water chemistry analysis apart from DOM optical composition analyses. DOC was measured as non-purgeable organic carbon and along with total dissolved nitrogen was analyzed using a Shimadzu TOC_L CPH Model Total Organic Carbon analyzer with an ASI-L and TNM-L (Shimadzu Corporation, 2015). Dissolved anions (ammonium (NH_4-N), chloride (Cl), nitrite (NO_2-N), nitrate (NO_3-N), soluble reactive phosphorous (SRP), and sulphate (SO_4-S)) were analyzed using a Thermo Gallery Plus Beermaster Autoanalyzer (Thermo Fisher Scientific, 2017). Dissolved metals (sodium (Na), potassium (K), magnesium (Mg), zinc (Zn), calcium (Ca), copper (Cu), iron (Fe), manganese (Mn), boron (B)) along with dissolved sulphur (S) and total dissolved phosphorus (TDP) were analysed using a Thermo iCAP6300 Duo (N. America) inductively coupled plasma-optical emission spectrometer (ICP – OES) (Thermo Fisher Corp., 2012).

Absorbance was measured using a UV_VIS Spectrometer (UV-1280, UV-VIS, Shimadzu Corporation, Japan) from 200 nm to 700 nm with a 1 nm interval. Samples were run using a 1 cm quartz cuvette. Samples were diluted with Milli-Q water if the measured absorbance value was close to or above 0.4 cm^{-1}. Milli-Q water blanks were run every 10 samples, and the absorbance measurements were blank subtracted post measurement. DOM absorbance was used to calculate the specific UV absorbance at 254 nm (SUVA). SUVA is a measure of DOC aromaticity and was calculated as UV absorbance at 254 nm divided by DOC mg L^{-1} and then multiplied by 100 (Weishaar et al. 2003). Absorbance values were also used to calculate the spectral slope between 275 – 295 nm ($S_{275-295}$) and the slope ratio for the two spectral slope regions of 275-295 nm and 350-400 nm (S_r), as these measures can give insight into the molecular weight and photochemical processing of DOM (Helms et al. 2008).

An excitation emission matrix (EEM) was used to measure DOM fluorescence of each sample and were attained using a Horiba Aqualog (Horiba Scientific, US). Samples were run in a 1 cm quartz cuvette with sample blanks run every 20 samples. Samples were run using an integration time of 0.5 seconds. Excitation was measured for wavelengths of 230 nm – 500 nm (increment of 5 nm) and the emission wavelengths ranged from 117 nm – 827 nm (increment of 2.33 nm). Samples were diluted with MilliQ water if the sum of absorbance values for any of the following wavelength pairs: 250 nm and 452 nm; 400 & 520 nm; or 300 nm & 352 nm, exceeded 1.5 cm^{-1} (Kothawala et al. 2013). Before analysis, fluorescence scans were corrected for inner filter effects, Raman normalization, blank subtraction, and dilutions (Murphy et al. 2013). Fluorescence analysis was done using the *drEEM* package version 0.6.5 (Murphy et al. 2013) in MATLAB version 9.14.0 (R2023a) Update 2 (The MathWorks Inc. 2023). The pickpeaks tool in the *drEEM* package was used to calculate common fluorescence peaks (Coble, 1996) as well as the fluorescence indices such as BIX, an indicator of how much autochthonous DOM is in the system (Huguet et al. 2009); HIX, an indicator of how humified the DOM is (Ohno, 2002; Fellman et al. 2010); Freshness Index (Freshness), another indicator of how freshly produced the DOM in the system is (Fellman et al. 2010; Williams et al. 2010) and Fluorescence index (FI), an indicator of whether the DOM is more terrestrial of microbially derived (Cory and McKnight, 2005; Fellman et al. 2010). Fluorescence scans were also analysed for independent components using parallel factor analysis (PARAFAC). PARAFAC analysis was run from a lab tutorial based on the paper and tutorial by Murphy et al. (2013) and consisted of the following: Rayleigh and Raman scatter peaks were removed and the EEM scans of independent samples were analysed for any clear errors and problem wavelengths identified were removed from these samples, sample outliers were then removed. Each EEM was normalized to its total signal to evaluate different models and outliers and then reversed back to true scores later in the analysis after validation. The final PARAFAC model was validated using split half analysis (Murphy et al. 2013).

2.2.4 Catchment delineation and characterization

Catchments were delineated for each sampling point using the Canadian digital elevation model (CDEM) (Natural Resources Canada, 2013) and the hydrology toolbox in ArcMap 10.8.2. (ESRI, 2021). Catchments were then corrected in one of two ways. First, where available, catchments were aligned to existing delineations from the National hydrometric network basin polygons

(Natural Resources Canada, 2022). Secondly, the remaining catchments were visually assessed based on google earth imagery and the watercourse dataset from the CanVec – Hydro 250K dataset for Alberta, B.C., and N.W.T. (Natural Resources Canada, 2017), the catchments were modified manually if there appeared to be large errors in the automatic delineation.

We used existing geospatial data to characterize the catchments, extracting information on several variables related to climatic, landscape, and topographic characteristics which were considered to have the potential to influence downstream water chemistry. One catchment characteristic of particular interest is the influence of permafrost extent. To explore this, we looked at the influence of mean annual air temperature (MAT) (°C), as air temperature has been shown to be a driving factor of permafrost (Chadburn et al. 2017; Biskaborn et al. 2019; Smith et al. 2022). Data of MAT and mean annual precipitation (MAP) over the period of 1991 – 2020 was accessed using the western North America dataset from ClimateNA v7.41 (Wang et al. 2016). ClimateNA data was developed by merging previous climate datasets (see references within Wang et al. 2016) and then downscaling it into scale free data using bilinear interpolation and local elevation (Wang et al. 2016). One of the products from ClimateNA is a gridded raster layer of historical climate data for western Canada at the resolution of around 800 by 800 m (Wang et al. 2016). We used the average data representing the period of 1991 – 2020 to calculate the spatial average of the MAT and MAP for each catchment. The area of the delineated catchments in km^2 was calculated within ArcMap using the calculate geometry function. The slope was calculated using the slope tool in ArcMap and was calculated in degrees based on the CDEM which had a resolution of 0.75 arc seconds. The mean slope of each catchment was then calculated. Geology data was accessed from Garrity & Soller (2009). The percentage of each geology unit in each catchment was calculated. The majority of the study area had either Cretaceous or Devonian geology (when simplified from classifications such as Upper, Middle, and Lower, Cretaceous or Devonian). Inclusion of geology in our statistical models was simplified to just percent cover of Devonian geology.

Land cover data and disturbance data for fire and harvesting was accessed from the National terrestrial monitoring system for Canada and related references (Hermosilla et al. 2016, 2018, 2022). The fires and harvesting data from Hermosilla et al. (2016) contain forest change data covering the years 1985-2020. The percent disturbed layer used in our analysis is the sum of both harvest and fire data from Hermosilla et al. (2016) and therefore represents the total percent of

each catchment which has been disturbed over 1985-2020. We were limited in accessing disturbance data for the years of 2021 and 2022 as from what we could find, it had not yet been added to spatial datasets of the Canadian National Fire Database or any other dataset which covered the entire study area. Spatial data of fire disturbance for 2021 was accessed individually for Alberta, British Columbia, and the Northwest Territories and for 2022 for Alberta and British Columbia from the provincial and territorial government (Government of Alberta, 2023; Government of British Columbia, 2023; NWT Center for Geomatics, 2022). Based on this data we determined that only a subset of catchments had burned at all during 2021 and 2022 and that only three catchments had burned over 1% of their catchment area. We therefore determined it was unlikely that disturbance in 2021 and 2022 would have a pertinent impact on downstream water chemistry and due to the lack of cohesive and complete datasets for both years, over the entire study area, disturbances in the years 2021 and 2022 were subsequently disregarded in our analysis.

The base land cover used for our study was the 2019 land cover map from Hermosilla et al. (2018 & 2022), which was generated using open Landsat data, with additional topologic and hydrologic information (see Hermosilla et al. 2022). However, as we were mainly interested in whether the landscape was functioning as peatland or forest, we modified the 2019 land cover map to limit the influence of fire and harvest, disturbances which often resulted in the transition of classification from forest to shrub land (Hermosilla et al. 2022). Using the disturbance datasets described above (Hermosilla et al. 2016), we removed land cover data from the 2019 dataset for areas which had been disturbed by fire and harvest in the years 1985 – 2019 and replaced it with land cover datasets representing years prior to the disturbance, also accessed from Hermosilla et al. (2018 & 2022). We reclassified the land cover in five-year intervals where, for example disturbances from 2011 – 2015 were all removed together and replaced with land cover from 2010. This modified land cover dataset was used to characterize the percent cover of water, wetlands (the sum to treed and non-treed wetlands), forest (sum of broadleaf, coniferous, and mixed wood), and other classes including rock, snow, barren rock, shrubs, bryoids, and herbs in the delineated catchments. We also calculated the percentage of each land cover class within 60 m of streams and lakes on the landscape. To calculate the land cover within 60 m of water features we used the watercourse and waterbody datasets from the CanVec – Hydro 250K datasets for Alberta, B.C., and N.W.T. (Natural Resources Canada, 2017) and created a 60 m buffer around these layers. When calculating the percent land cover within this buffer, any cells classified as water were removed from the

calculation (and not included in the sum) as we were interested in the land cover adjacent to water and having water within this area was likely due to slight differences in the identification of water features on the landscape between the CanVec layer and the land cover dataset.

2.2.5 Delineation of additional catchments and streams for un-sampled points

In addition to the investigation of sampled data, one of the target deliverables of this study was to predict concentrations within streams of the study area that were not sampled and subsequently map these predictions. To accomplish this, we first created the stream network we would like to predict concentrations for based on the Canadian DEM (Natural Resources Canada, 2013) and using a variety of tools (Breach Depressions Least Cost; Fill Depression Wang and Lui; D8 Flow Accumulation; Extract Streams; Raster Streams to Vector) for hydrological analysis within the *whitebox* package in R (Lindsay, 2016; Wu & Brown 2022). The number of streams was limited to larger streams based on a flow accumulation threshold. Points were then created at or just above each intersection of stream reaches within the dataset, this resulted in a total of 557 points. Catchments were delineated for each of these points using the Unnest Basins tool in the *whitebox* R package (Lindsay, 2016; Wu & Brown 2022). Due to the large number of points, very few manual adjustments were made to the delineation of the catchments created unless the error in the delineation was very large and/or obvious, we therefore expect there is some error in regard to catchment delineations. We opened the delineated catchments in ArcMap and extracted the catchment characteristics for each of the delineated catchments using the same datasets that characterized the original catchments as described above in section 2.4. This provided landscape data that was used in a random forest model (see section 2.2.7) to predict concentrations in more remote streams that had not been sampled.

2.2.6 Flow percentile calculation

Due to the large area of our study region, we found that even within each of our sampling trips there were hydrologic differences between regions of our study area including generally wetter conditions in the more southern catchments compared to northern catchments. To account for the differences in hydrologic conditions, spatially and temporally between our sampling campaigns we estimated the flow percentile at each sampling point for each sampling occasion. The flow percentile was defined as (100 - % flow exceedance). To calculate flow exceedance, we used data

from 15 hydrometric stations throughout the region operated by Environment and Climate Change Canada (2022). The majority of the stations used for flow calculations were stations that monitor rivers sampled for this project however, an additional two stations (Ocher River, NWT & Keg River, AB) were also used as they were in close proximity to sampled rivers in regions without a representative station on the sampled rivers. From these stations we used historic data from the years 2006 – 2018 except for 2014, 2016, and 2017 due to missing data for those years from one or more stations. We were limited in the length of years for our record as the Ochre River Station only had data dating back to 2006. We used only the months of May to September to capture the typical ice-free period for our sampling sites. In addition to data from 2006 – 2018, data was included for the days in 2021 and 2022 that rivers were sampled for each individual station (Environment and Climate Change Canada, 2022). Flow percentile was calculated as:

$$\textbf{Flow percentile} = 100 - ((m/n+1)*100)$$

Where m = the rank of discharge data within the time series and n = the number of discharge records used. A higher flow percentile represents a lower probability that this flow would be exceeded on a given day, i.e. higher flow for this catchment.

The station which was selected as proxy for each river depended on both the distance of the flow monitored river from the river in question and the size of the catchment of the flow monitored river compared to the size of the catchment for the river in question. If the station in closest proximity to the river was a station relatively similar in size, then only that station was used to calculate flow percentile. If the station in closest proximity to the sampled river had considerably different catchment sizes, than the flow percentile was calculated for both the station in closest proximity and the closest station more similar in size, and the average of both flow percentile values was used. There were a couple exceptions where the closest proximity river was not used at all if there were one or two other monitored catchments that were nearly the same distance away but with a catchment area that was more comparable. In addition, certain catchments such as the Willow Lake and Hay River catchments were so large that although they were closest in proximity to some sites, they were not used in any flow percentile calculations other than for their own catchment. There exist additional hydrometric stations within our study region such as at Petitot River and Kakisa River however these stations were not used due to missing a number of additional years between 2006 and 2018.

2.2.7 Statistical analysis

Our dataset included a number of samples with water chemistry parameters below the level of detection (LOD). For most water chemistry parameters this impacted only 0% - 1% of samples. The following parameters had more than 1% of samples below the LOD: Zn (6%), P (44%), Cu (57%), Al (14%), NO_2-N (80%), SRP (65%), SO_4S (27%), and NO_3-N (62%). If the lab responsible for sample analysis provided no values and instead listed values as < LOD, it was replaced with a value of half of the LOD, however, when provided, we used the raw instrument data even when below the level of detection (Antweiler, 2015). Our dataset also included missing observations for temperature for all three months for Little Buffalo River (FS2) and August flow percentile for WRI 12 (Willow Lake). These four missing values were filled by imputation using the rfImpute tool in the randomForest package in R (Liaw & Wiener, 2002). The input tool was used for each of the models (THg, TMeHg, DOC) and the overall average of the calculated input was then taken and used in the dataset for all analyses. Missing values were handled in these ways to ensure that most of the data could be used in all analyses. Certain sites including WRI15, HR41, and HR10 (Table A.2.1) had one or more months removed from all statistics analyses as they had clear outliers of MeHg which upon reflection was likely due to near stagnant conditions which we determined were therefore not representative of the catchment influence. All analyses were conducted in RStudio version 2023.06.1 (R Core Team, 2023). Additional packages *facttoextra* (Kassambara & Mundt, 2020), *ggplot2* (Wickham, 2016), *ggpubr* (Kassambara 2023a), and *ggcorrplot* (Kassambara, 2023) were additionally used for most of the data visualizations.

We ran a principal component analysis (PCA) using the princomp function in R to gain an overview of the relationships between water chemistry variables including Hg and MeHg. Concentration data was tested for normality using the Shapiro Wilk test and then was logged to improve normality and ensure the relationship among variables was linear. We ran the PCA using the correlation matrix. Due to missing approximately a third of the data, turbidity (no July data), DHg (no August data), and DMeHg (no August data) were not included in the PCA analysis. Instead, the relationships between THg and TMeHg concentrations with turbidity and the corresponding dissolved concentrations were investigated using spearman correlations.

DOM composition was explored using a PCA analysis which included the calculated fluorescence indices, absorbance indices, and the % of each PARAFAC component of the total fluorescence. The correlation matrix was used when performing the PCA. The relationship between DOC concentrations and DOM composition with Hg/MeHg was then investigated using linear models. The DOC, Hg, and MeHg concentrations were logged for these linear regression models.

We used random forest models (Breiman, 2001) to assess the importance of various landscape characteristics and stream measures such as pH, EC, turbidity, and flow percentile, in predicting concentrations of THg, DHg, TMeHg, DMeHg, DOC, and DOM composition. Random forest models are a nonparametric model which is essentially the iteration of classification and regression trees. Each tree is built using a subset of the data and the error is assessed using the subset not included. At each data split in the tree, a subset of the explanatory variables is evaluated for selection (Breiman, 2001; Genuer and Poggi, 2020). We chose to use random forest models because of its ability to be used for predictions, as well as give an indication of the importance of each explanatory variable within the model, and because random forests are not limited to linear relationships (Genuer and Poggi, 2020). Variable importance plots indicated which landscape characteristics were most important in each model and partial dependency plots (PDP) allowed us to investigate the relationship of individual landscape characteristics on the concentrations or composition scores. The package *randomForest* (Liaw and Wiener, 2002) was used to run all models and the package *pdp* (Greenwell, 2017) was used to generate the partial dependency plots. As we had a small number of explanatory variables, we included all of them within the model. We ran the models with 1000 tree iterations and using the default number of variables to be assessed at each node.

The first round of random forest models was run on all of the data collected from the three sampling campaigns and included dynamic explanatory variables such as pH, EC, water temperature, flow percentile, and turbidity. These dynamic variables were included in the model as additional indicators of processes which could be occurring on the landscape. For example, we expect pH and EC to be indicative of wetland or groundwater influence respectively (Bourbonniere, 2009; Burd et al. 2018). While higher soil and water temperature has been linked with higher MeHg (Sun et al. 2023; Thompson, Low et al. 2023) and therefore measured water temperature may provide an indication of conditions favoring MeHg production or mobilization within the catchment. As

hydrologic conditions and suspended sediment may mediate the transport of DOC, MeHg, and Hg downstream (Dittman et al. 2010; Ricassi et al. 2011; Staniszewska et al. 2023; Thompson, Low, et al. 2023), flow percentile and turbidity were also included in the model.

Although the final random forest models run included 100% of the collected data, to evaluate the model, we also cross validated it using five iterations where a different 20% of the data was removed in each iteration as test data. The average values of variance explained and mean squared residuals evaluated from the 20% test of each data subset was compared to the out of bag variance explained and mean squared residual supplied from our final model including all data. This was done as another way to evaluate the model and ensure similar results when including all data as opposed to excluding a subset of site as test data in the final model (Table A.2.2).

Additional models were run to the final models presented here to determine the influence of turbidity and non-independent catchments. As turbidity was not measured in July, we could not include it in the models without removing an entire month of collected data. We ran models for THg, TMeHg, DOC, and DOM aromaticity using data from the months of June and August, which included turbidity (Figure A.2.1). However, as turbidity was not one of the most important predictors in the models for TMeHg, DOC, and DOM aromaticity it was removed from these models in the interest of including data from the July sampling. An additional consideration in our dataset was that a subset of catchments were nested within one another in the southern region of our study area. To ensure that this did not heavily influence the random forest models, we ran the models while excluding the larger catchments that had smaller catchments nested within them. We found very little difference between models including nested catchments and those without (Figure A.2.2), and therefore in our final models we included all catchments.

A second objective of this project was to construct a model which could predict average DOC, THg, and TMeHg concentrations using only catchment characteristics that could be accessed remotely. This model would allow us to extrapolate our findings to streams and rivers within the study area which were not sampled but for which catchment characteristics were available. To accomplish this, a second round of random forest models was run and trained on the average concentrations collected at each site over the three sampling rounds. These random forest models included only catchment variables which were static and remotely available from online databases

such as the mean of historic climate variables. As such, we were able to access the catchment characteristic data for remote catchments over a large area. These random forest models were then applied to remote streams in the area to predict current and future concentrations of streams not sampled as a part of this project. We evaluated these models with the same method of cross validation described above (Table A.2.3).

2.3 Results

2.3.1 Catchment characteristics and differences between sampling periods

Land cover within catchments (Table 2.1) was primarily forest and wetland with an overall median value of 63% and 33% respectively. % Water cover was small in many catchments with an overall median of < 1%. Southern catchments generally had higher MAT, MAP, % wetlands, and were more disturbed than northern catchments which had slightly steeper catchments, more forest and lakes, and a high percent of Devonian geology (Table 2.1).

Table 2.1. Summary of land cover data from (a) northern catchments and (b) southern catchments.

	a) Northern catchments			b) Southern catchments		
	Median	Quartile 1	Quartile 3	Median	Quartile 1	Quartile 3
MAT (°C)	-2.5	-3.6	-2.3	-0.9	-1.4	-0.6
MAP (mm)	367	333	398	441	397	469
% Wetland	22	12	35	38	32	45
% Forest	73	54	83	59	53	67
% Water	1	0	4	1	0	1
% Wetland in a 60 m buffer	24	10	46	39	31	53
Area (Km^2)	97	28	545	215	85	983
Mean slope (°)	1.1	0.6	1.6	0.9	0.6	1.1
% Devonian geology	78	38	100	0	0	0
% Disturbed	0	0	6	7	2	13

Flow conditions changed between our June (2022), July (2021) and August (2022) samplings representing periods of both high and low flow. Flow was highest during the June sampling, followed by July and then August (Figure 2.2g). Although, our sampling campaigns did not catch peak flow during the spring freshet or during summer storms (Figure A.2.3). Due to the large size of our study area, there were differences in conditions between areas of the study region within the same sampling month. The greatest difference in flow between regions was during the July sampling where catchments within the southern region typically had higher flows compared to a

historical average (Figure A.2.3), while northern catchments had low flows. Water temperature in southern catchments was highest in August compared to June and July which were similar, while in northern catchments water temperature was cold in June compared to similar July and August samplings, following the general trend of differences in flow (Figure 2.2i).

2.3.2 Concentrations of Hg, MeHg, and DOC

Concentrations of Hg and MeHg in both southern and northern catchments were well below the water quality guidelines for aquatic health of 26 ng L^{-1} and 4 ng L^{-1} respectively (Canadian Council of Ministers of the Environment, 2003), except for two MeHg samples from very small streams which as described above were removed from analysis due to a blocked culvert and stagnant conditions. Median concentrations of DOC, THg, TMeHg, and % MeHg were 2.24, 2.02, 3.50, and 1.55 times higher respectively in southern catchments compared to northern catchments. (Table 2.2) (Figure 2.2. a-c). Dissolved fractions of MeHg and Hg were also sampled in July 2021 and June 2022 and followed the same south to north trend as total fractions with median concentrations of DHg 1.58 times higher and median concentrations of DMeHg 3.89 times higher in southern catchments compared to northern catchments (Table 2.2). Both MeHg and Hg were predominantly in the dissolved fraction. DMeHg made up a median of 96% (IQR: 91 – 100%) in southern catchments and 92% (81 – 98%) in northern catchments of TMeHg. DHg made up a median of 72% (56 – 87%) in southern catchments and 84% (74 – 91%) in northern catchments of THg concentrations.

TMeHg concentrations varied between the sampling months, with less apparent differences for THg and DOC concentrations. The sampling in July 2021 had higher MeHg concentrations than June and August 2022 based on their median and interquartile range (July: 0.30, 0.11 – 0.53 ng TMeHg L^{-1}; June: 0.16, 0.09 – 0.30 ng TMeHg L^{-1}; August: 0.19, 0.08 – 0.37 ng TMeHg L^{-1}). Median Hg concentrations were similar across sampling periods (July: 1.93, 1.43-3.23 ng THg L^{-1}; June: 2.06, 1.40 – 3.45 ng THg L^{-1}; August: 1.74, 1.01 – 2.42 ng THg L^{-1}); however, the June 2022 sampling had the largest interquartile range and highest Hg concentrations recorded. DOC concentrations remained consistent across sampling periods and also had very similar interquartile ranges (July: 23.33, 14.89 – 34.86 mg DOC L^{-1}; June: 21.90, 14.70 – 28.48 mg DOC L^{-1}; August: 23.73, 12.01 – 30.77 mg DOC L^{-1}).

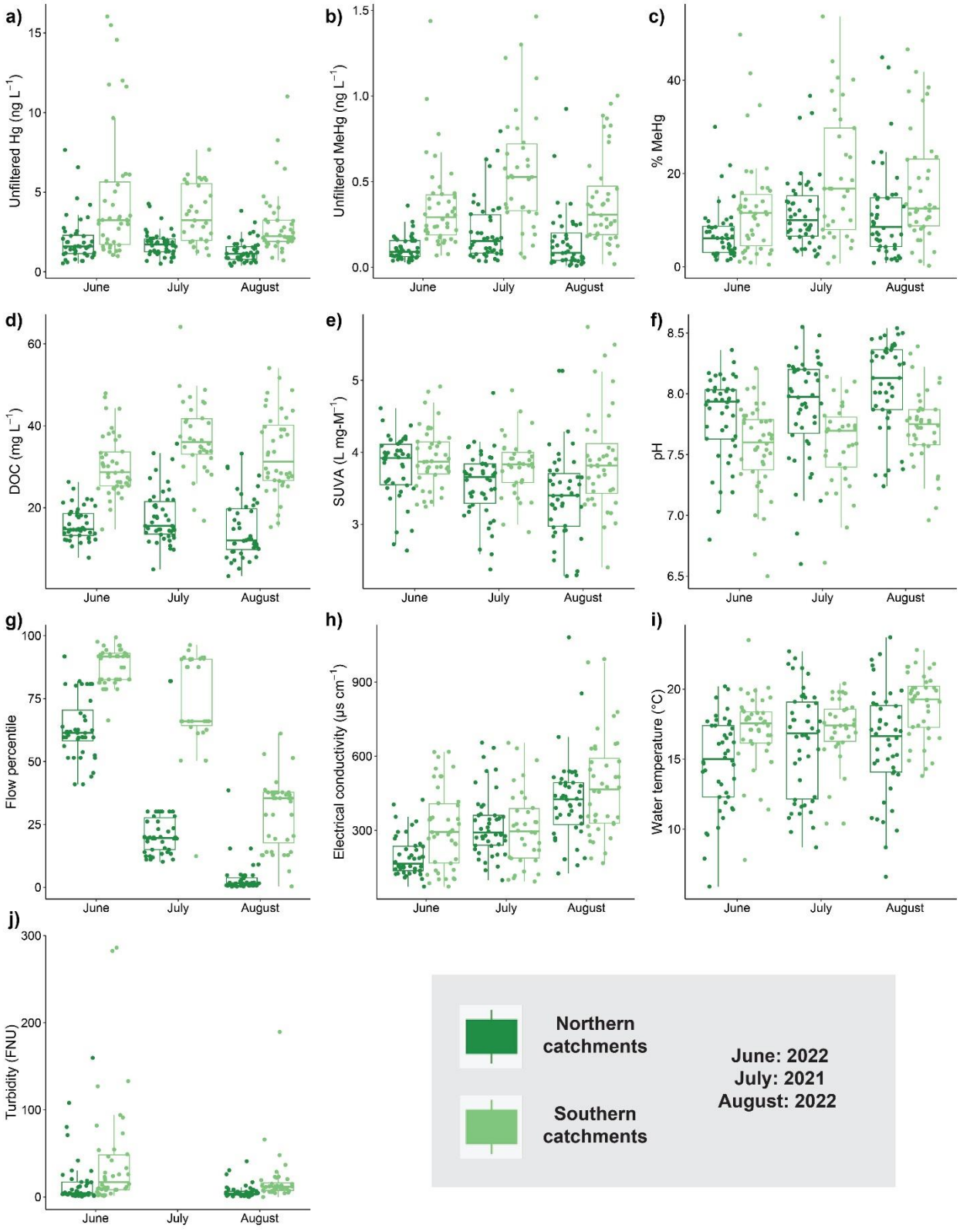

Figure 2.2. Boxplots of water chemistry concentrations and water conditions for each sampling month divided into general regions within the study area which are represented by colours. The line within the box is the median and the lower and upper limits of the box represent the first and third quartile respectively.

2.3.3 General water chemistry

Table 2.2. Summary of water chemistry data from (a) all sampling locations and divided into (b) northern catchments and (c) southern catchments.

	a) All data			b) Northern catchments			c) Southern catchments			
Variable	**Median**	**Quartile 1**	**Quartile 3**	**Median**	**Quartile 1**	**Quartile 3**	**Median**	**Quartile 1**	**Quartile 3**	**Units**
pH	7.8	7.5	8.1	8.0	7.7	8.2	7.7	7.5	7.8	-
Electrical conductivity	314	194	439	285	188	405	337	244	506	µS cm^{-1}
Turbidity*	8.5	3.5	18.9	4.1	2.3	10.5	12.3	8.0	26.0	FNRU
Flow percentile	40	14	81	20	5	59	66	38	91	%
THg	1.90	1.27	3.20	1.48	1.02	1.98	2.99	1.90	4.59	ng L^{-1}
DHg**	1.61	1.16	2.23	1.40	0.97	1.74	2.21	1.47	2.97	ng L^{-1}
TMeHg	0.19	0.09	0.37	0.10	0.06	0.18	0.35	0.21	0.55	ng L^{-1}
DMeHg**	0.18	0.08	0.37	0.09	0.06	0.16	0.35	0.24	0.59	ng L^{-1}
% MeHg	10.0	5.6	16.3	8.0	4.1	13.8	12.4	7.2	20.6	%
DOC	22.23	14.65	32.25	14.72	12.05	20.04	32.91	26.68	39.21	mg L^{-1}
TDN	0.65	0.48	0.92	0.51	0.43	0.63	0.92	0.70	1.14	mg L^{-1}
Na	7.25	3.50	13.40	3.94	2.27	7.67	10.90	7.81	21.81	mg L^{-1}
K	0.95	0.58	1.41	0.78	0.53	1.16	1.21	0.72	1.95	mg L^{-1}
Mg	10.55	7.20	14.23	9.72	6.83	12.58	11.58	7.90	16.59	mg L^{-1}
Zn	0.02	0.01	0.06	0.01	0.01	0.03	0.02	0.01	0.07	mg L^{-1}
P	0.02	0.01	0.04	0.01	0.01	0.01	0.04	0.02	0.07	mg L^{-1}
S	7.81	2.46	19.76	3.54	1.14	7.81	17.86	8.28	33.86	mg L^{-1}
Ca	41.61	29.57	57.21	42.07	29.82	56.00	41.10	28.56	58.17	mg L^{-1}
Cu	0.01	0.00	0.01	0.00	0.00	0.01	0.01	0.00	0.01	mg L^{-1}
Fe	0.37	0.16	0.77	0.18	0.09	0.33	0.68	0.44	0.91	mg L^{-1}
Mn	0.03	0.01	0.07	0.02	0.01	0.04	0.06	0.03	0.10	mg L^{-1}
B	0.03	0.01	0.04	0.01	0.01	0.02	0.04	0.03	0.05	mg L^{-1}
Al	0.08	0.04	0.14	0.06	0.00	0.09	0.12	0.08	0.20	mg L^{-1}
NH4N	16.74	11.36	28.87	14.69	7.31	19.02	27.55	13.55	37.34	µg L^{-1}
Cl	1.46	0.88	2.83	0.95	0.67	1.35	2.51	1.67	4.78	mg L^{-1}
SRP	3.19	2.71	6.12	2.82	2.58	3.13	6.53	3.61	23.80	µg L^{-1}
SO4S	6.88	0.22	19.11	1.97	0.20	7.01	17.44	8.34	34.47	mg L^{-1}
NO3-N & NO2-N	2.15	2.15	11.65	2.23	2.15	13.01	2.15	2.15	9.51	µg L^{-1}
CO3*	107.9	88.2	135.1	96.6	83.9	128.8	117.3	93.0	145.2	mg L^{-1}

* Data from June and August 2022 samplings.
** Data from July 2021 and June 2022 samplings.

Water chemistry parameters showed distinct north-south patterns (Table 2). Southern catchments were more nutrient-rich than the northern catchments, with higher concentrations of TDP, SRP, TDN, and NH4-N. Southern catchments were also characterized by a lower pH, higher EC, and higher concentrations of major ions and metals, except for Ca which remained similar across regions.

A PCA was used to explore associations between water chemistry parameters including Hg, MeHg, and DOC, explaining a total of 50% of variation of water chemistry (Figure 2.3). PC1 was generally representative of the different regions of our study area with positive scores representing more southern sites with higher concentrations of solutes, while more northern sites generally had negative PC1 scores. PC2 appeared to be representative of different water sources, where positive scores were associated with parameters typically derived from weathering processes and generally representative of groundwater influence, including Ca, Mg, and EC. While negative PC2 scores were representative of more peatland influenced waters (increasing DOM aromaticity, Hg, MeHg, DOC, Fe, decreasing pH) (Bourbonniere, 2009). The PCA analysis distinguished some seasonal trends where June samples and July samples from southern sites generally appeared to be associated with higher concentrations of solutes representative of more peatland influenced water, while samples taken during August, as well as in July for northern catchments were generally more associated with parameters derived from weathering processes.

Certain parameters including turbidity (sampled June and August 2022), carbonate (CO_3) (sampled June and August 2022) and DHg and DMeHg (sampled July 2021 and June 2022) were not included in the PCA due to missing data for one of the sampling campaigns. Instead, spearman correlations were used to investigate the relationship between these values with concentrations of THg and TMeHg. Turbidity was highly correlated to both THg and DHg concentrations ($\rho = 0.78$, $\rho = 0.71$) (Figure A.2.4). Dissolved fractions of Hg and MeHg were strongly related to their corresponding total fractions (Hg $\rho = 0.90$, MeHg $\rho = 0.94$). CO_3 was more correlated with weathering parameters such as Ca ($\rho = 0.77$) and Mg ($\rho = 0.73$) (Figure A.2.4). SO_4-S and SRP were also sampled but were not included in the PCA as they were highly correlated with S and TDP respectively.

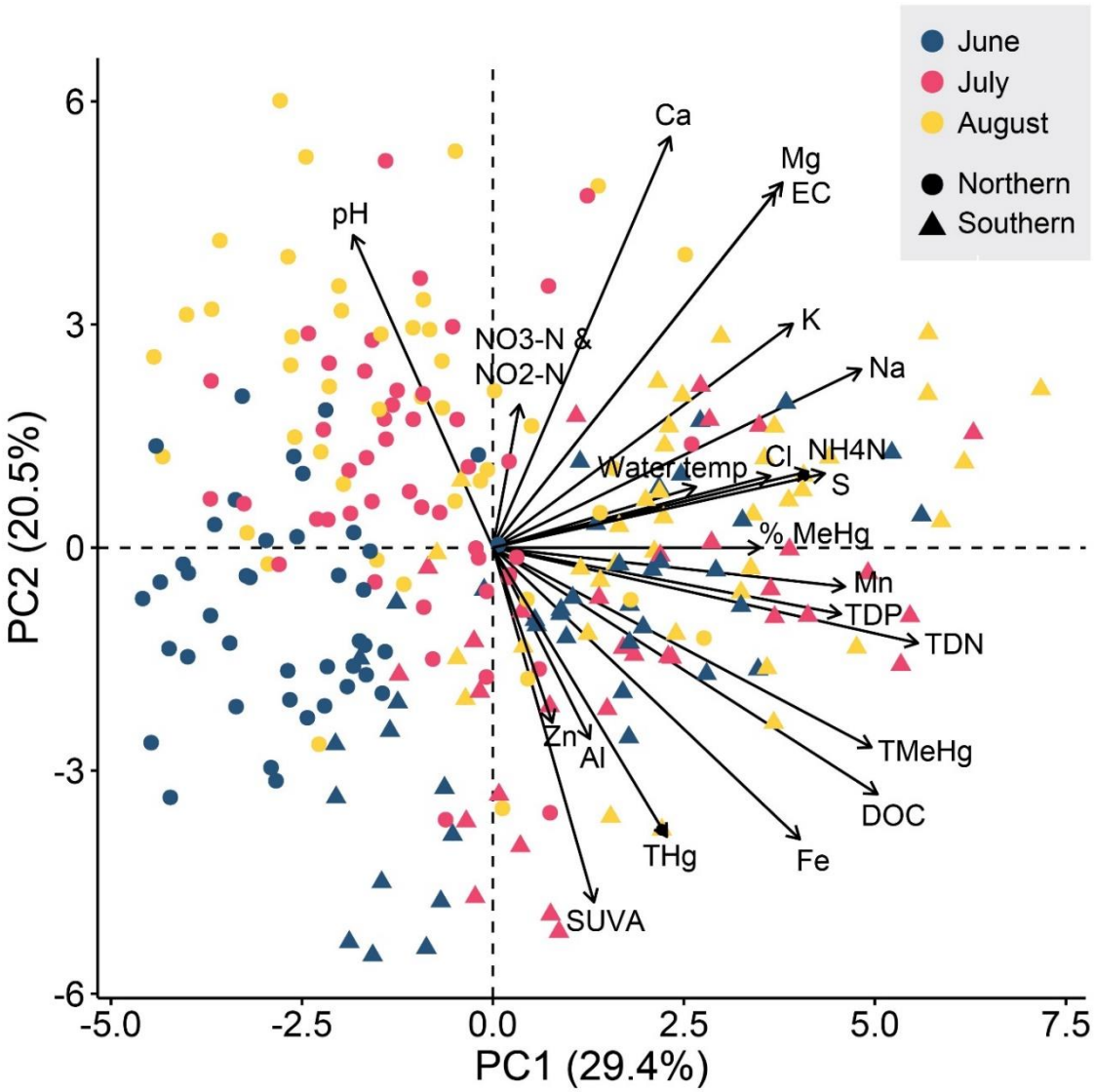

Figure 2.3. PCA analysis of water chemistry. Colours represent the sampling months of June 2022 (blue), July 2021 (pink) and August 2022 (yellow). Shapes represent the general region where the sample was collected divided into northern and southern regions within the study area. Water chemistry data excluding pH, electrical conductivity (EC), SUVA, Water temperature, and % MeHg are logged.

2.3.4 Relationships of Hg and MeHg with DOC concentration and DOM composition

The majority of DOM in our study was characterized as terrestrial humic like using parallel factor analysis where four unique components were identified (Table 2.3). All components had matches to previous datasets published on OpenFluor (Murphy et al., 2014) (Table 2.3). Component 1 was classified as terrestrial humic-like (associated with Peak A and Peak C; Table 2.3; Figure A.2.5; Coble, 1996), and typically made up the majority of the fluorescence in our dataset with a median value of 50% of the total fluorescence for a sample. Component 2 was well matched on OpenFluor

and classified as microbial, humic like, highly associating with the Coble Peak M. Component 3 typically represented around 11% of the total fluorescence, with the least matches on the OpenFluor database. Some of the matches on OpenFluor suggested their related component was terrestrial, humic like (Du et al. 2016; Eder et al. 2022) while other suggested it may be representative of more microbial sources (Cory & McKnight, 2005) or from multiple signals or origins (Wunsch & Murphy, 2021; Bouchachi et al. 2023) (Table 2.3). In our dataset, Component 3 plotted differently from the other components and associated more closely with the Coble Peak T, generally associated with more Tryptophan, protein-like (Coble, 1996). Component 4 was classified as terrestrial humic like or fulvic like by previous studies with an association to Coble Peaks A and C (Coble, 1996) (Figure A.2.5).

Table 2.3. Summary of PARAFAC components including peak excitation and emission values and the likely source of DOM this component represents. Italicized values represent secondary peaks.

PARAFAC Component	Ex	Em	Probable source/characteristics	Selected studies with similar component
C1	< 250, *335*	451	Terrestrial, humic like	Thompson et al., 2023 (C1), Osburn et al., 2018 (C1), Lambert et al., 2016 (C1), Wauthy et al., 2018 (C1),
C2	< 250, *310*	391	Microbial, humic like	Thompson et al. 2023 (C2), Osburn et al. 2018 (C2), Lambert et al. 2016 (C3), Wauthy et al., 2018 (C4)
C3	< 250	416	Humic like, terrestrial and/or microbial origin. Possibly some protein – like.	Wünsch & Murphy, 2021 (C1) Bouchachi et al. 2023 (C6) Cory & McKnight, 2005 (C6) Du et al. 2016 (C1)
C4	275, *400*	> 500	Terrestrial, humic like or soil, fulvic like	Thompson et al., 2023 (C3), Osburn et al. 2018 (C3), Kothawala et al. 2014 (C3)

We used a PCA analysis to examine the DOM composition using both absorbance (SUVA, SR, S275-295) and fluorescence indices (% C1 - % C4, FI, Freshness, BIX, HIX) (Figure 2.4). PC1 explained the majority of DOM composition variance (69.4 %). This axis increased with the aromaticity of DOM, where higher scores were associated with higher values of SUVA, % C1, % C4, and HIX, whereas negative scores were indicative of higher values of BIX and the freshness index. The second component only explained 14.5% of the variance and was driven mainly by a higher % C3 and lower FI values.

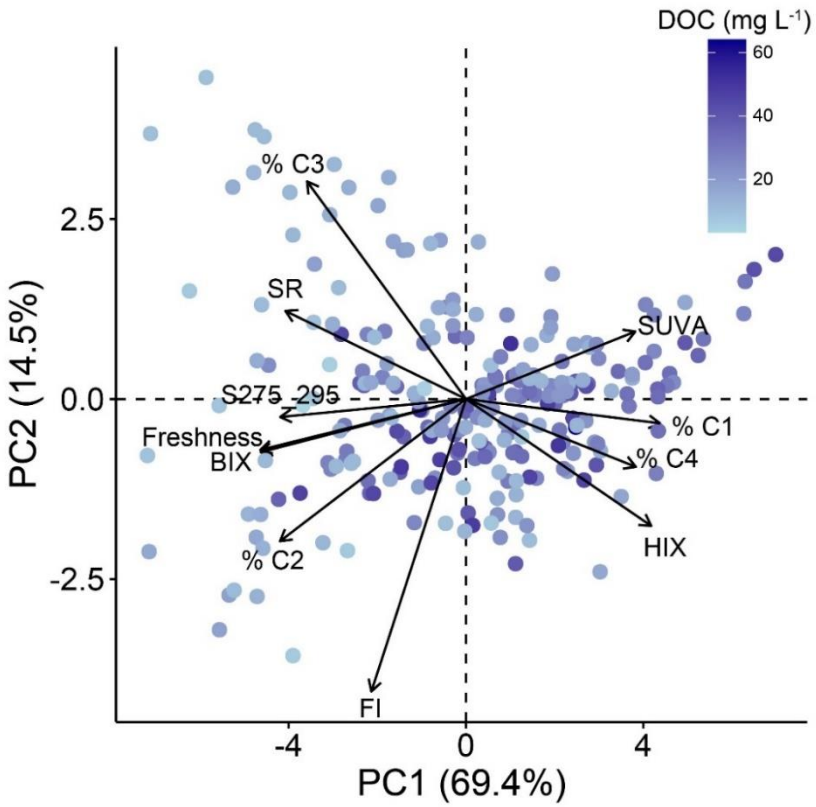

Figure 2.4. Principal component analysis for indices of DOM composition.

We assessed the influence of DOC concentration and DOM composition on Hg and MeHg concentrations using linear regressions (Figure 2.5) and the PC scores from the PCA of DOM composition (Figure 2.4) as a representation of the aromaticity of DOM. DOC, MeHg, and Hg concentrations were logged for these linear regressions. DOC was highly correlated with DMeHg and TMeHg ($R^2_{adj} = 0.70$, $R^2_{adj} = 0.63$) but less so with DHg and THg ($R^2_{adj} = 0.19$, $R^2_{adj} = 0.16$). This relationship remained consistently high across sampling months for TMeHg (June: $R^2_{adj} = 0.61$; July: $R^2_{adj} = 0.61$; August: $R^2_{adj} = 0.66$). However, for THg, the relationship with bulk DOC was weakest during June (June: $R^2_{adj} = 0.07$; July: $R^2_{adj} = 0.22$; August: $R^2_{adj} = 0.22$).

The relationship between MeHg and DOC did not appear to be influenced by the aromaticity of the DOM indicated by the very similar linear relationship between TMeHg or DMeHg concentrations with DOC concentrations when utilizing all data (gray line, Figure 2.5. a, c) compared to when data was grouped by low (light blue) vs high (dark blue) aromaticity (Figure 2.5. a, c). THg and DHg appeared to be preferentially associated with DOC of high aromaticity indicated by the consistently higher values of THg or DHg concentrations when utilizing half of

the data with high aromaticity compared to the half of data group by low aromaticity (Figure 2.5. b, d). These relationships are further supported by looking directly at the relationship between PC1 scores and concentrations. TMeHg and DMeHg concentrations did not correlate well with DOM aromaticity ($R^2_{adj} = 0.15$, $R^2_{adj} = 0.16$ respectively). Whereas THg and DHg were more correlated with DOM aromaticity ($R^2_{adj} = 0.36$, $R^2_{adj} = 0.49$ respectively) than with bulk DOC concentrations. TMeHg, DMeHg, THg, and DHg did not appear to be associated preferentially with any portion of PC2 scores from Figure 2.4, which represented a higher percentage of PARAFAC C3 and lower FI values (Figure A.2.6).

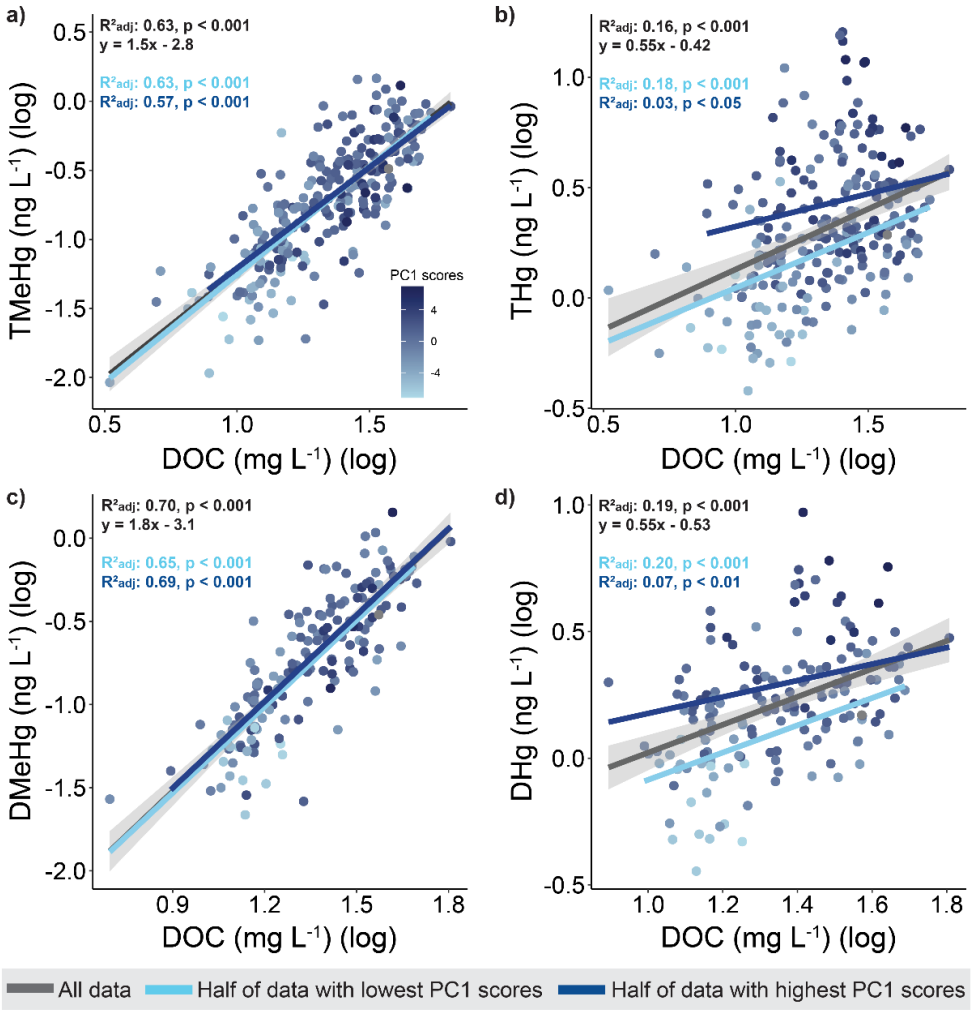

Figure 2.5. Relationship between concentrations of DOC and a) TMeHg, b) THg, c) DMeHg, d) DHg. Relationships were investigated for different groups of data including, all data (grey/black), half of the data with the lowest PC1 scores (light blue), half of the data with the highest PC1 scores (dark blue), scores are from the PCA of DOM composition (Figure 2.4). Higher scores represent more aromatic DOM. Adjusted R^2 values and p-values are displayed for each regression line. The regression formula, and a 95% confidence interval surrounds the best fit line for the regression which utilizes all data. All axes are log transformed.

2.3.5 Influence of landscape characteristics on downstream concentrations and DOM composition

The random forest model for TMeHg concentrations explained 34% of the variability in TMeHg concentrations (Figure 2.6.a.). MAT was the most important variable in the model. The PDP for MAT indicated a threshold within the model at approximately -2°C where at colder temperatures, MeHg concentrations remained fairly steady but quickly increased once hitting this threshold before stabilizing at warmer temperatures. pH was additionally a highly important variable for MeHg concentrations, with PDP indicating an almost linear negative relationship between MeHg concentrations and pH. MeHg concentrations also appeared to increase with lower mean slopes, higher water temperatures, and when the flow percentile hit a threshold of 85%. MAP and the percent of Devonian geology in the catchment were also identified as important variables, however, their effect does not appear to be well characterized by the model.

DOC concentrations had the highest percent of variability explained by random forest models (77%) (Figure 2.6.b.). The DOC random forest model was similar to that of MeHg with MAT and pH identified as the two most important variables. The relationship between concentrations of DOC and MAT matched the trend of TMeHg concentrations with a notable increase at -2°C. pH had a negative relationship to DOC concentrations where concentrations remained high up to a pH of between 7.0 and 7.3 after which concentrations decreased gradually. In addition to MAT and pH, wetlands also appeared important for DOC, as concentrations increased with the proportion of wetlands within 60 m of a water feature and with the proportion of wetlands across the whole catchment. DOC concentrations also declined with steeper mean slopes and the percent of Devonian geology within a catchment.

The random forest model for THg concentrations had a high level of explained variance (73%) (Figure 2.6.c.). This model only utilized data from June and August 2022 due to the importance of turbidity as an explanatory variable for THg. Turbidity was the most important predictor, and concentrations of THg increased exponentially with turbidity. In addition to turbidity, MAP, MAT, and flow percentile were all relatively important for predicting THg concentrations. Concentrations of THg remained steady up to a point (MAP: ~ 450mm, MAT: ~ -1.5°C, Flow percentile: ~ 90) after which they increased. Concentrations of THg also had a slight decrease with an increase in EC. For THg, Devonian geology was not an important contributor to the model.

The landscape characteristics identified as important in the model for predicting DOM aromaticity (inferred from higher PC1 scores; Figure 2.4) differed than those identified for DOC concentrations and were more similar to the predictors for THg concentrations which included MAP, flow percentile, and EC as important predictors. The percent of variance explained for DOM aromaticity was relatively high at 73% (Figure 2.6.d.). EC was the most important variable for predicting DOM aromaticity and aromaticity declined exponentially with increasing EC. The predictive strength of EC was closely followed by pH and MAP, where aromaticity was stable up to a pH of approximately 7.5 after which it decreased. Aromaticity remained stable or increased with increasing precipitation and had a sharp increase at 450 mm yr^{-1}. Aromaticity also increased with increasing flow percentile, a higher mean catchment slope, and colder water temperatures.

Full random forest models with all PDP can be found in the appendix (Figure A.2.7 – A.2.10). Random forest models for DHg and DMeHg were similar to their corresponding models of THg and TMeHg, although there were some differences, likely attributable to the fact that these models were limited to data collected in July and June 2022 (only June for DHg) and were therefore missing the variability in conditions represented by the August sampling. These models can be found in the supplemental material (Figure A.2.11 & Figure A.2.12).

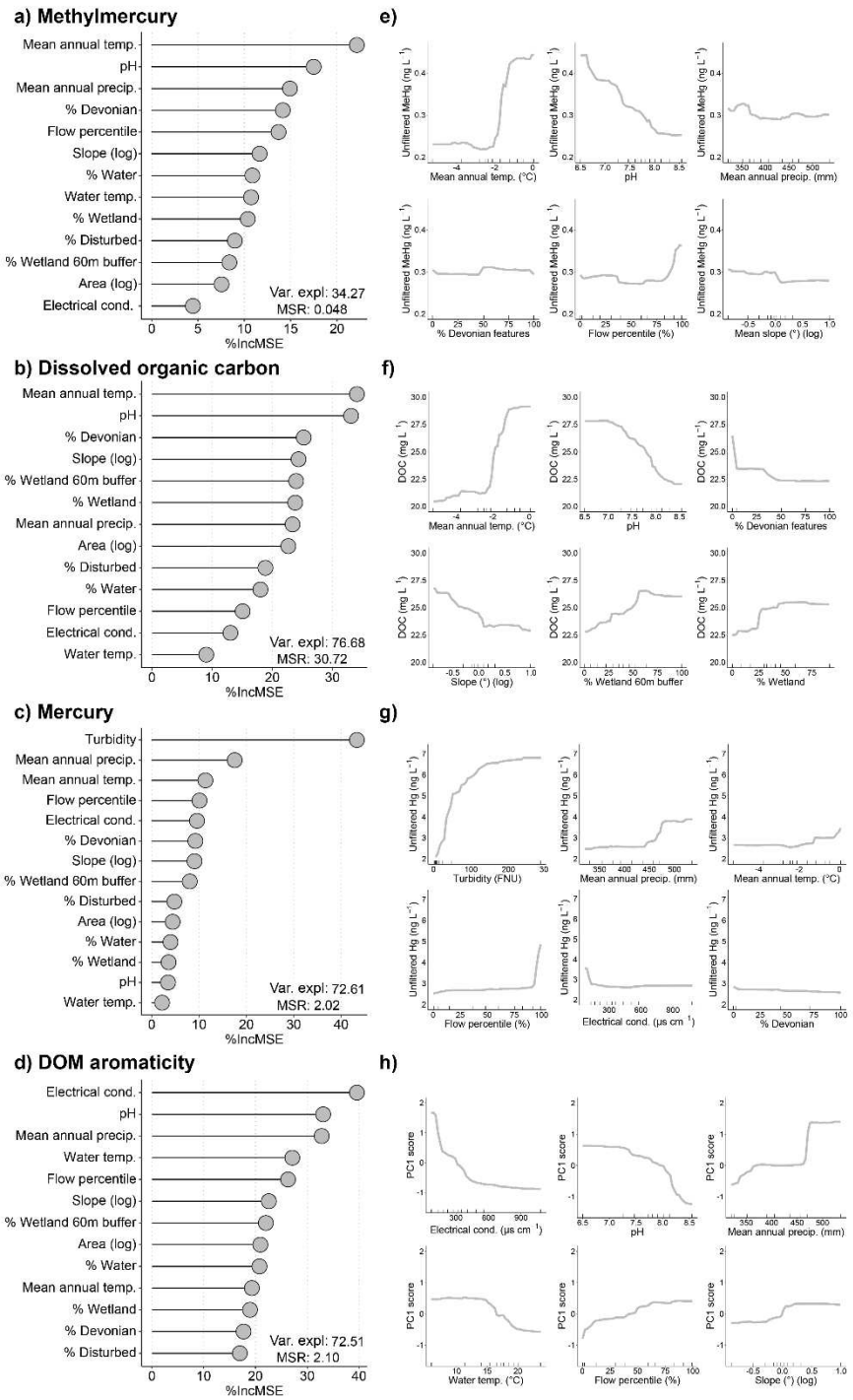

Figure 2.6. Random Forest model variable importance figures for a) TMeHg, b) DOC, c) THg, and d) DOM aromaticity inferred from PC1 scores (Figure 2.4). Models for DOC concentration, DOM composition, and TMeHg include data for June, July, and August. The model for THg includes data for June and August only as turbidity was not measured in July. The higher the variable on the y-axis the more important this variable is for predicting the concentrations of the parameter of interest. The x-axis shows the increase in mean squared error (MSE) of the model if that variable is removed from the model. Variance explained (Var. expl) and mean squared residuals (MSR) shows are based on predicting out of bag (OOB) samples. Figures e-h) partial dependency plots which show the marginal effect for the top six predictor variables on the response variables of e) TMeHg, f) DOC, g) THg, and h) DOM aromaticity. Rug lines at the bottom show data min/max and deciles.

2.3.6 Predicting unsampled stream concentrations and future concentrations

A second round of random forest models exclusively assessed predictors relating to climate and landscape for average TMeHg, THg, and DOC concentrations over the three sampling periods (Figure 2.7. d-f.). These random forest models were generated to predict concentrations in unsampled streams of the study area as opposed to evaluating the importance of each explanatory variable. As such, these random forest models were run using only explanatory variables which could be accessed remotely, and dynamic variables such as flow percentile, EC, pH, and turbidity were not included.

The model used to predict average TMeHg concentrations explained 45% of the variance within the training dataset, an increase in variability explained from the random forest models run on all data as opposed to averages. MAT, % Devonian geology, and MAP remained as highly important variables in the average model and the trend of the relationships remained similar to those discussed above (Figure A.2.13). In addition, wetlands were an important predictor for average TMeHg concentrations; concentrations increased with increasing wetland cover in the catchment with a peak around 30 – 40 % cover and a slight decline after that. Concentrations increased rapidly at 30% wetland cover within a 60m buffer of water features and then remained steady at the higher concentration.

The variance explained for average DOC concentrations was 65% which is a slight decrease from the previous model. The new model was very similar with MAT, MAP, wetlands, and mean slope remaining as important predictor variables. % Devonian geology was the second most important predictor after MAT in this model, with concentrations decreasing with an increase in the percent of Devonian geology (Figure A.2.14).

The model used to predict Hg concentrations explained 41% of the variance in concentrations, representing a large decrease in variance explained from the previous model including turbidity. As with MeHg, MAP, MAT, and % Devonian geology features remained important variables in the average model and the trend of the relationships remained similar to those discussed above (Figure A.2.15). Wetland cover within a 60m buffer of the stream was also an important predictor in this model. Concentrations decreased with increasing wetland cover within a 60m buffer of water features.

The modelled THg, TMeHg, and DOC concentrations for unsampled streams in the study region (Figure 2.7. a-c) reflected the observed latitudinal trends, where catchments in the southern region of the Interior Plains generally had higher concentrations than the northern catchments.

In consideration of the rapid and ongoing changes to climate in the Interior Plains, we predicted concentrations of THg, TMeHg, and DOC under a future climate scenario for catchments in the northern region of the study area (Table 2.4) Using the same random forest models for average concentrations, we replaced values of MAT and MAP in our model with predicted future values, while all other values of the explanatory variables were kept the same. We used the 8-model ensemble of downscaled future climate data from Mahony et al. (2022) which represents a subset of the models in the coupled model intercomparison project phase 6 (CMIP6) ScenarioMIP holdings (Mahony et al. 2022). We investigated future climate change impacts on downstream concentrations based on the ensemble modelled future MAT and MAP for the years 2041 – 2070 under the CMIP6 scenario based on the shared socio-economic pathway (SSP) 2-4.5, which represents a "middle of the road" scenario (O'Neill et al. 2017). Predicted concentrations under the future climate scenario were compared to the predicted stream values under the current climate (Table 2.4). Concentrations of TMeHg are predicted to have the greatest increase (+ 93% increase in the mean concentration). Increases of THg (+ 32%) and DOC (+ 45%) are also expected.

Table 2.4. Comparison of predicted concentrations for Northern catchments under current climate conditions and future climate scenarios. Climate conditions of interest were mean annual temperature and mean annual precipitation all other catchment characteristics were assumed to be the same under both scenarios. Climate datasets were accessed from ClimateNA (Wang et al. 2016; Mahony et al. 2022).

	Current Climate (MAT & MAP for 1991-2020)			Future Climate (8GCMs ensemble ssp245 2041-2070)			Percent Increase		
	Mean	Min	Max	Mean	Min	Max	Mean	Min	Max
DOC	18.9	9.7	32.1	27.4	13.0	40.9	45	33	27
TMeHg	0.18	0.08	0.31	0.36	0.11	0.54	93	37	75
THg	2.1	1.1	3.4	2.8	1.3	6.3	32	26	89
MAT	-3.2	-5.3	-1.4	-1.1	-3.1	0.5	66	41	138
MAP	359	286	439	401	327	484	12	15	10

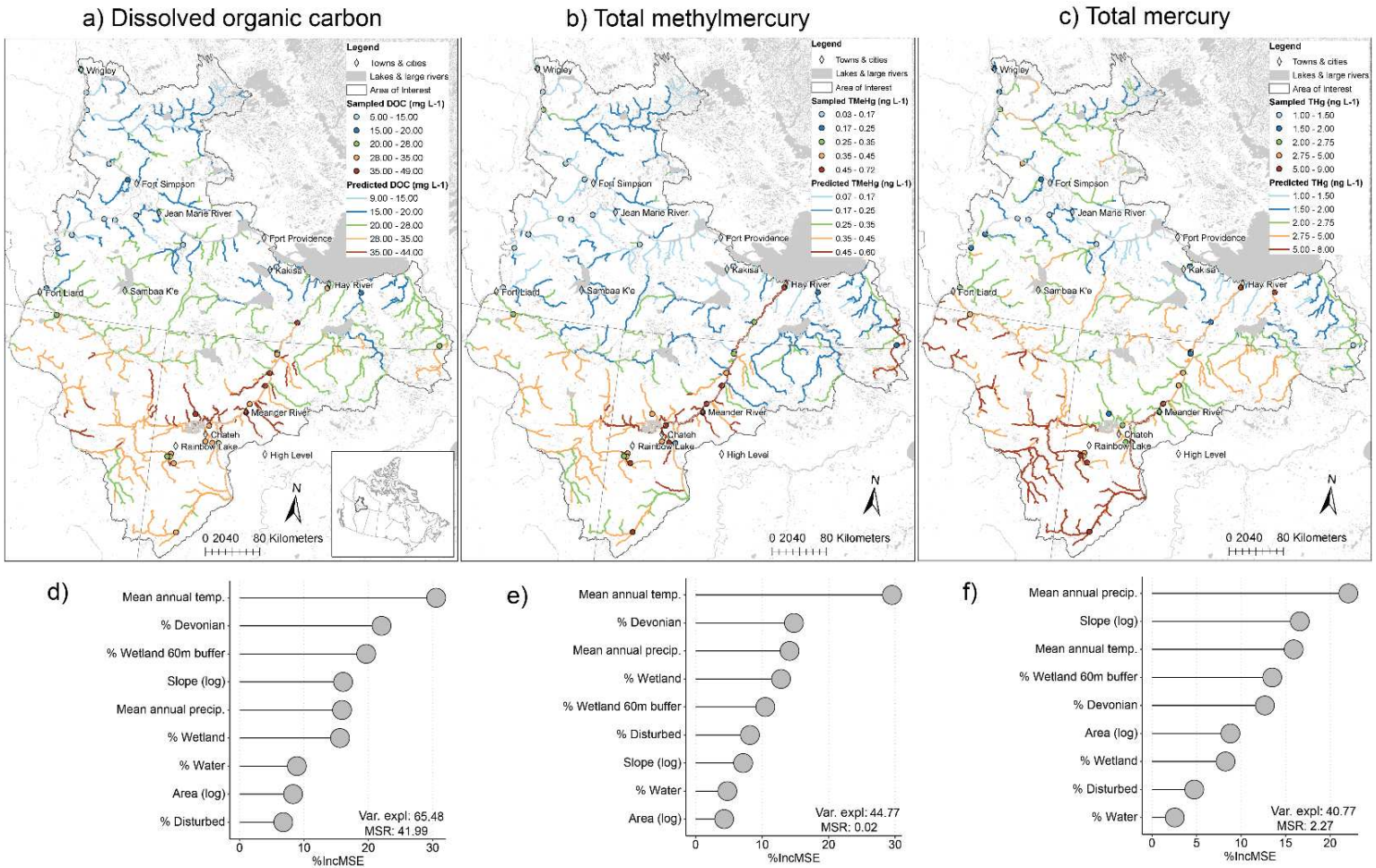

Figure 2.7. Random forest model predictions of average stream concentrations for unsampled streams in the study region. Figures a) – c) show predicted concentrations of a) DOC, b) TMeHg, c) THg. The point values show a subset of measured values which fall onto the streams used for predicting concentrations. Concentrations were predicted using average measured values from 93 streams and remotely available climate and land cover data. Figures d) – f) show the variable importance plots. The higher the variable on the y-axis, the more important this variable is for predicting the concentrations of the parameter of interest. The x-axis shows the increase in mean squared error (MSE) of the model if that variable is removed from the model. Variance explained (Var. expl.) and mean squared residuals (MSR) are based on predicting out of bag samples.

2.4 Discussion

Ongoing climate change threatens to alter the Hg cycle in northern catchments, but the influence on Hg and MeHg concentrations at catchment outlets is not well established. We sampled 93 streams three times in a region with permafrost ranging from isolated sporadic to discontinuous, throughout the open water seasons of 2021 and 2022. We found a strong climate gradient for TMeHg and DOC concentrations even while considering landcover and hydrologic influences. THg was strongly predicted by turbidity and hydrologic conditions and correlated more strongly with aromatic DOM than bulk DOC concentrations. Here, we further discuss the influence of permafrost, landcover, and hydrological variables on driving downstream water chemistry.

2.4.1 Hg and MeHg concentrations

Overall, concentrations of Hg and MeHg measured in this study were below water quality guidelines for aquatic life (CCME, 2003) and were within the range of reported values for streams and rivers within the Boreal zone of Canada. A few samples of Hg were on the higher range of those typically found in peatland dominated catchments (St. Louis et al. 1994; Wasiuta et al. 2019; Fink-Mercier, Lapierre, et al. 2022; Emmerton et al. 2022; Thompson, Khun, et al. 2023; Thompson, Low, et al. 2023). % MeHg concentrations were also similar to other studies from the boreal forest region (St. Louis et al. 1994; Emmerton et al. 2022; Thompson, Khun, et al.; Thompson, Low, et al. 2023). The THg and MeHg sampled in our study was predominantly in the dissolved fraction, although the proportion of DHg made up less than 50% of THg in some of the more turbid rivers. Overall, the dominance of the dissolved fraction aligns with low relief catchments across boreal regions of Canada (Emmerton et al. 2022; Campeau et al. 2022; Thompson, Khun, et al. 2023; Thompson, Low, et al. 2023).

2.4.2 Hydrologic conditions and MeHg concentrations changed with sampling campaigns.

Environmental conditions were different for each sampling campaign. The highest flows percentiles were measured in June, and in some of the northern catchments, the June sampling occurred immediately after the falling limb of the spring freshet. Our PCA findings of general water chemistry showed that June samples, especially from northern catchments, had generally lower median water temperatures and were characterized by lower electrical conductivity and low concentrations of solutes generally associated with groundwater contributions including Mg, and

Ca. The July sampling represented a period of moderate flow, but southern catchments generally had higher flows than northern catchments. Samples from southern catchments during June and July were generally characteristic of contributions from peatland sources, as indicated by the high concentrations of DOC, iron, and high DOM aromaticity (Bourbonniere, 2009). In northern catchments, July and August had low flow conditions with similar water chemistry consisting of high pH and lower concentrations of DOC consistent with lower peatland influence. In the southern catchments, August low flows had water chemistry indicative of groundwater (high EC, Mg, Ca) at some sites, although some sites had water chemistry more indicative of peatland influence.

MeHg concentrations were highest in July 2021, particularly in the southern catchments. MeHg concentrations in June may have been lower than July due to recent flushing of MeHg from soils during the snowmelt and/or less production of MeHg in this earlier colder season (Demers et al. 2010; Shanley et al. 2022). MeHg concentrations or production have been shown to peak around midsummer in some systems (Ramlal et al. 1993; Gerson et al. 2017) and are associated with higher soil or water temperatures (Sun et al. 2023; Thompson, Low, et al. 2023). The greater concentrations of MeHg in July may be attributed to an accumulation of MeHg in the soils, which was then flushed by relatively high flows, particularly in the southern catchments. Low MeHg concentrations during low August flows, dominated by groundwater in many catchments, may be related to limited transport of MeHg from organic subsurface flow pathways. MeHg is likely more supply or production limited than Hg and DOC on the landscape (Wasiuta et al. 2019; Fink-Mercier, del Giorgio, et al. 2022; Shanley et al. 2022; Thompson, Low, et al. 2023).

Hg and DOC concentrations were more similar between sampling months. However, the highest measured concentrations of Hg were sampled in June, which also had the highest flow percentiles and turbidity. Additional sampling within this region of THg and TMeHg with high temporal frequency, including during the spring freshet, and during the peak flow of summer storms would be beneficial to further contextualize the broad seasonal trends shown here. For example, in some catchments DOC or THg are high during snowmelt (Demers et al. 2010; Shanley et al. 2022; Thompson, Low, et al. 2023) while others are diluted or depleted throughout snowmelt (Oswald and Branfireun, 2014; Burd et al. 2018) but it is unclear which if any of these processes are occurring from the limited temporal frequency collected here.

2.4.3 MeHg shows strong relationship with bulk DOC, Hg stronger relationship with aromatic DOM

DOC concentrations within this study correlated strongly with TMeHg and DMeHg and, to a lesser extent, THg and DHg concentrations. Positive correlations between DOC and both MeHg and Hg are common across landscapes, particularly those with wetland influence, although the relationship between DOC and MeHg is generally weaker than that of DOC and Hg (Selvendiran et al. 2008; Lescord et al. 2018; Lavoie et al. 2019; Fink-Mercier, del Giorgio, et al. 2022; Shanley et al. 2022). However, the strong relationships between MeHg and DOC found here are consistent with peatland influenced catchments within our study region (Thompson, Khun, et al. 2023; Thompson, Low, et al. 2023). Strong relationships persisted between MeHg and DOC for June, July, and August, however the relationship between THg and DOC was particularly weak in June compared to July or August. This contrasts with findings from Fink-Mercier, del Giorgio, et al. (2022) who found stronger relationships of THg and DOC during periods of high flow.

The weaker relationship between THg and DOC concentrations in June could be representative of several processes including that early in the open water season, the frost table may not have reached its maximum depth, limiting flow to the upper layer within peatlands (Morison et al. 2017). Early in the season mobile DOC and THg pools may have also been depleted due to the recent snowmelt (Oswald and Branfireun, 2014). However, higher flows often result in more channel erosion and sediment loads (Vercruysse et al. 2017) which may lead to higher loadings of particulate bound Hg (Dittman et al 2010; Staniszewska et al. 2023) and could result in the decoupling of DOC and Hg concentrations.

THg and DHg associated preferentially with terrestrial aromatic DOM, based on the PC1 scores of the DOM composition PCA (Figure 2.4), where higher scores represented more terrestrial aromatic DOM. Several studies have reported stronger correlations between more coloured or aromatic DOM and Hg (Bravo et al. 2018; Lavoie et al. 2019; Fink – Mercier, del Giorgio et al. 2022). Aromatic DOM has higher binding affinities and likely contains more binding sites than non-aromatic DOM (Wang et al. 2022). The strong relationship between aromatic DOC and Hg has generally been attributed to co-mobilization from similar source areas within the catchments (Lavoie et al. 2019). It has also been suggested to be a function of the preferential loss of both Hg

and coloured DOC compared to bulk DOC throughout the water column (Fink-Mercier, del Giorgio, et al. 2022). In addition, this relationship may be more indicative of hydrologic conditions influencing aromatic DOM and Hg in the same direction but through both similar and different processes. This is discussed further in section 2.4.5.

In our study, MeHg did not appear to associate preferentially with DOM of a particular composition. Although MeHg was positively correlated to aromatic indices such as SUVA, and A254, the strongest correlation was to bulk DOC concentrations suggesting that these positive relationships were in part because as DOC increased so did aromatic DOM. MeHg concentrations have been shown to correlate more strongly with aromatic or humic components of DOM than bulk DOC (Shanley et al. 2022), including a meta-analysis of the literature (Lavoie et al. 2019), although MeHg and methylation has also been found to associate more strongly with autochthonous DOM in some streams and lakes (Bravo et al. 2017; Bravo et al. 2018). In our study streams, although MeHg correlated very strongly with bulk DOC, it did not appear to associate preferentially with metrics of DOM of a specific composition.

2.4.4. Stream concentrations of MeHg and DOC relate to permafrost and wetland influence

All of the water chemistry constituents, including Hg, MeHg, and DOC, with the exception of NO_3-N and Ca had generally higher concentrations in the southern catchments compared to northern catchments of the study area. Additionally, most landscape characteristics showed overall trends of higher (MAT; MAP; % wetland; % wetland in 60m stream buffer; area; % disturbed) or lower values (% forest; % water; mean slope; % Devonian geology) in southern catchments compared to northern catchments. As such, a number of these variables were correlated. To better understand the role of the landscape characteristics, we used random forest models to determine the importance of each landscape characteristic for predicting downstream concentrations of THg, TMeHg, and DOC.

MAT was the most important landscape variable for predicting concentrations of MeHg and DOC, followed by indices of wetland influence. A potential mechanism for this trend could be attributed to warmer long-term air temperatures corresponding to warming soil temperatures, particularly in the spring and summer (Qian et al. 2011), which may stimulate microbial activity and, consequently DOC and MeHg production (Dieleman et al. 2016; Paranjape & Hall, 2017; Sun et

al. 2023). TMeHg and DOC concentrations in peatland influenced catchments, are typically higher during warmer months or with higher water temperatures (Dittman et al. 2010; Thompson, Low, et al. 2023). However, the MAT used here represents a 30-year average (1991-2020) (Wang et al. 2016) and as such, we also used it to assess the influence of permafrost extent, as MAT is a primary driver for permafrost conditions (Chadburn et al. 2017; Biskaborn et al. 2019; Smith et al. 2022). Concentrations of TMeHg and DOC increased with warmer MAT, especially at a threshold of -2ºC where concentrations increased substantially. At - 2 ºC, permafrost extent is estimated to be quite low (Chadburn et al. 2017) and has previously been identified as an important temperature threshold for increasing concentrations of DOC in west Siberia (Frey and Smith, 2005).

Limited studies have investigated the influence of permafrost on downstream MeHg concentrations. St. Pierre et al. (2018) found an extreme increase of MeHg downstream of a large thaw slump, although this is uncharacteristic of the permafrost disturbances in our study region. While Staniszewska et al. (2022) and Thompson, Khun, et al. (2023) found little influence of permafrost extent or thaw on downstream MeHg concentrations. Observations from Thompson, Khun, et al. (2023) encompassed similar streams to our study, but their work spanned a more extensive latitudinal gradient and a single sampling period in mid-summer. Here, a clear climatic trend was observed from our repeated sampling campaign of a more limited geographic region around the boundary of permafrost. In addition to the effects on microbial methylation (Sun et al. 2023), temperature also affects the distribution and change in permafrost extent (Shur and Jogenson 2007; Chadburn et al. 2017; Smith et al. 2022).

As permafrost thaws within the Taiga Plains region, elevated permafrost plateaus can collapse into thawed peatlands (Gordon et al. 2016; Fahnestock et al. 2019; Wright et al. 2022), which are areas of higher MeHg production (Gordon et al. 2016; Fahnestock et al. 2019; Tarbier et al. 2021; Thompson, 2023). As thaw can also increase the hydrologic connectivity of a landscape (Connon et al. 2014), these processes are likely contributing to the elevated downstream MeHg concentrations found in our study.

Compared to MeHg, there is more extensive research on how permafrost degradation and thaw influence downstream concentrations of DOC. DOC has been shown to both increase and decrease with permafrost thaw (Frey and McClelland, 2009; Tank et al. 2012; Tank et al. 2020), dependant

on a variety of landscape characteristics as well as the type of permafrost disturbance (Frey and McClelland, 2009; Tank et al. 2020). Decreasing DOC concentrations with permafrost thaw has been attributed to greater interaction with mineral soil layers to which DOC adsorbs (Petrone et al. 2006; Frey and McClelland 2009; Pokorovsky et al. 2020). However, our results of higher DOC concentrations in areas with less permafrost correspond well with studies from peatland-rich areas in the discontinuous permafrost region (Frey and Smith, 2005; Olefeldt et al. 2014). In our study region, as discussed above, permafrost thaw is thought to increase the hydrologic connectivity on the landscape where the collapse of permafrost plateaus may result in more connection of previously isolated landscapes, including peatlands (Connon et al. 2014), and this increased connectivity may result in an increase of DOC concentrations downstream (Olefeldt et al. 2014).

pH was the second most important predictor of TMeHg and DOC within the random forest model; more acidic streams had higher concentrations of TMeHg and DOC. Water from peatland environments is generally more acidic (Bourbonniere, 2009; Gordon et al. 2016), and within our study, waters with lower pH associated with higher concentrations of water chemistry characteristic of peatlands including high DOC (Bourbonniere, 2009). Therefore, this relationship is likely indicative of the role of peatlands as a source of MeHg and DOC within these catchments, as is commonly found elsewhere (Olefeldt and Roulet, 2014, Fink-Mercier, Lapierre, et al. 2022; Thompson, Khun, et al. 2023). It is interesting that pH was a more important predictor than wetland cover within our models. We attribute this to the fact that pH was a dynamic variable throughout the three samplings as opposed to wetland cover, which remained constant. Therefore, pH may have been more representative of actual peatland influence at the time of each sampling as opposed to wetland cover, which may have included wetlands that were hydrologically disconnected from the stream network for some or all sampling periods.

Wetland cover appeared as an important predictor variable for DOC, further supported by the importance of less steep catchments, highlighting lowland areas. The lesser importance of wetland cover for TMeHg concentrations may have been due to the fact that the wetland map we used to define wetland cover did not distinguish between different peatland types. Although, plateaus and thawed peatlands generally have high soil and pore water concentrations of DOC (Olefeldt and Roulet, 2014; Gordon et al. 2016; Thompson, 2023), plateaus typically have very low concentrations and production of MeHg compared to thawed peatlands, especially fens (Gordon

et al. 2016; Fahnestock et al. 2019; Tarbier et al. 2021; Thompson, 2023). The differing influence of peatland types on MeHg may have limited the identification of wetlands as a more important predictor of TMeHg concentrations.

Although random forest models for TMeHg and DOC had similar important predictors and relationships, the statistical model estimated DOC much better than TMeHg. This is likely due to the complexity of MeHg production and cycling on the landscape or could be reflective of the additional reliance on DOC for the transport of MeHg downstream limiting the influence of landscape characteristics without accounting for this transport mechanism.

2.4.5 THg related to turbidity while both THg and aromatic DOM are explained by hydrologic conditions

The random forest models for THg concentrations and DOM aromaticity appear to be more driven by hydrologic conditions as opposed to MAT or wetland cover. Turbidity dominated the random forest model for THg and along with the importance of high flow percentile, indicates the importance of erosive processes mobilizing particulate or colloidal bound Hg in driving higher concentrations of THg, likely occurring in the steeper forested areas of the catchments. The positive relationship between TSS or turbidity with THg in rivers has been shown previously (Dittman et al. 2010; Ricassi et al. 2011; St. Pierre et al. 2018; Staniszewska et al. 2023).

High THg and aromatic DOM associating with high flow percentiles and lower EC is likely indicative of the importance of high flow events for the co-mobilization of THg and aromatic DOM from organic soils. In forested or mixed catchments, which are common within our study area, higher flows during summer typically represent increased contributions from more organic subsurface flow pathways of uplands or riparian areas (Laudon et al. 2011; Burd et al. 2018; Werner et al. 2019). Runoff may also be generated from peatland areas of the catchment (Quinton et al. 2009; Olefeldt and Roulet, 2014). Both peatlands and riparian organic soils are important sources of aromatic DOC (Olefeldt, Roulet, et al. 2013; Olefeldt and Roulet, 2014; Ledesma et al. 2018; Werner et al. 2019) and Hg has been suggested to be more mobile within the upper soil layers (Jiskra et al. 2017). SUVA and THg concentrations sampled here negatively associated with indicators of groundwater influence such as EC, Mg, and Ca concentrations based on the PCA analysis, further supporting the role of higher subsurface flow pathways for their delivery

downstream. Our findings align with previous studies where THg and aromatic DOC have been shown to increase with spring or summer high flows in other catchments and are generally attributed to changing flow paths or hydrologic connectivity within the catchment (Demers et al. 2010; Werner et al. 2019; Thompson, Low, et al. 2023).

The positive relationship of aromatic DOM with steeper slopes, higher flow percentiles, and the negative relationship with water temperature may additionally point to the importance of high flows resulting in shorter water residence times for DOM aromaticity. The importance of short water residence time has been identified as an important consideration for terrestrial or coloured fractions of DOC (Kothawala et al. 2014; Fink-Mercier, del Giorgio, et al. 2022) as well as Hg (Richardson et al. 2021; Fink-Mercier, del Giorgio, et al. 2022) in other studies. Shorter water residence times are likely to limit processing within the system, and as aromatic DOC can be lost preferentially via photo chemical processes and flocculation (Olefeldt, Turetsky and Blodau, 2013; Kothawala et al. 2014; Hutchins et al. 2017) shorter water residence times may promote more persistence of coloured or aromatic DOC throughout the aquatic network (Kothawala et al. 2014; Fink-Mercier, del Giorgio, et al. 2022).

MAP was the second most important predictor for aromatic DOM and THg concentrations. Long-term MAP could be related to a variety of landscape and hydrologic processes. The MAP used here is modelled MAP and elevation was used in the modelling (Wang et al. 2016), meaning that it is also related to topographic characteristics. Our dataset cannot determine the influence of MAP at a process level and overall, the importance of MAP in our models is likely due to a general relationship with various hydrologic processes. Future investigations and models would likely benefit from a more specific estimate of precipitation.

MAT was also an important predictor for THg, although it appears to influence much less of the variability than for DOC or TMeHg concentrations. A few studies have investigated the relationship between THg dynamics in aquatic systems and permafrost thaw and have generally attributed increasing trends of exports or concentrations to increased thaw resulting in a deeper active layer (Rydberg et al. 2010; Lim et al. 2019; Mu et al. 2020). This includes a study by Lim et al. (2019) which investigated 32 rivers in the western Siberia Lowlands, spanning a gradient of continuous to isolated permafrost and found the highest concentrations of particulate Hg in the

sporadic zone (Lim et al. 2019), similar to our findings. It is possible that the deepening active layer may also play a role in the increased mobilization and resulting concentrations within our study, along with the increased hydrologic connectivity from plateau collapse discussed above.

Unlike the clear climatic pattern of bulk DOC, MAT was not an important predictor for the aromaticity of DOM. Some studies have suggested that carbon mobilized from permafrost may be more aliphatic or labile in nature (Mann et al. 2015; Spencer et al. 2015; Fouché et al. 2020; Starr et al. 2024). However, Gandois et al. (2019) showed contrasting results in permafrost peatlands, where they showed that DOM aromaticity was higher in bogs with more permafrost DOM (Gandois et al. 2019). The lack of the detection of a large temperature influence on DOM aromaticity in our study may be because MAT is likely a better indicator of permafrost extent on the landscape as opposed to capturing thaw features which are releasing permafrost DOM. In addition, permafrost DOM being released within our catchments may undergo processing before it reaches our sampling locations. Several studies have shown that permafrost DOC can be highly bioavailable and likely quickly taken up by microbes (Mann et al. 2015; Spencer et al. 2015; Vonk et al. 2015). Gandois et al. (2019) also showed a shift in the proportion of permafrost DOC throughout the peatland thaw gradient, and they attributed this to dilution by other DOM sources or processing of DOM. In addition, as the permafrost gradient within our study ranges from isolated/sporadic to discontinuous permafrost and this may also limit detection of a permafrost influence. A study investigating biodegradability of DOM as opposed to composition, found the highest bioavailability was in more continuous permafrost soils, and discussed the possibility of attributing this to the more limited processing which may occur while in permafrost in the continuous zone (Vonk et al. 2015).

2.4.6 Highest predicted concentrations in southern catchments

We predicted average summer concentrations of THg, TMeHg, and DOC in unsampled streams of the region based on our random forest models executed using solely remotely available data. Within these models, MAT and wetlands remained important variables for TMeHg and DOC. However, Devonian geology became the second most important variable (after MAT) in the models for average TMeHg and DOC concentrations. The influence of Devonian geology on MeHg concentrations remains poorly characterized in the average models. Although DOC

concentrations decrease with increasing cover of Devonian geology. The Devonian geology in the area is likely to be mainly limestone (Ecosystem Classification Group, 2007) and is somewhat positively correlated to pH and a higher Ca:Ca+Mg, suggesting an influence on water chemistry. This may in turn influence the solubility or mobility of DOC and potentially MeHg and Hg. However, it is difficult to say with certainty the process-based influence of Devonian geology within our model. The model for THg remained similar with MAP now the most important predictor in the absence of turbidity.

Concentrations of Hg and MeHg in freshwater are of great concern due to the health implications of MeHg within the food chain (Mergler et al. 2007). However, compared to other water chemistry analysis the cost of Hg and MeHg analysis is relatively very high. In northern systems the challenge of sampling is expanded due to limited access roads and extra costs. The importance of understanding the Hg risk in these systems remains high due to the importance of fish in traditional diets of many northern communities (Houde et al. 2022). The resulting maps give an indication of streams and rivers with potentially high THg and TMeHg concentrations. As the accuracy of our statistical models is moderate, the intent of this map is not to provide fully accurate concentration data but instead to provide high level information on trends in concentrations of DOC, TMeHg, and THg to inform future monitoring and research activities. Overall, we found that concentrations tend to be highest in the Hay River Basin of northern Alberta, an area in which very limited water chemistry and Hg sampling has taken place.

2.4.7 Expected concentration increase under a warming climate

With ongoing change in Northern environments, concentrations of DOC, THg, and TMeHg are likely to increase in the future. We used a random forest model updated with future values of MAT and MAP to estimate expected changes under a future climate change scenario. We expect TMeHg concentrations to be most sensitive to an increase in MAT and MAP followed by smaller increases in DOC and THg concentrations. However, it is important to note the uncertainty within our models and that even with the large, predicted increases, concentrations of TMeHg and THg will likely remain below guidelines for aquatic health in the near future. The influence of MAT in our statistical models is likely representative of a number of processes including temperature and landcover change due to permafrost thaw which may influence downstream concentrations as

discussed above. However, permafrost thaw often lags behind increases in air temperature and may even continue to persist depending on the ecosystem in which it is found (Shur & Jorgenson, 2007). Therefore, although we predict future concentrations based on MAT and MAP for the years 2041 – 2070 there may be a lag for the estimated increase in concentrations. Yet, there may be a small increase within the estimated time frame based on a more immediate impact of the warming of active layer soils and water, stimulating microbial activity. Although we expect an increase in downstream concentrations to occur as the coverage of thermokarst peatlands with greater potential for MeHg production expands with thaw, over a longer term the stability of this increase is uncertain. Recent work has suggested that the development of peatlands due to thaw may be one stage in a series of successional stages where peatlands may further develop in the future into re established forest area without the underlying permafrost (Carpino et al. 2018) and this shift could further change the Hg dynamics on the landscape. Continued monitoring of Hg dynamics in these ecosystems is warranted to fully understand the future impacts of the changing climate. Therefore, our data provides important insights for predicting the influence of ongoing changes and will provide an important baseline to understand future changes.

Chapter 3: Conclusions, limitations, and future study directions

3.1 Summary of findings

We sampled 93 streams throughout the Taiga Plains in western Canada and found that TMeHg and DOC concentrations were best predicted by mean annual temperature and peatland influence within their catchment, while THg and DOM aromaticity was more related to hydrologic parameters. TMeHg and DOC concentrations increased with MAT, likely due to increased areas of high MeHg production and increased potential for downstream transport resulting from expanding thawed peatland areas on the landscape. The warmer temperatures may have also stimulated microbial activity and subsequent DOC production and Hg methylation. Both TMeHg and DOC also increased with lower pH further confirming the role of peatlands as a source of MeHg and DOC at the catchment scale. Turbidity was the most important predictor for THg concentrations demonstrating the importance of erosive processes and particulate bound Hg in driving higher concentrations within these systems. Hydrologic parameters including higher flow percentiles, MAP, and decreasing electrical conductivity were important predictors for THg concentrations and DOM aromaticity, likely indicating the importance of inputs from organic flow paths and (or) low water residence time for the persistence of aromatic DOM in these systems. Understandably, given the similarity in predictors, MeHg correlated most strongly to bulk DOC, while THg appeared to associate most strongly with the aromatic fraction of DOM, likely due to similar mobilization processes. Overall, our findings suggest that ongoing climate change will result in an increase of TMeHg, THg, and DOC concentrations at the catchment scale and therefore will likely have implications for the functioning and health of aquatic systems and food webs.

3.2 Limitations and future study directions

Incorporating more detailed landscape and permafrost feature data may have improved the accuracy of our models. However, a particular challenge of this project was finding spatially available data with an appropriate level of detail, but which also spanned two provinces and a territory of Canada, with areas both above and below the 60th parallel. Peatland types differ in their efficiency producing MeHg (Gordon et al. 2016; Fahnestock et al. 2019; Tarbier et al. 2021; Thompson, 2023) and therefore additional consideration of broad peatland types may improve the

variance explained by models and confirm of some of the processes suggested here such as the reasons for wetlands as a more important predictor for DOC compared to TMeHg.

Hydrology was found to be an important consideration for THg and aromatic DOM in particular, which aligns with a number of other studies (Demers et al. 2010; Werner et al. 2019; Thompson, Low, et al. 2023). However, as flow percentile in our catchment was estimated using a subset of streams monitored by Environment and Climate Change Canada, the strength of flow in predicting concentrations may have changed had true flow been measured at each sampling location. Permafrost thaw is expected to alter the hydrology within the Taiga Plains in a number of ways (Wright et al. 2022). Although several studies have investigated the influence of flow on downstream concentrations of DOC, or less commonly Hg, in northern catchments (Gandois et al. 2021; Shrogen et al. 2021; Thompson, Low, et al. 2023), in our study the influence of permafrost temporal dynamics and role of hydrology in permafrost regions on downstream concentrations of MeHg, Hg, and DOC may benefit from comparisons of similar catchments across this boundary and with more consideration of seasonality.

In our study, landscape disturbance, including wildfire and harvesting, was not an important predictor for THg, MeHg, or DOC concentrations or DOM composition. However, the disturbances included in our study were limited to disturbances occurring at least a few years before sampling, likely limiting the ability to detect any effects. However, these results do support those of other studies which find limited influence of wildfire of downstream Hg or DOC in northern regions (Burd et al. 2018; Hutchins et al. 2023). Limited studies have investigated the influence of wildfires on downstream concentrations of MeHg at the catchments scale, yet Ackley et al. (2021) found elevated concentrations within pore waters of burned wetlands, indicating the necessity of further evaluating the risk of elevated concentrations downstream.

This study looks at MeHg in peatland areas where it is highly related to DOC concentrations and may be representative of the influence of permafrost thaw for other regions with similar landscapes. However, the influence of permafrost thaw on DOC concentrations varies across regions (Frey and McClelland, 2009; Tank et al. 2020) and therefore we might expect the influence of permafrost to vary for other water chemistry parameters as well. The relationship between DOC and MeHg can be variable (Lavoie et al. 2019) making DOC a less reliable proxy for systems

where the relationship is not established. Therefore, the understanding of how permafrost thaw may influence downstream MeHg concentrations remains uncertain and understudied in comparison to Hg and DOC within some systems, highlighting the need for future studies and long-term monitoring programs to include sampling of MeHg.

Hg in aquatic systems is generally of concern because of the possibility of bioaccumulation and bio magnification in food webs. Although we expect increasing concentrations of MeHg in water with ongoing climate warming, it is difficult to predict to what extent this increase will translate to an increase in fish concentrations. Hg in fish can be reflective of the concentrations of Hg or MeHg in the surrounding waters (Emmerton et al. 2022), yet a number of biological and environmental variables may also play a role in the accumulation of Hg within fish, including additional water chemistry (Moslemi-Aqdam et al. 2022). THg concentrations in fish or other aquatic biota have been shown to positively relate to concentrations of DOC or nutrients in the water (Ahonen et al. 2018; Moslemi-Aqdam et al. 2023; Rask et al. 2024). However, DOC or TOC concentrations have also been shown to decrease the bioaccumulation rates of THg in invertebrates and fish after a threshold around 5.8 to 8.6 mg L-1 DOC (French et al 2014; Braaten et al. 2018). DOC concentrations within our streams are higher than these thresholds and are likely to increase alongside MeHg, which may influence the future trends in fish Hg. Additional studies investigating Hg concentrations and bioaccumulation in the Hay River catchment may provide important insights into these relationships and would likely provide an interesting comparison to studies which have been completed in the northern regions of the study area (Moslemi-Aqdam et al. 2022; Moslemi-Aqdam et al. 2023).

Overall, this study provides important findings relating to the influence of catchment drivers on downstream concentrations of TMeHg, THg, and DOC concentrations. The clear climatic gradient influencing TMeHg and DOC concentrations highlights the risk of elevated future concentrations with continued warming. This emphasizes the need for continued monitoring of MeHg in aquatic systems and organisms within northern regions. The data presented here provides an important dataset, particularly in the understudied Hay River watershed, to which the impact of future disturbance may be compared.

References

Ackley, C., Tank, S. E., Haynes, K. M., Rezanezhad, F., McCarter, C., & Quinton, W. L. (2021). Coupled hydrological and geochemical impacts of wildfire in peatland-dominated regions of discontinuous permafrost. *Science of The Total Environment*, *782*, 146841. https://doi.org/10.1016/j.scitotenv.2021.146841

Ahonen, S. A., Hayden, B., Leppänen, J. J., & Kahilainen, K. K. (2018). Climate and productivity affect total mercury concentration and bioaccumulation rate of fish along a spatial gradient of subarctic lakes. *Science of The Total Environment*, *637–638*, 1586–1596. https://doi.org/10.1016/j.scitotenv.2018.04.436

Antweiler, R. C. (2015). Evaluation of Statistical Treatments of Left-Censored Environmental Data Using Coincident Uncensored Data Sets. II. Group Comparisons. *Environmental Science & Technology*, *49*(22), 13439–13446. https://doi.org/10.1021/acs.est.5b02385

BASL. (2023). *BASL - Low-level Mercury Analysis*. (n.d.). Retrieved March 21, 2024, from https://www.biology.ualberta.ca/basl/mercury.html

Biskaborn, B. K., Smith, S. L., Noetzli, J., Matthes, H., Vieira, G., Streletskiy, D. A., Schoeneich, P., Romanovsky, V. E., Lewkowicz, A. G., Abramov, A., Allard, M., Boike, J., Cable, W. L., Christiansen, H. H., Delaloye, R., Diekmann, B., Drozdov, D., Etzelmüller, B., Grosse, G., … Lantuit, H. (2019). Permafrost is warming at a global scale. *Nature Communications*, *10*(1), 264. https://doi.org/10.1038/s41467-018-08240-4

Bouchachi, N., Obernosterer, I., Marie, B., Crispi, O., & Ortega-Retuerta, E. (2023). Phosphorus limitation determines the quality of dissolved organic matter released by marine heterotrophic prokaryotes. *Limnology and Oceanography Letters*, *8*(2), 330–339. https://doi.org/10.1002/lol2.10287

Bourbonniere, R. A. (2009). Review of Water Chemistry Research in Natural and Disturbed Peatlands. *Canadian Water Resources Journal*, *34*(4), 393–414. https://doi.org/10.4296/cwrj3404393

Braaten, H. F. V., De Wit, H. A., Larssen, T., & Poste, A. E. (2018). Mercury in fish from Norwegian lakes: The complex influence of aqueous organic carbon. *Science of The Total Environment*, *627*, 341–348. https://doi.org/10.1016/j.scitotenv.2018.01.252

Branfireun, B. A., Cosio, C., Poulain, A. J., Riise, G., & Bravo, A. G. (2020). Mercury cycling in freshwater systems—An updated conceptual model. *Science of The Total Environment*, *745*, 140906. https://doi.org/10.1016/j.scitotenv.2020.140906

Bravo, A. G., Bouchet, S., Tolu, J., Björn, E., Mateos-Rivera, A., & Bertilsson, S. (2017). Molecular composition of organic matter controls methylmercury formation in boreal lakes. *Nature Communications*, *8*(1), 14255. https://doi.org/10.1038/ncomms14255

Bravo, A. G., & Cosio, C. (2020). Biotic formation of methylmercury: A bio–physico–chemical conundrum. *Limnology and Oceanography, 65*(5), 1010–1027. https://doi.org/10.1002/lno.11366

Bravo, A. G., Kothawala, D. N., Attermeyer, K., Tessier, E., Bodmer, P., Ledesma, J. L. J., Audet, J., Casas-Ruiz, J. P., Catalán, N., Cauvy-Fraunié, S., Colls, M., Deininger, A., Evtimova, V. V., Fonvielle, J. A., Fuß, T., Gilbert, P., Herrero Ortega, S., Liu, L., Mendoza-Lera, C., … Amouroux, D. (2018). The interplay between total mercury, methylmercury and dissolved organic matter in fluvial systems: A latitudinal study across Europe. *Water Research*, *144*, 172–182. https://doi.org/10.1016/j.watres.2018.06.064

Breiman, L. (2001). Random Forests. *Machine Learning*, *45*(1), 5–32. https://doi.org/10.1023/A:1010933404324

Brigham, M. E., Wentz, D. A., Aiken, G. R., & Krabbenhoft, D. P. (2009). Mercury Cycling in Stream Ecosystems. 1. Water Column Chemistry and Transport. *Environmental Science & Technology, 43*(8), 2720–2725. https://doi.org/10.1021/es802694n.

Brown, J., O. Ferrians, J. A. Heginbottom, and E. Melnikov. (2002). Circum-Arctic Map of Permafrost and Ground-Ice Conditions, Version 2 [Data Set]. Boulder, Colorado USA. National Snow and Ice Data Center. https://doi.org/10.7265/skbg-kf16. Date Accessed 03-20-2024.

Burd, K., Tank, S. E., Dion, N., Quinton, W. L., Spence, C., Tanentzap, A. J., & Olefeldt, D. (2018). Seasonal shifts in export of DOC and nutrients from burned and unburned peatland-rich catchments, Northwest Territories, Canada. *Hydrology and Earth System Sciences*, *22*(8), 4455–4472. https://doi.org/10.5194/hess-22-4455-2018

Bush, E. and Lemmen, D.S., editors (2019): Canada's Changing Climate Report; Government of Canada, Ottawa, ON. 444 p.

Campeau, A., Eklöf, K., Soerensen, A. L., Åkerblom, S., Yuan, S., Hintelmann, H., Bieroza, M., Köhler, S., & Zdanowicz, C. (2022). Sources of riverine mercury across the Mackenzie River Basin; inferences from a combined Hg C isotopes and optical properties approach. *Science of The Total Environment*, *806*, 150808. https://doi.org/10.1016/j.scitotenv.2021.150808

Canadian Council of Ministers of the Environment. (2003). Canadian Water Quality Guidelines for the Protection of Aquatic Life - Mercury - Inorganic mercury and methylmercury, 6.

Carpino, O. A., Berg, A. A., Quinton, W. L., & Adams, J. R. (2018). Climate change and permafrost thaw-induced boreal forest loss in northwestern Canada. *Environmental Research Letters*, *13*(8), 084018. https://doi.org/10.1088/1748-9326/aad74e

Carpino, O., Haynes, K., Connon, R., Craig, J., Devoie, É., & Quinton, W. (2021). Long-term climate-influenced land cover change in discontinuous permafrost peatland complexes. *Hydrology and Earth System Sciences*, *25*(6), 3301–3317. https://doi.org/10.5194/hess-25-3301-2021

Chadburn, S. E., Burke, E. J., Cox, P. M., Friedlingstein, P., Hugelius, G., & Westermann, S. (2017). An observation-based constraint on permafrost loss as a function of global warming. *Nature Climate Change*, *7*(5), 340–344. https://doi.org/10.1038/nclimate3262

Chupakov, A. V., Pokrovsky, O. S., Moreva, O. Y., Kotova, E. I., Vorobyeva, T. Y., & Shirokova, L. S. (2023). Export of organic carbon, nutrients and metals by the mid-sized Pechora River to the Arctic Ocean. *Chemical Geology*, *632*, 121524. https://doi.org/10.1016/j.chemgeo.2023.121524

Clarkson, T. W., Magos, L., & Myers, G. J. (2003). The Toxicology of Mercury—Current Exposures and Clinical Manifestations. *New England Journal of Medicine, 349*(18), 1731–1737. https://doi.org/10.1056/NEJMra022471

Coble, P. G. (1996). Characterization of marine and terrestrial DOM in seawater using excitation-emission matrix spectroscopy. *Marine Chemistry*, *51*(4), 325–346. https://doi.org/10.1016/0304-4203(95)00062-3

Connon, R. F., Quinton, W. L., Craig, J. R., & Hayashi, M. (2014). Changing hydrologic connectivity due to permafrost thaw in the lower Liard River valley, NWT, Canada. *Hydrological Processes*, *28*(14), 4163–4178. https://doi.org/10.1002/hyp.10206

Cory, R. M., & McKnight, D. M. (2005). Fluorescence Spectroscopy Reveals Ubiquitous Presence of Oxidized and Reduced Quinones in Dissolved Organic Matter. *Environmental Science & Technology*, *39*(21), 8142–8149. https://doi.org/10.1021/es0506962

Creed, I. F., McKnight, D. M., Pellerin, B. A., Green, M. B., Bergamaschi, B. A., Aiken, G. R., Burns, D. A., Findlay, S. E. G., Shanley, J. B., Striegl, R. G., Aulenbach, B. T., Clow, D. W., Laudon, H., McGlynn, B. L., McGuire, K. J., Smith, R. A., & Stackpoole, S. M. (2015). The river as a chemostat: Fresh perspectives on dissolved organic matter flowing down the river continuum. *Canadian Journal of Fisheries and Aquatic Sciences*, *72*(8), 1272–1285. https://doi.org/10.1139/cjfas-2014-0400

Dastoor, A., Ryzhkov, A., Durnford, D., Lehnherr, I., Steffen, A., & Morrison, H. (2015). Atmospheric mercury in the Canadian Arctic. Part II: Insight from modeling. *Science of The Total Environment, 509–510,* 16–27. https://doi.org/10.1016/j.scitotenv.2014.10.112

Demers, J. D., Driscoll, C. T., & Shanley, J. B. (2010). Mercury mobilization and episodic stream acidification during snowmelt: Role of hydrologic flow paths, source areas, and supply of dissolved organic carbon. *Water Resources Research*, *46*(1), 2008WR007021. https://doi.org/10.1029/2008WR007021

Dieleman, C. M., Lindo, Z., McLaughlin, J. W., Craig, A. E., & Branfireun, B. A. (2016). Climate change effects on peatland decomposition and porewater dissolved organic carbon biogeochemistry. *Biogeochemistry*, *128*(3), 385–396. https://doi.org/10.1007/s10533-016-0214-8

Dittman, J. A., Shanley, J. B., Driscoll, C. T., Aiken, G. R., Chalmers, A. T., Towse, J. E., & Selvendiran, P. (2010). Mercury dynamics in relation to dissolved organic carbon concentration and quality during high flow events in three northeastern U.S. streams. *Water Resources Research*, *46*(7), 2009WR008351. https://doi.org/10.1029/2009WR008351

Du, Y., Zhang, Y., Chen, F., Chang, Y., & Liu, Z. (2016). Photochemical reactivities of dissolved organic matter (DOM) in a sub-alpine lake revealed by EEM-PARAFAC: An insight into the fate of allochthonous DOM in alpine lakes affected by climate change. *Science of The Total Environment*, *568*, 216–225. https://doi.org/10.1016/j.scitotenv.2016.06.036

Ducharme, A. A., Casson, N. J., Higgins, S. N., & Friesen-Hughes, K. (2021). Hydrological and catchment controls on event-scale dissolved organic carbon dynamics in boreal headwater streams. *Hydrological Processes*, *35*(7), e14279. https://doi.org/10.1002/hyp.14279

Eckley, C. S., & Hintelmann, H. (2006). Determination of mercury methylation potentials in the water column of lakes across Canada. Science of The Total Environment, 368(1), 111–125. https://doi.org/10.1016/j.scitotenv.2005.09.042

Ecosystem Classification Group. (2007, rev. 2009). Ecological Regions of the Northwest Territories – Taiga Plains. Department of Environmental and Natural Resources, Government of the Northwest Territories, Yellowknife, NT, Canada. viii + 173 pp. folded insert map.

Eder, A., Weigelhofer, G., Pucher, M., Tiefenbacher, A., Strauss, P., Brandl, M., & Blöschl, G. (2022). Pathways and composition of dissolved organic carbon in a small agricultural catchment during base flow conditions. *Ecohydrology & Hydrobiology*, *22*(1), 96–112. https://doi.org/10.1016/j.ecohyd.2021.07.012

Emmerton, C. A., Cooke, C. A., Hustins, S., Silins, U., Emelko, M. B., Lewis, T., Kruk, M. K., Taube, N., Zhu, D., Jackson, B., Stone, M., Kerr, J. G., & Orwin, J. F. (2020). Severe western Canadian wildfire affects water quality even at large basin scales. Water Research, 183, 116071. https://doi.org/10.1016/j.watres.2020.116071

Emmerton, C. A., Drevnick, P. E., Serbu, J. A., Cooke, C. A., Graydon, J. A., Reichert, M., et al. (2022). Downstream Modification of Mercury in Diverse River Systems Underscores the Role of Local Conditions in Fish Bioaccumulation. *Ecosystems*, *26*, 114–133. https://doi.org/10.1007/s10021-022-00745-w

Environment and Climate Change Canada. (2022). Historical Hydrometric Data Search. Government of Canada, Ottawa, ON.

Environment and Climate Change Canada. (2023). Canadian Climate Normals. Government of Canada. Retrieved November 22, 2023, from https://climate.weather.gc.ca/climate_normals/index_e.html.

Fahnestock, M. F., Bryce, J. G., McCalley, C. K., Montesdeoca, M., Bai, S., Li, Y., et al. (2019). Mercury reallocation in thawing subarctic peatlands. *Geochemical Perspectives Letters*, 33–38. https://doi.org/10.7185/geochemlet.1922

Fellman, J. B., Hood, E., & Spencer, R. G. M. (2010). Fluorescence spectroscopy opens new windows into dissolved organic matter dynamics in freshwater ecosystems: A review. *Limnology and Oceanography*, *55*(6), 2452–2462. https://doi.org/10.4319/lo.2010.55.6.2452

Fink-Mercier, C., Lapierre, J., Amyot, M., & Del Giorgio, P. A. (2022). Concentrations and Yields of Total Hg and MeHg in Large Boreal Rivers Linked to Water and Wetland Coverage in the Watersheds. Journal of Geophysical Research: Biogeosciences, 127(5), e2022JG006892. https://doi.org/10.1029/2022JG006892

Fink-Mercier, C., del Giorgio, P., Amyot, M., & Lapierre, J. (2022). Hydrology and seasonality shape the coupling of dissolved Hg and methyl-Hg with DOC in boreal rivers in northern Québec. *Water Resources Research*, *58*, e2022WR033036. https://doi.org/10.1029/2022WR033036

Fouché, J., Christiansen, C. T., Lafrenière, M. J., Grogan, P., & Lamoureux, S. F. (2020). Canadian permafrost stores large pools of ammonium and optically distinct dissolved organic matter. Nature Communications, 11(1), 4500. https://doi.org/10.1038/s41467-020-18331-w

French, T. D., Houben, A. J., Desforges, J.-P. W., Kimpe, L. E., Kokelj, S. V., Poulain, A. J., et al. (2014). Dissolved organic carbon thresholds affect mercury bioaccumulation in Arctic lakes. *Environmental Science and Technology*, *48*(6), 3162–3168. https://doi.org/10.1021/es403849d

Frey, K. E., & McClelland, J. W. (2009). Impacts of permafrost degradation on arctic river biogeochemistry. Hydrological Processes: *An International Journal, 23*(1), 169–182.

Frey, K. E., & Smith, L. C. (2005). Amplified carbon release from vast West Siberian peatlands by 2100. *Geophysical Research Letters*, *32*(9), 1–4. https://doi.org/10.1029/2004GL022025

Gandois, L., Hoyt, A. M., Hatté, C., Jeanneau, L., Teisserenc, R., Liotaud, M., & Tananaev, N. (2019). Contribution of Peatland Permafrost to Dissolved Organic Matter along a Thaw Gradient in North Siberia. *Environmental Science & Technology*, *53*(24), 14165–14174. https://doi.org/10.1021/acs.est.9b03735

Gandois, L., Tananaev, N. I., Prokushkin, A., Solnyshkin, I., & Teisserenc, R. (2021). Seasonality of DOC Export From a Russian Subarctic Catchment Underlain by Discontinuous Permafrost, Highlighted by High-Frequency Monitoring. *Journal of Geophysical Research: Biogeosciences*, *126*(10), e2020JG006152. https://doi.org/10.1029/2020JG006152

Garrity, C.P., and Soller, D.R. (2009). Database of the Geologic Map of North America; adapted from the map by J.C. Reed, Jr. and others (2005): U.S. Geological Survey Data Series 424. https://pubs.usgs.gov/ds/424/.

Gascón Díez, E., Loizeau, J.-L., Cosio, C., Bouchet, S., Adatte, T., Amouroux, D., & Bravo, A.G. (2016). Role of Settling Particles on Mercury Methylation in the Oxic Water Column of Freshwater Systems. Environmental Science & Technology, 50(21), 11672–11679. https://doi.org/10.1021/acs.est.6b03260

Genuer, R., & Poggi, J.-M. (2020). *Random Forests with R*. Springer International Publishing. https://doi.org/10.1007/978-3-030-56485-8

Gerson, J. R., Driscoll, C. T., Demers, J. D., Sauer, A. K., Blackwell, B. D., Montesdeoca, M. R., Shanley, J. B., & Ross, D. S. (2017). Deposition of mercury in forests across a montane elevation gradient: Elevational and seasonal patterns in methylmercury inputs and production. *Journal of Geophysical Research: Biogeosciences*, *122*(8), 1922–1939. https://doi.org/10.1002/2016JG003721

Gibson, C. M., Chasmer, L. E., Thompson, D. K., Quinton, W. L., Flannigan, M. D., & Olefeldt, D. (2018). Wildfire as a major driver of recent permafrost thaw in boreal peatlands. *Nature Communications*, *9*(1), 3041. https://doi.org/10.1038/s41467-018-05457-1

Giesler, R., Clemmensen, K. E., Wardle, D. A., Klaminder, J., & Bindler, R. (2017). Boreal Forests Sequester Large Amounts of Mercury over Millennial Time Scales in the Absence of Wildfire. Environmental Science & Technology, 51(5), 2621–2627. https://doi.org/10.1021/acs.est.6b06369

Goodbrand, A., Westbrook, C. J., & Van Der Kamp, G. (2019). Hydrological functions of a peatland in a Boreal Plains catchment. *Hydrological Processes*, *33*(4), 562–574. https://doi.org/10.1002/hyp.13343

Gordon, J., Quinton, W., Branfireun, B. A., & Olefeldt, D. (2016). Mercury and methylmercury biogeochemistry in a thawing permafrost wetland complex, Northwest Territories, Canada. Hydrological Processes, 30(20), 3627–3638. https://doi.org/10.1002/hyp.10911

Government of Alberta. (2023). Historical Wildfire Perimeter Data: 1931 to 2022 [Dataset]. Wildfire maps and data | Alberta.ca. (n.d.). Retrieved December 2023, from https://www.alberta.ca/wildfire-maps-and-data

Government of British Columbia. (2023). BC Fire Perimeters 2020 – 2022 [Dataset]. Fire Perimeters – Historical, Data Catalogue. (n.d.). Retrieved December 2023, from https://catalogue.data.gov.bc.ca/dataset/fire-perimeters-historical

Graham, A. M., Aiken, G. R., & Gilmour, C. C. (2012). Dissolved Organic Matter Enhances Microbial Mercury Methylation Under Sulfidic Conditions. Environmental Science & Technology, 46(5), 2715–2723. https://doi.org/10.1021/es203658f

Greenwell BM (2017). "pdp: An R Package for Constructing Partial Dependence Plots." The R Journal, 9(1), 421–436. https://journal.r-project.org/archive/2017/RJ-2017-016/index.html.

Gustin, M. S. (2011). Exchange of Mercury between the Atmosphere and Terrestrial Ecosystems. In G. Liu, Y. Cai, & N. O'Driscoll (Eds.), Environmental Chemistry and Toxicology of Mercury (1st ed., pp. 423–451). Wiley. https://doi.org/10.1002/9781118146644.ch13

Hamelin, S., Planas, D., & Amyot, M. (2015). Mercury methylation and demethylation by periphyton biofilms and their host in a fluvial wetland of the St. Lawrence River (QC, Canada). Science of The Total Environment, 512–513, 464–471. https://doi.org/10.1016/j.scitotenv.2015.01.040

Hammerschmidt, C. R., & Fitzgerald, W. F. (2006). Photodecomposition of Methylmercury in an Arctic Alaskan Lake. Environmental Science & Technology, 40(4), 1212–1216. https://doi.org/10.1021/es0513234

Helms, J. R., Stubbins, A., Ritchie, J. D., Minor, E. C., Kieber, D. J., & Mopper, K. (2008). Absorption spectral slopes and slope ratios as indicators of molecular weight, source, and photobleaching of chromophoric dissolved organic matter. *Limnology and Oceanography*, *53*(3), 955–969. https://doi.org/10.4319/lo.2008.53.3.0955

Hermosilla, T., Wulder, M.A., White, J.C., Coops, N.C., Hobart, G.W., Campbell, L.B. (2016). Mass data processing of time series Landsat imagery: pixels to data products for forest monitoring. *International Journal of Digital Earth 9(11), 1035-1054*.

Hermosilla, T., Wulder, M.A., White, J.C., Coops, N.C., Hobart, G.W. (2018). Disturbance Informed Annual Land Cover Classification Maps of Canada's Forested Ecosystems for a 29-Year Landsat Time Series. *Canadian Journal of Remote Sensing. 44(1), 67-87.*

Hermosilla, T., Wulder, M.A., White, J.C., Coops, N.C. (2022). Land cover classification in an era of big and open data: Optimizing localized implementation and training data selection to improve mapping outcomes. *Remote Sensing of Environment. No. 112780*.

Herndon, E. M., Dere, A. L., Sullivan, P. L., Norris, D., Reynolds, B., & Brantley, S. L. (2015). Landscape heterogeneity drives contrasting concentration–discharge relationships in shale headwater catchments. *Hydrology and Earth System Sciences*, *19*(8), 3333–3347. https://doi.org/10.5194/hess-19-3333-2015

Hines, N. A., & Brezonik, P. L. (2007). Mercury inputs and outputs at a small lake in northern Minnesota. Biogeochemistry, 84(3), 265–284. https://doi.org/10.1007/s10533-007-9114-2

Hintelmann H. & Ogrinc, N. (2002). Determination of stable mercury isotopes by ICP/MS and their application in environmental studies. In Y. Cai, & O.C. Braids (Eds.), Biogeochemistry of Environmentally Important Trace Elements (pp. 321-338). ACS Symposium Series, Vol. 835. American Chemical Society. 10.1021/bk-2003-0835.ch021

Holloway, J. E., & Lewkowicz, A. G. (2020). Half a century of discontinuous permafrost persistence and degradation in western Canada. *Permafrost and Periglacial Processes*, *31*(1), 85–96. https://doi.org/10.1002/ppp.2017

Holmes, C. D., Jacob, D. J., & Yang, X. (2006). Global lifetime of elemental mercury against oxidation by atomic bromine in the free troposphere. Geophysical Research Letters, 33(20), 2006GL027176. https://doi.org/10.1029/2006GL027176

Houde, M., Krümmel, E. M., Mustonen, T., Brammer, J., Brown, T. M., Chételat, J., Dahl, P. E., Dietz, R., Evans, M., Gamberg, M., Gauthier, M.-J., Gérin-Lajoie, J., Hauptmann, A. L., Heath, J. P., Henri, D. A., Kirk, J., Laird, B., Lemire, M., Lennert, A. E., … Whiting, A. (2022). Contributions and perspectives of Indigenous Peoples to the study of mercury in the Arctic. *Science of The Total Environment*, *841*, 156566. https://doi.org/10.1016/j.scitotenv.2022.156566

Huang, H., & Mitchell, C. P. J. (2023). Spatial and seasonal patterns of mercury concentrations, methylation and demethylation in central Canadian boreal soils and stream sediment. *Science of The Total Environment*, *891*, 164447. https://doi.org/10.1016/j.scitotenv.2023.164447

Hugelius, G., Loisel, J., Chadburn, S., Jackson, R. B., Jones, M., MacDonald, G., et al. (2020). Large stocks of peatland carbon and nitrogen are vulnerable to permafrost thaw. *Proceedings of the National Academy of Sciences*, *117*(34), 20438–20446. https://doi.org/10.1073/pnas.1916387117

Huguet, A., Vacher, L., Relexans, S., Saubusse, S., Froidefond, J. M., & Parlanti, E. (2009). Properties of fluorescent dissolved organic matter in the Gironde Estuary. *Organic Geochemistry*, *40*(6), 706–719. https://doi.org/10.1016/j.orggeochem.2009.03.002

Hutchins, R. H. S., Aukes, P., Schiff, S. L., Dittmar, T., Prairie, Y. T., & Del Giorgio, P. A. (2017). The Optical, Chemical, and Molecular Dissolved Organic Matter Succession Along a Boreal Soil-Stream-River Continuum. *Journal of Geophysical Research: Biogeosciences*, *122*(11), 2892–2908. https://doi.org/10.1002/2017JG004094

Hutchins, R. H. S., Tank, S. E., Olefeldt, D., Quinton, W. L., Spence, C., Dion, N., & Mengistu, S. G. (2023). Influence of Wildfire on Downstream Transport of Dissolved Carbon, Nutrients, and Mercury in the Permafrost Zone of Boreal Western Canada. *Journal of Geophysical Research: Biogeosciences*, *128*(10), e2023JG007602. https://doi.org/10.1029/2023JG007602

Jeremiason, J. D., Kanne, L. A., Lacoe, T. A., Hulting, M., & Simcik, M. F. (2009). A comparison of mercury cycling in Lakes Michigan and Superior. Journal of Great Lakes Research, 35(3), 329–336. https://doi.org/10.1016/j.jglr.2009.06.001

Jiang, T., Bravo, A. G., Skyllberg, U., Björn, E., Wang, D., Yan, H., & Green, N. W. (2018). Influence of dissolved organic matter (DOM) characteristics on dissolved mercury (Hg) species composition in sediment porewater of lakes from southwest China. Water Research, 146, 146–158. https://doi.org/10.1016/j.watres.2018.08.054

Jiskra, M., Wiederhold, J. G., Skyllberg, U., Kronberg, R.-M., & Kretzschmar, R. (2017). Source tracing of natural organic matter bound mercury in boreal forest runoff with mercury stable isotopes. *Environmental Science: Processes & Impacts*, *19*(10), 1235–1248. https://doi.org/10.1039/C7EM00245A

Jonsson, S., Skyllberg, U., Nilsson, M. B., Westlund, P.-O., Shchukarev, A., Lundberg, E., & Björn, E. (2012). Mercury Methylation Rates for Geochemically Relevant Hg II Species in Sediments. Environmental Science & Technology, 46(21), 11653–11659. https://doi.org/10.1021/es3015327

Kassambara, A. (2023). ggcorrplot: Visualization of a Correlation Matrix using 'ggplot2'. R package version 0.1.4.1. https://CRAN.R-project.org/package=ggcorrplot.

Kassambara, A. (2023a). ggpubr: 'ggplot2' Based Publication Ready Plots. R package version 0.6.0. https://CRAN.R-project.org/package=ggpubr.

Kassambara, A. and Mundt F. (2020). factoextra: Extract and Visualize the Results of Multivariate Data Analyses. R package version 1.0.7. https://CRAN.R-project.org/package=factoextra.

Kidd, K., Clayden, M., & Jardine, T. (2011). Bioaccumulation and Biomagnification of Mercury through Food Webs. In G. Liu, Y. Cai, & N. O'Driscoll (Eds.), Environmental Chemistry and Toxicology of Mercury (1st ed., pp. 453–499). Wiley. https://doi.org/10.1002/9781118146644.ch14

Klapstein, S. J., & O'Driscoll, N. J. (2018). Methylmercury Biogeochemistry in Freshwater Ecosystems: A Review Focusing on DOM and Photodemethylation. Bulletin of Environmental Contamination and Toxicology, 100(1), 14–25. https://doi.org/10.1007/s00128-017-2236-x

Kothawala, D. N., Murphy, K. R., Stedmon, C. A., Weyhenmeyer, G. A., & Tranvik, L. J. (2013). Inner filter correction of dissolved organic matter fluorescence. *Limnology and Oceanography: Methods*, *11*(12), 616–630. https://doi.org/10.4319/lom.2013.11.616

Kothawala, D. N., Stedmon, C. A., Müller, R. A., Weyhenmeyer, G. A., Köhler, S. J., & Tranvik, L. J. (2014). Controls of dissolved organic matter quality: Evidence from a large-scale boreal lake survey. *Global Change Biology*, *20*(4), 1101–1114. https://doi.org/10.1111/gcb.12488

Lambert, T., Teodoru, C. R., Nyoni, F. C., Bouillon, S., Darchambeau, F., Massicotte, P., & Borges, A. V. (2016). Along-stream transport and transformation of dissolved organic matter in a large tropical river. *Biogeosciences*, *13*(9), 2727–2741. https://doi.org/10.5194/bg-13-2727-2016

Laudon, H., Berggren, M., Ågren, A., Buffam, I., Bishop, K., Grabs, T., Jansson, M., & Köhler, S. (2011). Patterns and Dynamics of Dissolved Organic Carbon (DOC) in Boreal Streams: The Role of Processes, Connectivity, and Scaling. Ecosystems, 14(6), 880–893. https://doi.org/10.1007/s10021-011-9452-8.

Lavoie, R. A., Amyot, M., & Lapierre, J. (2019). Global Meta-Analysis on the Relationship Between Mercury and Dissolved Organic Carbon in Freshwater Environments. *Journal of Geophysical Research: Biogeosciences*, *124*(6), 1508–1523. https://doi.org/10.1029/2018JG004896

Le Faucheur, S., Campbell, P. G. C., Fortin, C., & Slaveykova, V. I. (2014). Interactions between mercury and phytoplankton: Speciation, bioavailability, and internal handling. Environmental Toxicology and Chemistry, 33(6), 1211–1224. https://doi.org/10.1002/etc.2424

Ledesma, J. L. J., Kothawala, D. N., Bastviken, P., Maehder, S., Grabs, T., & Futter, M. N. (2018). Stream Dissolved Organic Matter Composition Reflects the Riparian Zone, Not Upslope Soils in Boreal Forest Headwaters. *Water Resources Research*, *54*(6), 3896–3912. https://doi.org/10.1029/2017WR021793

Lescord, G. L., Emilson, E. J. S., Johnston, T. A., Branfireun, B. A., & Gunn, J. M. (2018). Optical Properties of Dissolved Organic Matter and Their Relation to Mercury Concentrations in Water and Biota Across a Remote Freshwater Drainage Basin. *Environmental Science & Technology*, *52*(6), 3344–3353. https://doi.org/10.1021/acs.est.7b05348

Liaw A, Wiener M (2002). "Classification and Regression by randomForest." R News, 2(3), 18 22. https://CRAN.R-project.org/doc/Rnews/.

Lim, A. G., Sonke, J. E., Krickov, I. V., Manasypov, R. M., Loiko, S. V., & Pokrovsky, O. S. (2019). Enhanced particulate Hg export at the permafrost boundary, western Siberia. *Environmental Pollution*, *254*, 113083. https://doi.org/10.1016/j.envpol.2019.113083

Lindsay JB (2016). "Whitebox GAT: A case study in geomorphometric analysis." Computers & Geosciences, 95, 75-84. http://dx.doi.org/10.1016/j.cageo.2016.07.003.

Liu, M., Zhang, Q., Maavara, T., Liu, S., Wang, X., & Raymond, P. A. (2021). Rivers as the largest source of mercury to coastal oceans worldwide. Nature Geoscience, 14(9), 672–677. https://doi.org/10.1038/s41561-021-00793-2

Ma, M., Du, H., & Wang, D. (2019). Mercury methylation by anaerobic microorganisms: A review. Critical Reviews in Environmental Science and Technology, 49(20), 1893–1936. https://doi.org/10.1080/10643389.2019.1594517

Mahony, CR, Wang, T; Hamann, A and Cannon, AJ, 2022. A CMIP6 ensemble for downscaled monthly climate normals over North America. International Journal of Climatology 42 (11), 5871-5891 DOI: https://doi.org/10.1002/joc.7566.

Mann, P. J., Eglinton, T. I., McIntyre, C. P., Zimov, N., Davydova, A., Vonk, J. E., Holmes, R. M., & Spencer, R. G. M. (2015). Utilization of ancient permafrost carbon in headwaters of Arctic fluvial networks. *Nature Communications*, *6*(1), 7856. https://doi.org/10.1038/ncomms8856

Marvin-DiPasquale, M., Lutz, M. A., Brigham, M. E., Krabbenhoft, D. P., Aiken, G. R., Orem, W. H., & Hall, B. D. (2009). Mercury Cycling in Stream Ecosystems. 2. Benthic Methylmercury Production and Bed Sediment−Pore Water Partitioning. *Environmental Science & Technology*, *43*(8), 2726–2732. https://doi.org/10.1021/es802698v

Mauro, J.B.N., Guimarães, J.R.D., Hintelmann, H., Watras, C.J., Haack, E.A., & Coelho-Souza. (2002). Mercury methylation in macrophytes, periphyton, and water - Comparative studies with stable and radio-mercury additions. Analytical and Bioanalytical Chemistry, 374(6), 983–989. https://doi.org/10.1007/s00216-002-1534-1

Mergler, D., Anderson, H. A., Chan, L. H. M., Mahaffey, K. R., Murray, M., Sakamoto, M., & Stern, A. H. (2007). Methylmercury Exposure and Health Effects in Humans: A Worldwide Concern. AMBIO: A Journal of the Human Environment, 36(1), 3–11. https://doi.org/10.1579/0044-7447(2007)36[3:MEAHEI]2.0.CO;2

Mitchell, C. P. J., Branfireun, B. A., & Kolka, R. K. (2008). Assessing sulfate and carbon controls on net methylmercury production in peatlands: An in situ mesocosm approach. Applied Geochemistry, 23(3), 503–518. https://doi.org/10.1016/j.apgeochem.2007.12.020

Morison, M. Q., Macrae, M. L., Petrone, R. M., & Fishback, L. (2016). Seasonal dynamics in shallow freshwater pond-peatland hydrochemical interactions in a subarctic permafrost environment. *Hydrological Processes*, *31*(2), 462–475. https://doi.org/10.1002/hyp.11043

Moslemi-Aqdam, M., Baker, L. F., Baltzer, J. L., Branfireun, B. A., Evans, M. S., Laird, B. D., Low, G., Low, M., & Swanson, H. K. (2022). Understanding among-lake variability of mercury concentrations in Northern Pike (Esox lucius): A whole-ecosystem study in subarctic lakes. *Science of The Total Environment*, *822*, 153430. https://doi.org/10.1016/j.scitotenv.2022.153430

Moslemi-Aqdam, M., Low, G., Low, M., Laird, B. D., Branfireun, B. A., & Swanson, H. K. (2023). Estimates, spatial variability, and environmental drivers of mercury biomagnification rates through lake food webs in the Canadian subarctic. *Environmental Research*, *217*, 114835. https://doi.org/10.1016/j.envres.2022.114835

Mu, C., Schuster, Paul. F., Abbott, Benjamin. W., Kang, S., Guo, J., Sun, S., Wu, Q., & Zhang, T. (2020). Permafrost degradation enhances the risk of mercury release on Qinghai-Tibetan Plateau. Science of The Total Environment, 708, 135127. https://doi.org/10.1016/j.scitotenv.2019.135127

Murphy, K. R., Stedmon, C. A., Graeber, D., & Bro, R. (2013). Fluorescence spectroscopy and multi-way techniques. PARAFAC. *Analytical Methods*, *5*(23), 6557. https://doi.org/10.1039/c3ay41160e

Murphy, K. R., Stedmon, C. A., Wenig, P., & Bro, R. (2014). OpenFluor– an online spectral library of auto-fluorescence by organic compounds in the environment. *Anal. Methods*, *6*(3), 658–661. https://doi.org/10.1039/C3AY41935E

Natural Resources Canada. (2013). Canadian Digital Elevation Model. Government of Canada.

Natural Resources Canada. (2017). Lakes, Rivers and Glaciers in Canada - CanVec Series – Hydrographic Features. Government of Canada.

Natural Resources Canada. (2022). National Hydrometric Network Basin Polygons. Government of Canada.

NWT Center for Geomatics. (2022). Fire History [Dataset]. Government of Northwest Territories. Retrieved December 2023, from https://www.geomatics.gov.nt.ca/en/resources?search_api_views_fulltext=fire&sort_by=field_resource_publication_date&sort_order=DESC

O'Neill, B. C., Kriegler, E., Ebi, K. L., Kemp-Benedict, E., Riahi, K., Rothman, D. S., Van Ruijven, B. J., Van Vuuren, D. P., Birkmann, J., Kok, K., Levy, M., & Solecki, W. (2017). The roads ahead: Narratives for shared socioeconomic pathways describing world futures in the 21st century. *Global Environmental Change*, *42*, 169–180. https://doi.org/10.1016/j.gloenvcha.2015.01.004

Obrist, D., Agnan, Y., Jiskra, M., Olson, C. L., Colegrove, D. P., Hueber, J., Moore, C. W., Sonke, J. E., & Helmig, D. (2017). Tundra uptake of atmospheric elemental mercury drives Arctic mercury pollution. Nature, 547(7662), 201–204. https://doi.org/10.1038/nature22997

Ohno, T. (2002). Fluorescence Inner-Filtering Correction for Determining the Humification Index of Dissolved Organic Matter. *Environmental Science & Technology*, *36*(4), 742–746. https://doi.org/10.1021/es0155276

Olefeldt, D., Persson, A., & Turetsky, M. R. (2014). Influence of the permafrost boundary on dissolved organic matter characteristics in rivers within the Boreal and Taiga plains of western Canada. *Environmental Research Letters*, *9*(3), 035005. https://doi.org/10.1088/1748-9326/9/3/035005

Olefeldt, D., & Roulet, N. T. (2014). Permafrost conditions in peatlands regulate magnitude, timing, and chemical composition of catchment dissolved organic carbon export. *Global Change Biology*, *20*(10), 3122–3136. https://doi.org/10.1111/gcb.12607

Olefeldt, D., Roulet, N., Giesler, R., & Persson, A. (2013). Total waterborne carbon export and DOC composition from ten nested subarctic peatland catchments-importance of peatland cover, groundwater influence, and inter-annual variability of precipitation patterns: WATERBORNE CARBON EXPORT FROM SUBARCTIC CATCHMENTS. *Hydrological Processes*, *27*(16), 2280–2294. https://doi.org/10.1002/hyp.9358

Olefeldt, D., Turetsky, M. R., & Blodau, C. (2013). Altered Composition and Microbial versus UV-Mediated Degradation of Dissolved Organic Matter in Boreal Soils Following Wildfire. *Ecosystems*, *16*(8), 1396–1412. https://doi.org/10.1007/s10021-013-9691-y

Osburn, C. L., Oviedo-Vargas, D., Barnett, E., Dierick, D., Oberbauer, S. F., & Genereux, D. P. (2018). Regional Groundwater and Storms Are Hydrologic Controls on the Quality and Export of Dissolved Organic Matter in Two Tropical Rainforest Streams, Costa Rica. Journal of Geophysical Research: Biogeosciences, 123(3), 850–866. https://doi.org/10.1002/2017JG003960.

Oswald, C. J., & Branfireun, B. A. (2014). Antecedent moisture conditions control mercury and dissolved organic carbon concentration dynamics in a boreal headwater catchment. *Water Resources Research*, *50*(8), 6610–6627. https://doi.org/10.1002/2013WR014736

Pak, K.-R., & Bartha, R. (1998). Mercury Methylation and Demethylation in Anoxic Lake Sediments and by Strictly Anaerobic Bacteria. Applied and Environmental Microbiology, 64(3), 1013–1017. https://doi.org/10.1128/AEM.64.3.1013-1017.1998

Paranjape, A. R., & Hall, B. D. (2017). Recent advances in the study of mercury methylation in aquatic systems. FACETS, 2(1), 85–119. https://doi.org/10.1139/facets-2016-0027

Parks, J. M., Johs, A., Podar, M., Bridou, R., Hurt, R. A., Smith, S. D., Tomanicek, S. J., Qian, Y., Brown, S. D., Brandt, C. C., Palumbo, A. V., Smith, J. C., Wall, J. D., Elias, D. A., & Liang, L. (2013). The Genetic Basis for Bacterial Mercury Methylation. Science, 339(6125), 1332–1335. https://doi.org/10.1126/science.1230667

Petrone, K. C., Jones, J. B., Hinzman, L. D., & Boone, R. D. (2006). Seasonal export of carbon, nitrogen, and major solutes from Alaskan catchments with discontinuous permafrost. Journal of Geophysical Research: Biogeosciences, 111(G2), 2005JG000055. https://doi.org/10.1029/2005JG000055

Pokrovsky, O. S., Manasypov, R. M., Kopysov, S. G., Krickov, I. V., Shirokova, L. S., Loiko, S. V., Lim, A. G., Kolesnichenko, L. G., Vorobyev, S. N., & Kirpotin, S. N. (2020). Impact of Permafrost Thaw and Climate Warming on Riverine Export Fluxes of Carbon, Nutrients and Metals in Western Siberia. *Water*, *12*(6), 1817. https://doi.org/10.3390/w12061817

Poulin, B. A., Ryan, J. N., Tate, M. T., Krabbenhoft, D. P., Hines, M. E., Barkay, T., Schaefer, J., & Aiken, G. R. (2019). Geochemical Factors Controlling Dissolved Elemental Mercury and Methylmercury Formation in Alaskan Wetlands of Varying Trophic Status. Environmental Science & Technology, 53(11), 6203–6213. https://doi.org/10.1021/acs.est.8b06041

Qian, B., Gregorich, E. G., Gameda, S., Hopkins, D. W., & Wang, X. L. (2011). Observed soil temperature trends associated with climate change in Canada. *Journal of Geophysical Research*, *116*(D2), D02106. https://doi.org/10.1029/2010JD015012

Quinton, W. L., Hayashi, M., & Pietroniro, A. (2003). Connectivity and storage functions of channel fens and flat bogs in northern basins. *Hydrological Processes*, *17*(18), 3665–3684. https://doi.org/10.1002/hyp.1369

Quinton, W. L., Hayashi, M., & Chasmer, L. E. (2009). Peatland Hydrology of Discontinuous Permafrost in the Northwest Territories: Overview and Synthesis. *Canadian Water Resources Journal*, *34*(4), 311–328. https://doi.org/10.4296/cwrj3404311

R Core Team (2023). R: A language and environment for statistical computing. R Foundation for Statistical Computing, Vienna, Austria. https://www.R-project.org/

Ramlal, P. S., Kelly, C. A., Rudd, J. W. M., & Furutani, A. (1993). Sites of Methyl Mercury Production in Remote Canadian Shield. *Canadian Journal of Fisheries and Aquatic Sciences*, *50*(5), 972–979. https://doi.org/10.1139/f93-112

Rask, M., Malinen, T., Nyberg, K., Olin, M., Kurkilahti, M., Blauberg, T.-R., Salonen, M., Vesala, S., Ruuhijärvi, J., Tiainen, J., Vuorenmaa, J., Lodenius, M., Arzel, C., Nummi, P., Kahilainen, K. K., Verta, M., & Arvola, L. (2024). Pike Mercury Concentration in Small Boreal Headwater Lakes During Four Decades of Regional and Local Changes. *Water, Air, & Soil Pollution*, *235*(1), 85. https://doi.org/10.1007/s11270-024-06894-z

Riscassi, A. L., Hokanson, K. J., & Scanlon, T. M. (2011). Streamwater Particulate Mercury and Suspended Sediment Dynamics in a Forested Headwater Catchment. *Water, Air, & Soil Pollution*, *220*(1), 23–36. https://doi.org/10.1007/s11270-010-0731-3

Rice, K. M., Walker, E. M., Wu, M., Gillette, C., & Blough, E. R. (2014). Environmental Mercury and Its Toxic Effects. Journal of Preventive Medicine & Public Health, 47(2), 74–83. https://doi.org/10.3961/jpmph.2014.47.2.74

Richardson, M., Chételat, J., MacMillan, G. A., & Amyot, M. (2021). Mercury concentrations and associations with dissolved organic matter are modified by water residence time in eastern Canadian lakes along a 30° latitudinal gradient. *Limnology and Oceanography*, *66*(S1). https://doi.org/10.1002/lno.11580

Rose, L. A., Karwan, D. L., & Godsey, S. E. (2018). Concentration–discharge relationships describe solute and sediment mobilization, reaction, and transport at event and longer timescales. *Hydrological Processes*, *32*(18), 2829–2844. https://doi.org/10.1002/hyp.13235

Rutkowski, C., Lenz, J., Lang, A., Wolter, J., Mothes, S., Reemtsma, T., Grosse, G., Ulrich, M., Fuchs, M., Schirrmeister, L., Fedorov, A., Grigoriev, M., Lantuit, H., & Strauss, J. (2021). Mercury in Sediment Core Samples From Deep Siberian Ice-Rich Permafrost. Frontiers in Earth Science, 9, 718153. https://doi.org/10.3389/feart.2021.718153

Rydberg, J., Klaminder, J., Rosén, P., & Bindler, R. (2010). Climate driven release of carbon and mercury from permafrost mires increases mercury loading to sub-arctic lakes. Science of The Total Environment, 408(20), 4778–4783. https://doi.org/10.1016/j.scitotenv.2010.06.056

Schaefer, K., Elshorbany, Y., Jafarov, E., Schuster, P. F., Striegl, R. G., Wickland, K. P., & Sunderland, E. M. (2020). Potential impacts of mercury released from thawing permafrost. Nature Communications, 11(1), 4650. https://doi.org/10.1038/s41467-020-18398-5

Schroeder, W.H., & Munthe, J. (1998). Atmospheric mercury—An overview. Atmospheric Environment, 32(5), 809-822. https://doi.org/10.1016/S1352-2310(97)00293-8

Schuster, P. F., Schaefer, K. M., Aiken, G. R., Antweiler, R. C., Dewild, J. F., Gryziec, J. D., Gusmeroli, A., Hugelius, G., Jafarov, E., Krabbenhoft, D. P., Liu, L., Herman-Mercer, N., Mu, C., Roth, D. A., Schaefer, T., Striegl, R. G., Wickland, K. P., & Zhang, T. (2018). Permafrost Stores a Globally Significant Amount of Mercury. Geophysical Research Letters, 45(3), 1463–1471. https://doi.org/10.1002/2017GL075571

Schütze, M., Gatz, P., Gilfedder, B., & Biester, H. (2021). Why productive lakes are larger mercury sedimentary sinks than oligotrophic brown water lakes. Limnology and Oceanography, 66(4), 1316–1332. https://doi.org/10.1002/lno.11684

Selvendiran, P., Driscoll, C. T., Montesdeoca, M. R., & Bushey, J. T. (2008). Inputs, storage, and transport of total and methyl mercury in two temperate forest wetlands. *Journal of Geophysical Research: Biogeosciences*, *113*(G2), 2008JG000739. https://doi.org/10.1029/2008JG000739

Shanley, J. B., Taylor, V. F., Ryan, K. A., Chalmers, A. T., Perdrial, J., & Stubbins, A. (2022). Using dissolved organic matter fluorescence to predict total mercury and methylmercury in forested headwater streams, Sleepers River, Vermont USA. Hydrological Processes, 36(5), e14572. https://doi.org/10.1002/hyp.14572

Shogren, A. J., Zarnetske, J. P., Abbott, B. W., Iannucci, F., Medvedeff, A., Cairns, S., Duda, M. J., & Bowden, W. B. (2021). Arctic concentration–discharge relationships for dissolved organic carbon and nitrate vary with landscape and season. *Limnology and Oceanography*, *66*(S1). https://doi.org/10.1002/lno.11682

Shur, Y. L., & Jorgenson, M. T. (2007). Patterns of permafrost formation and degradation in relation to climate and ecosystems. *Permafrost and Periglacial Processes*, *18*(1), 7–19. https://doi.org/10.1002/ppp.582

Smith, S. L., O'Neill, H. B., Isaksen, K., Noetzli, J., & Romanovsky, V. E. (2022). The changing thermal state of permafrost. *Nature Reviews Earth & Environment*, *3*(1), 10–23. https://doi.org/10.1038/s43017-021-00240-1

Spencer, R. G. M., Mann, P. J., Dittmar, T., Eglinton, T. I., McIntyre, C., Holmes, R. M., Zimov, N., & Stubbins, A. (2015). Detecting the signature of permafrost thaw in Arctic rivers. *Geophysical Research Letters*, *42*(8), 2830–2835. https://doi.org/10.1002/2015GL063498

St. Louis, V. L., Rudd, J. W. M., Kelly, C. A., Beaty, K. G., Bloom, N. S., & Flett, R. J. (1994). Importance of Wetlands as Sources of Methyl Mercury to Boreal Forest Ecosystems. Canadian Journal of Fisheries and Aquatic Sciences, 51(5), 1065–1076. https://doi.org/10.1139/f94-106

St. Pierre, K. A., St. Louis, V. L., Lehnherr, I., Gardner, A. S., Serbu, J. A., Mortimer, C. A., Muir, D. C. G., Wiklund, J. A., Lemire, D., Szostek, L., & Talbot, C. (2019). Drivers of Mercury Cycling in the Rapidly Changing Glacierized Watershed of the High Arctic's Largest Lake by Volume (Lake Hazen, Nunavut, Canada). Environmental Science & Technology, 53(3), 1175–1185. https://doi.org/10.1021/acs.est.8b05926

St. Pierre, K. A., Zolkos, S., Shakil, S., Tank, S. E., St. Louis, V. L., & Kokelj, S. V. (2018). Unprecedented Increases in Total and Methyl Mercury Concentrations Downstream of Retrogressive Thaw Slumps in the Western Canadian Arctic. Environmental Science & Technology, 52(24), 14099–14109. https://doi.org/10.1021/acs.est.8b05348

Staniszewska, K. J., Reyes, A. V., & Cooke, C. A. (2023). Glacial Erosion Drives High Summer Mercury Exports from the Yukon River, Canada. *Environmental Science & Technology Letters*, *10*(11), 1117–1124. https://doi.org/10.1021/acs.estlett.3c00427

Staniszewska, K. J., Reyes, A. V., Cooke, C. A., Miller, B. S., & Woywitka, R. J. (2022). Permafrost, geomorphic, and hydroclimatic controls on mercury, methylmercury, and lead concentrations and exports in Old Crow River, arctic western Canada. *Chemical Geology*, *596*, 120810. https://doi.org/10.1016/j.chemgeo.2022.120810

Stantec Consulting Ltd. (2016). State of aquatic knowledge for the Hay River Basin. Prepared for: Government of the Northwest Territories, Department of Environment & Natural Resources. https://www.gov.nt.ca/sites/ecc/files/aquatic_knowledge_hay_river_basin.pdf.

Starr, S. F., Frey, K. E., Smith, L. C., Kellerman, A. M., McKenna, A. M., & Spencer, R. G. M. (2024). Peatlands Versus Permafrost: Landscape Features as Drivers of Dissolved Organic Matter Composition in West Siberian Rivers. *Journal of Geophysical Research: Biogeosciences*, *129*(2), e2023JG007797. https://doi.org/10.1029/2023JG007797

Steffen, A., Lehnherr, I., Cole, A., Ariya, P., Dastoor, A., Durnford, D., Kirk, J., & Pilote, M. (2015). Atmospheric mercury in the Canadian Arctic. Part I: A review of recent field measurements. Science of The Total Environment, 509–510, 3–15. https://doi.org/10.1016/j.scitotenv.2014.10.109

Streets, D. G., Devane, M. K., Lu, Z., Bond, T. C., Sunderland, E. M., & Jacob, D. J. (2011). All Time Releases of Mercury to the Atmosphere from Human Activities. Environmental Science & Technology, 45(24), 10485–10491. https://doi.org/10.1021/es202765m

Sun, T., Lindo, Z., & Branfireun, B. A. (2023). Ground warming releases inorganic mercury and increases net methylmercury production in two boreal peatland types. *Frontiers in Environmental Science*, *11*, 1100443. https://doi.org/10.3389/fenvs.2023.1100443

Sundseth, K., Pacyna, J., Pacyna, E., Pirrone, N., & Thorne, R. (2017). Global Sources and Pathways of Mercury in the Context of Human Health. International Journal of Environmental Research and Public Health, 14(1), 105. https://doi.org/10.3390/ijerph14010105

Takaoka, S., Fujino, T., Hotta, N., Ueda, K., Hanada, M., Tajiri, M., & Inoue, Y. (2014). Signs and symptoms of methylmercury contamination in a First Nations community in Northwestern Ontario, Canada. Science of The Total Environment, 468–469, 950–957. https://doi.org/10.1016/j.scitotenv.2013.09.015

Tank, S. E., Frey, K. E., Striegl, R. G., Raymond, P. A., Holmes, R. M., McClelland, J. W., & Peterson, B. J. (2012). Landscape-level controls on dissolved carbon flux from diverse catchments of the circumboreal. *Global Biogeochemical Cycles*, *26*(4), 2012GB004299. https://doi.org/10.1029/2012GB004299

Tank, S. E., Vonk, J. E., Walvoord, M. A., McClelland, J. W., Laurion, I., & Abbott, B. W. (2020). Landscape matters: Predicting the biogeochemical effects of permafrost thaw on aquatic networks with a state factor approach. *Permafrost and Periglacial Processes*, *31*(3), 358–370. https://doi.org/10.1002/ppp.2057

Tarbier, B., Hugelius, G., Kristina Sannel, A. B., Baptista-Salazar, C., & Jonsson, S. (2021). Permafrost Thaw Increases Methylmercury Formation in Subarctic Fennoscandia. *Environmental Science & Technology*, *55*(10), 6710–6717. https://doi.org/10.1021/acs.est.0c04108

The MathWorks Inc. (2023). MATLAB version: 9.14.0 (R2023a) Update 2, Natick, Massachusetts: The MathWorks Inc. https://www.mathworks.com

Thompson, L. (2023). Enhanced methylmercury formation in thawing permafrost peatlands of northwestern Canada. Methylmercury production and export across the terrestrial-aquatic continuum in permafrost peatland catchments. https://doi.org/10.7939/r3-2py0-wb68

Thompson, L. M., Kuhn, M. A., Winder, J. C., Braga, L. P. P., Hutchins, R. H. S., Tanentzap, A. J., St. Louis, V. L., & Olefeldt, D. (2023). Controls on methylmercury concentrations in lakes and streams of peatland-rich catchments along a 1700 km permafrost gradient. Limnology and Oceanography, 68(3), 583–597. https://doi.org/10.1002/lno.12296

Thompson, L. M., Low, M., Shewan, R., Schulze, C., Simba, M., Sonnentag, O., Tank, S. E., & Olefeldt, D. (2023b). Concentrations and Yields of Mercury, Methylmercury, and Dissolved Organic Carbon From Contrasting Catchments in the Discontinuous Permafrost Region, Western Canada. *Water Resources Research*, *59*(11), e2023WR034848.

Tjerngren, I., Karlsson, T., Björn, E., & Skyllberg, U. (2012). Potential Hg methylation and MeHg demethylation rates related to the nutrient status of different boreal wetlands. Biogeochemistry, 108(1–3), 335–350. https://doi.org/10.1007/s10533-011-9603-1

Tsui, M. T. K., Blum, J. D., Finlay, J. C., Balogh, S. J., Kwon, S. Y., & Nollet, Y. H. (2013). Photodegradation of methylmercury in stream ecosystems. *Limnology and Oceanography*, *58*(1), 13–22. https://doi.org/10.4319/lo.2013.58.1.0013

UN Environment. (2019). Global Mercury Assessment 2018. UN Environment Programme Chemicals and Health Branch Geneva Switzerland. ISBN: 978-92-807-3744-8

U.S. Environmental Protection Agency. (1996). Method 1669: Sampling Ambient Water for Trace Metals at EPA Water Quality Criteria Levels.

U.S. Environmental Protection Agency. (1998). Method 1630, Methyl Mercury in Water by Distillation, Aqueous Ethylation, Purge and Trap and Cold Vapor Atomic Fluorescence Spectrometry.

U.S. Environmental Protection Agency. (2002). Method 1631, Revision E: Mercury in Water by Oxidation, Purge and Trap, and Cold Vapor Atomic Fluorescence Spectrometry.

Vercruysse, K., Grabowski, R. C., & Rickson, R. J. (2017). Suspended sediment transport dynamics in rivers: Multi-scale drivers of temporal variation. *Earth-Science Reviews*, *166*, 38–52. https://doi.org/10.1016/j.earscirev.2016.12.016

Vonk, J. E., Tank, S. E., Mann, P. J., Spencer, R. G. M., Treat, C. C., Striegl, R. G., Abbott, B. W., & Wickland, K. P. (2015). Biodegradability of dissolved organic carbon in permafrost soils and aquatic systems: A meta-analysis. *Biogeosciences*, *12*(23), 6915–6930. https://doi.org/10.5194/bg-12-6915-2015

Wang T, Hamann A, Spittlehouse D, Carroll C (2016) Locally Downscaled and Spatially Customizable Climate Data for Historical and Future Periods for North America. PLoS ONE 11(6): e0156720. doi:10.1371/journal.pone.0156720.

Wang, Y., Liu, J., Liem-Nguyen, V., Tian, S., Zhang, S., Wang, D., & Jiang, T. (2022). Binding strength of mercury (II) to different dissolved organic matter: The roles of DOM properties and sources. *Science of The Total Environment*, *807*, 150979. https://doi.org/10.1016/j.scitotenv.2021.150979

Wang, X., Yuan, W., Lin, C.-J., Luo, J., Wang, F., Feng, X., Fu, X., & Liu, C. (2020). Underestimated Sink of Atmospheric Mercury in a Deglaciated Forest Chronosequence. Environmental Science & Technology, 54(13), 8083–8093. https://doi.org/10.1021/acs.est.0c01667

Wasiuta, V., Kirk, J. L., Chambers, P. A., Alexander, A. C., Wyatt, F. R., Rooney, R. C., & Cooke, C. A. (2019). Accumulating Mercury and Methylmercury Burdens in Watersheds Impacted by Oil Sands Pollution. *Environmental Science & Technology*, *53*(21), 12856–12864. https://doi.org/10.1021/acs.est.9b02373

Wauthy, M., Rautio, M., Christoffersen, K. S., Forsström, L., Laurion, I., Mariash, H. L., Peura, S., & Vincent, W. F. (2018). Increasing dominance of terrigenous organic matter in circumpolar freshwaters due to permafrost thaw. *Limnology and Oceanography Letters*, *3*(3), 186–198. https://doi.org/10.1002/lol2.10063

Weishaar, J. L., Aiken, G. R., Bergamaschi, B. A., Fram, M. S., Fujii, R., & Mopper, K. (2003). Evaluation of Specific Ultraviolet Absorbance as an Indicator of the Chemical Composition and Reactivity of Dissolved Organic Carbon. *Environmental Science & Technology*, *37*(20), 4702–4708. https://doi.org/10.1021/es030360x

Werner, B. J., Musolff, A., Lechtenfeld, O. J., De Rooij, G. H., Oosterwoud, M. R., & Fleckenstein, J. H. (2019). High-frequency measurements explain quantity and quality of dissolved organic carbon mobilization in a headwater catchment. *Biogeosciences*, *16*(22), 4497–4516. https://doi.org/10.5194/bg-16-4497-2019

Wickham, H. (2016). ggplot2: Elegant Graphics for Data Analysis. Springer-Verlag New York.

Williams, C. J., Yamashita, Y., Wilson, H. F., Jaffé, R., & Xenopoulos, M. A. (2010). Unraveling the role of land use and microbial activity in shaping dissolved organic matter characteristics in stream ecosystems. *Limnology and Oceanography*, *55*(3), 1159–1171. https://doi.org/10.4319/lo.2010.55.3.1159

Wright, S. N., Thompson, L. M., Olefeldt, D., Connon, R. F., Carpino, O. A., Beel, C. R., & Quinton, W. L. (2022). Thaw-induced impacts on land and water in discontinuous permafrost: A review of the Taiga Plains and Taiga Shield, northwestern Canada. *Earth-Science Reviews*, *232*, 104104. https://doi.org/10.1016/j.earscirev.2022.104104

Wu Q, Brown A (2022). *'whitebox': 'WhiteboxTools' R Frontend*. R package version 2.2.0, https://CRAN.R-project.org/package=whitebox

Wünsch, U. J., & Murphy, K. (2021). A simple method to isolate fluorescence spectra from small dissolved organic matter datasets. *Water Research*, *190*, 116730. https://doi.org/10.1016/j.watres.2020.116730

Xiang, Y., Guo, Y., Liu, G., Liu, Y., Song, M., Shi, J., Hu, L., Yin, Y., Cai, Y., & Jiang, G. (2022). Particle-Bound Hg(II) is Available for Microbial Uptake as Revealed by a Whole-Cell Biosensor. Environmental Science & Technology, 56(10), 6754–6764. https://doi.org/10.1021/acs.est.1c08946

Zampella, R. A. (1994). CHARACTERIZATION OF SURFACE WATER QUALITY ALONG A WATERSHED DISTURBANCE GRADIENT 1. JAWRA Journal of the American Water Resources Association, 30(4), 605–611. https://doi.org/10.1111/j.1752-1688.1994.tb03315.x

Zhang, T., Kim, B., Levard, C., Reinsch, B. C., Lowry, G. V., Deshusses, M. A., & Hsu-Kim, H. (2012). Methylation of Mercury by Bacteria Exposed to Dissolved, Nanoparticulate, and Microparticulate Mercuric Sulfides. Environmental Science & Technology, 46(13), 6950–6958. https://doi.org/10.1021/es203181m

Zhao, L., Li, Y., Zhang, L., Zheng, J., Pierce, E. M., & Gu, B. (2019). Mercury Adsorption on Minerals and Its Effect on Microbial Methylation. ACS Earth and Space Chemistry, 3(7), 1338–1345. https://doi.org/10.1021/acsearthspacechem.9b00039

Zolkos, S., Krabbenhoft, D. P., Suslova, A., Tank, S. E., McClelland, J. W., Spencer, R. G. M., Shiklomanov, A., Zhulidov, A. V., Gurtovaya, T., Zimov, N., Zimov, S., Mutter, E. A., Kutny, L., Amos, E., & Holmes, R. M. (2020). Mercury Export from Arctic Great Rivers. *Environmental Science & Technology*, *54*(7), 4140–4148. https://doi.org/10.1021/acs.est.9b07145

Appendix:

Table A.2.1: Table summarizing each stream and river sampling location and the characteristics of their catchments.

Site code	Number of times sampled	Missing sampling month	Lat	Long	Area (km^2)	MAT (°C)	MAP (mm)	% Wetland	% Forest	% Water	% Wetland in 60m buffer	% Devonian geology	Mean Slope (degrees)	% Disturbed
FS1	3	NA	60.7150	-114.9078	18070	-2.2	372	53	39	6	43	43	0.9	19
FS2	3	NA	60.0472	-112.7712	3344	-1.5	355	36	60	5	50	96	0.3	33
HR1	3	NA	60.7527	-115.8227	51955	-0.9	441	41	57	1	37	3	1.0	10
HR2	3	NA	60.5265	-116.2152	215	-2.1	336	63	36	1	46	100	0.2	1
HR3	3	NA	60.4419	-116.3415	187	-2.1	342	62	33	4	68	100	0.1	0
HR4	3	NA	60.2717	-116.5659	526	-2.4	361	38	58	3	30	32	1.6	5
HR5	3	NA	60.0186	-116.9504	178	-2.5	375	17	81	1	13	0	2.5	12
HR6	3	NA	59.8591	-117.0375	468	-2.8	391	36	58	6	30	0	1.6	9
HR7	3	NA	59.8363	-117.0393	193	-1.8	376	47	52	0	36	0	0.8	8
HR8	3	NA	59.6845	-117.1393	115	-2.0	384	40	60	0	23	0	1.0	16
HR9	3	NA	59.5761	-117.1929	2647	-1.6	399	45	54	1	35	0	0.8	24
HR10	3	August removed	59.4582	-117.2154	20	-1.2	378	66	33	1	63	0	0.3	43
HR11	3	NA	59.1491	-117.6367	37489	-0.5	463	38	60	1	37	0	1.0	7
HRX	3	NA	59.4059	-117.2813	296	-1.1	383	51	49	0	46	0	0.3	7
HR16	3	NA	58.5914	-118.1280	36	-0.4	435	30	69	0	64	0	0.4	40
HR17	3	NA	58.6089	-118.2766	278	-0.3	441	43	55	2	71	0	0.3	31
HR18	3	NA	58.5961	-118.3345	10591	-0.2	499	34	64	1	31	0	1.4	4
HR20	3	NA	57.3736	-119.1452	3996	0.1	527	36	62	1	33	0	1.6	5
HR21	3	NA	58.5916	-118.4908	836	-0.5	457	27	72	1	29	0	0.9	10
HR22	3	NA	58.5998	-118.6676	984	-0.6	457	40	58	0	35	0	0.7	8
HR24	3	NA	58.3912	-119.4947	243	-0.7	468	37	59	2	41	0	0.7	10
HR25	2	June	58.3498	-119.5081	1335	-0.7	475	42	57	1	39	0	1.0	2
HR26	3	NA	58.3506	-119.5807	983	-0.9	490	41	58	0	35	0	1.3	2
HR28	2	June	58.8132	-118.6176	21189	-0.7	459	41	57	2	41	0	1.0	7

HR40	3	NA	58.3999	-119.4149	121	-0.9	470	34	62	1	39	0	0.8	7
HR41	3	June & August removed	58.4582	-119.4365	6	-1.0	470	37	63	0	50	0	0.7	0
HR42	3	NA	58.5051	-119.2606	11	-1.2	472	33	66	0	15	0	1.0	2
HR45	3	NA	57.3348	-119.0529	26	-1.0	506	24	73	0	1	0	2.7	2
HR46	2	August	57.3873	-119.4245	5	-0.1	511	80	20	0	100	0	0.6	0
HR47	2	August	57.3593	-119.5906	580	-0.6	536	36	63	0	38	0	1.5	0
HR48	2	August	57.3812	-119.2812	46	-0.2	512	35	64	0	54	0	1.2	0
HR50	3	NA	59.0897	-117.6939	83	-0.9	396	45	55	0	63	0	0.3	3
HR51	3	NA	59.0328	-117.7117	1503	-0.8	403	32	67	1	31	0	0.7	14
HR62	1	June & July	58.9449	-118.9921	743	-1.6	437	59	39	2	65	0	0.6	29
HR66	1	July & August	58.5926	-119.5847	19	-0.7	460	7	93	0	6	0	1.4	0
HR67	2	July	58.5955	-119.7221	59	-0.6	460	20	79	0	8	0	0.8	1
HR68	2	June	58.6126	-119.8869	435	-0.3	462	31	68	0	37	0	0.9	0
HR69	2	August	58.6312	-119.9967	92	-0.2	458	54	46	0	55	0	1.0	1
HR72	2	July	59.1337	-118.3213	187	-1.3	415	40	56	1	52	0	0.8	48
HR73	1	June & July	59.0716	-118.7192	87	-1.2	424	25	74	0	24	0	0.8	8
HR75	2	July	58.5983	-118.1757	33	-0.4	436	30	69	0	59	0	0.5	35
HR76	2	July	58.4506	-119.2002	87	-0.6	462	66	31	1	89	0	0.3	8
HR77	2	July	58.2705	-119.3980	824	-0.7	476	38	61	1	41	0	1.1	2
HR80	1	July & August	58.5980	-119.8362	25	-0.4	457	18	82	0	30	0	0.8	0
HR82	2	July	59.1141	-118.5871	185	-1.3	422	30	68	0	29	0	0.9	12
HR83	2	July	58.8095	-117.4177	124	-0.8	401	46	53	1	55	0	0.3	10
MAC1	3	NA	60.6339	-116.3494	13	-2.2	332	35	33	32	48	100	0.6	0
MAC2	3	NA	60.7782	-116.5772	204	-2.3	323	46	54	0	71	100	0.3	0
MAC3	3	NA	60.9847	-117.2447	15844	-2.4	361	47	44	8	38	33	0.9	12
MAC4	3	NA	61.0595	-118.4305	63	-2.5	327	42	55	3	47	100	0.5	0
MAC5	3	NA	61.0912	-118.7199	529	-2.3	334	59	36	3	73	100	0.4	9

MAC6	2	August	61.1221	-118.9529	14	-2.1	326	77	22	0	89	100	0.3	4
MAC7	3	NA	61.1441	-119.2338	32	-2.0	334	92	7	1	92	100	0.2	1
MAC8	3	NA	61.1520	-119.3422	1852	-2.4	366	63	34	3	51	37	0.5	7
MAC9	3	NA	61.1448	-119.8460	9063	-2.8	405	45	46	8	42	4	0.8	10
MAC10	3	NA	61.1554	-119.8957	9	-1.9	356	21	77	0	15	100	0.5	89
MAC12	3	NA	61.2241	-120.3801	29	-2.2	371	66	23	6	60	100	0.3	14
MAC13	3	NA	61.2916	-120.6215	31	-2.4	376	31	60	4	35	100	0.6	0
MAC14	3	NA	61.3236	-120.6747	134	-2.2	368	17	78	3	19	100	1.1	15
MAC15	3	NA	61.4449	-121.2378	1263	-2.5	389	33	64	2	26	71	0.8	4
LIA1	3	NA	61.4159	-121.4552	130	-2.3	391	41	54	2	52	100	0.4	0
LIA2	3	NA	61.3413	-121.7968	1652	-2.6	401	33	62	4	26	51	0.9	0
LIA3	3	NA	61.3323	-122.0957	551	-2.4	406	31	67	1	23	86	1.1	0
LIA4	3	NA	61.0599	-122.8953	1409	-2.6	415	22	76	1	15	44	1.2	10
LIA5	3	NA	61.0558	-122.8977	384	-2.3	421	9	90	0	7	2	1.9	0
LIA6	3	NA	61.0071	-122.9758	135	-2.4	424	25	75	0	15	0	1.2	0
LIA7	3	NA	60.8456	-123.2097	1142	-2.0	432	14	86	0	11	0	1.3	0
LIA8	2	June	60.7328	-123.3062	2	-1.4	431	59	33	7	48	0	0.2	0
LIA9	3	NA	60.4625	-123.3688	107	-1.4	439	14	83	2	25	0	0.9	0
LIA10	3	NA	60.4213	-123.3489	27	-1.3	440	21	73	6	47	0	0.7	0
LIA11	3	NA	60.3042	-123.3171	6206	-2.3	432	30	67	1	27	0	1.2	2
LIA12	3	NA	60.6431	-123.5001	2	-1.5	449	23	77	0	3	0	1.9	0
LIA13	3	NA	59.9810	-122.9226	21351	-1.8	441	56	38	5	53	0	1.2	17
WRI1	3	NA	61.7805	-121.3019	2	-2.5	376	19	75	0	13	100	0.5	0
WRI2	3	NA	61.8935	-121.6132	2073	-2.8	390	26	71	2	22	71	1.3	2
WRI3	3	NA	61.9559	-121.7923	44	-2.6	374	20	80	0	9	100	0.8	0
WRI4	3	NA	61.9922	-121.9279	111	-2.9	378	6	92	1	4	68	1.5	1
WRI5	3	NA	62.0625	-122.2060	231	-3.3	383	15	83	0	10	70	1.6	0
WRI6	3	NA	62.1199	-122.5212	7	-2.8	370	0	98	0	1	100	1.7	10
WRI7	3	NA	62.1623	-122.5352	88	-3.0	366	8	89	2	14	100	1.1	0
WRI8	3	NA	62.2580	-122.5854	56	-3.6	365	32	63	1	57	64	1.1	0
WRI9	3	NA	62.3222	-122.7168	56	-3.6	364	28	67	1	41	57	1.0	0

WRI10	3	NA	62.4599	-123.0114	69	-3.8	361	6	93	0	5	42	2.1	0
WRI11	3	NA	62.6731	-123.0785	42	-3.6	351	12	85	0	7	70	2.0	0
WRI12	3	NA	62.7107	-123.0858	21060	-4.0	326	33	48	6	41	60	1.0	39
WRI13	3	NA	62.8696	-123.1575	12	-3.8	338	4	87	8	10	100	4.8	0
WRI14	3	NA	62.9420	-123.1994	3414	-4.5	327	9	69	8	15	13	2.4	25
WRI15	2	August, June removed	63.0446	-123.1959	7	-4.0	328	0	100	0	0	100	6.0	0
WRI16	3	NA	63.0905	-123.2331	83	-4.6	330	1	93	2	5	100	7.8	8
WRI17	3	NA	63.1126	-123.2488	6	-3.9	322	16	81	1	40	100	1.2	0
WRI18	3	NA	63.1431	-123.2587	13	-3.9	321	20	74	4	41	100	1.4	1
WRI20	3	NA	63.1740	-123.3377	151	-4.7	324	4	86	1	5	100	7.8	0
WRI21	3	NA	63.2337	-123.4828	317	-5.3	326	3	81	1	7	86	9.8	0

Table A.2.2: Results from running cross validations to compare the results from having independent test data with results from our final model using all data (green). For each model run we removed 20% of the data prior to analysis (Groups "A", "B", "C", "D", "E") and then tested the model against the excluded data (Column 4 & 5). Columns 3 and 4 represent the values calculated within the model run. The comparison we were most interested in are the values in red which represent our final model results compared to the average values from testing cross validation models on the excluded subset of data.

a) TMeHg				
1. Data Included / Excluded	**2. Variance Explained (OOB values)**	**3. Mean squared residuals (OOB values)**	**4. Variance explained of subset of data excluded**	**5. MSE (RMSE) evaluated on subset of data excluded.**
No Group "A"	45.56	0.038	16.48	0.076, (0.276)
No Group "B"	21.76	0.052	44.66	0.055, (0.235)
No Group "C"	28.60	0.051	40.01	0.046, (0.215)
No Group "D"	32.76	0.050	37.04	0.041, (0.202)
No Group "E"	28.11	0.057	51.30	0.022, (0.149)
Avg. of groups	31.36	0.050	37.90	0.048, (0.215)
No excluded data	34.27	0.048	NA	NA
b) DOC				
Data Excluded from model	**Variance Explained (OOB values)**	**Mean squared residuals (OOB values)**	**Variance explained of subset of data excluded**	**MSE (RMSE) evaluated on subset of data excluded.**
No Group "A"	76.73	31.68	70.58	34.11, (5.84)
No Group "B"	76.23	32.59	71.82	30.76, (5.55)
No Group "C"	75.09	33.12	77.09	32.14, (5.67)
No Group "D"	73.86	31.79	77.05	46.04, (6.79)
No Group "E"	71.03	37.77	88.17	19.15, (4.38)
Avg. of groups	74.59	33.39	76.94	32.44, (5.64)
No excluded data	76.68	30.72	NA	NA
c) THg				
Data Excluded from model	**Variance Explained (OOB values)**	**Mean squared residuals (OOB values)**	**Variance explained of subset of data excluded**	**MSE (RMSE) evaluated on subset of data excluded.**
No Group "A"	65.84	2.25	83.82	2.41, (1.55)
No Group "B"	74.51	2.18	62.19	1.30, (1.14)
No Group "C"	72.53	2.38	69.03	0.56, (0.74)
No Group "D"	63.82	1.82	86.04	5.15, (2.27)
No Group "E"	69.62	2.37	79.06	1.28, (1.13)
Avg. of groups	69.26	2.20	76.03	2.14, (1.37)
No excluded data	72.61	2.02	NA	NA
d) DOM aromaticity				
Data Excluded from model	**Variance Explained (OOB values)**	**Mean squared residuals (OOB values)**	**Variance explained of subset of data excluded**	**MSE (RMSE) evaluated on subset of data excluded.**
No Group "A"	68.24	2.47	75.69	1.94, (1.39)
No Group "B"	70.01	2.42	78.27	1.40, (1.18)
No Group "C"	73.28	2.03	70.91	2.64, (1.62)
No Group "D"	70.06	2.22	71.57	2.79, (1.67)
No Group "E"	68.36	2.31	82.23	2.24, (1.50)
Avg. of groups	69.99	2.29	75.73	2.20, (1.47)
No excluded data	72.51	2.10	NA	NA

Table A.2.3. Results from running cross validations to compare the results from having independent test data with results from our final average model using all data (green). For each model run we removed 20% of the data prior to analysis (Groups "A", "B", "C", "D", "E") and then tested the model against the excluded data (Column 4 & 5). Columns 3 and 4 represent the values calculated within the model run. The comparison we were most interested in are the values in red which represent our final model results compared to the average values from testing cross validation models on the excluded subset of data.

a) Average TMeHg				
Data Included / Excluded	**Variance Explained (OOB values)**	**Mean squared residuals (OOB values)**	**Variance explained of subset of data excluded**	**MSE (RMSE) evaluated on subset of data excluded.**
No Group "A"	39.54	0.025	61.13	0.015, (0.122)
No Group "B"	42.56	0.019	46.16	0.041, (0.201)
No Group "C"	40.47	0.026	42.75	0.014, (0.119)
No Group "D"	37.55	0.025	62.54	0.019, (0.137)
No Group "E"	45.29	0.023	32.26	0.020, (0.141)
Avg of groups	41.082	0.024	48.97	0.022, (0.144)
No excluded data	44.77	0.022	NA	NA
b) Average THg				
Data Included / Excluded	**Variance Explained (OOB values)**	**Mean squared residuals (OOB values)**	**Variance explained of subset of data excluded**	**MSE (RMSE) evaluated on subset of data excluded.**
No Group "A"	32.80	2.16	50.16	3.28, (1.81)
No Group "B"	38.18	2.65	45.93	1.20, (1.10)
No Group "C"	44.73	1.93	36.78	3.20, (1.79)
No Group "D"	33.80	2.56	51.91	2.19, (1.48)
No Group "E"	39.65	2.59	51.30	0.85, (0.92)
Avg of groups	37.83	2.38	47.22	2.15, (1.42)
No excluded data	40.77	2.27	NA	NA
c) Average DOC				
Data Included / Excluded	**Variance Explained (OOB values)**	**Mean squared residuals (OOB values)**	**Variance explained of subset of data excluded**	**MSE (RMSE) evaluated on subset of data excluded.**
No Group "A"	67.96	35.77	53.59	72.79, (8.53)
No Group "B"	62.31	45.01	76.57	32.55, (5.71)
No Group "C"	66.66	44.65	38.34	50.94, (7.14)
No Group "D"	57.30	52.85	81.92	24.75, (4.97)
No Group "E"	62.88	43.76	60.27	58.20, (7.63)
Average of excluded groups	63.42	44.41	62.14	47.85, (6.80)
No excluded data	65.48	41.99	NA	NA

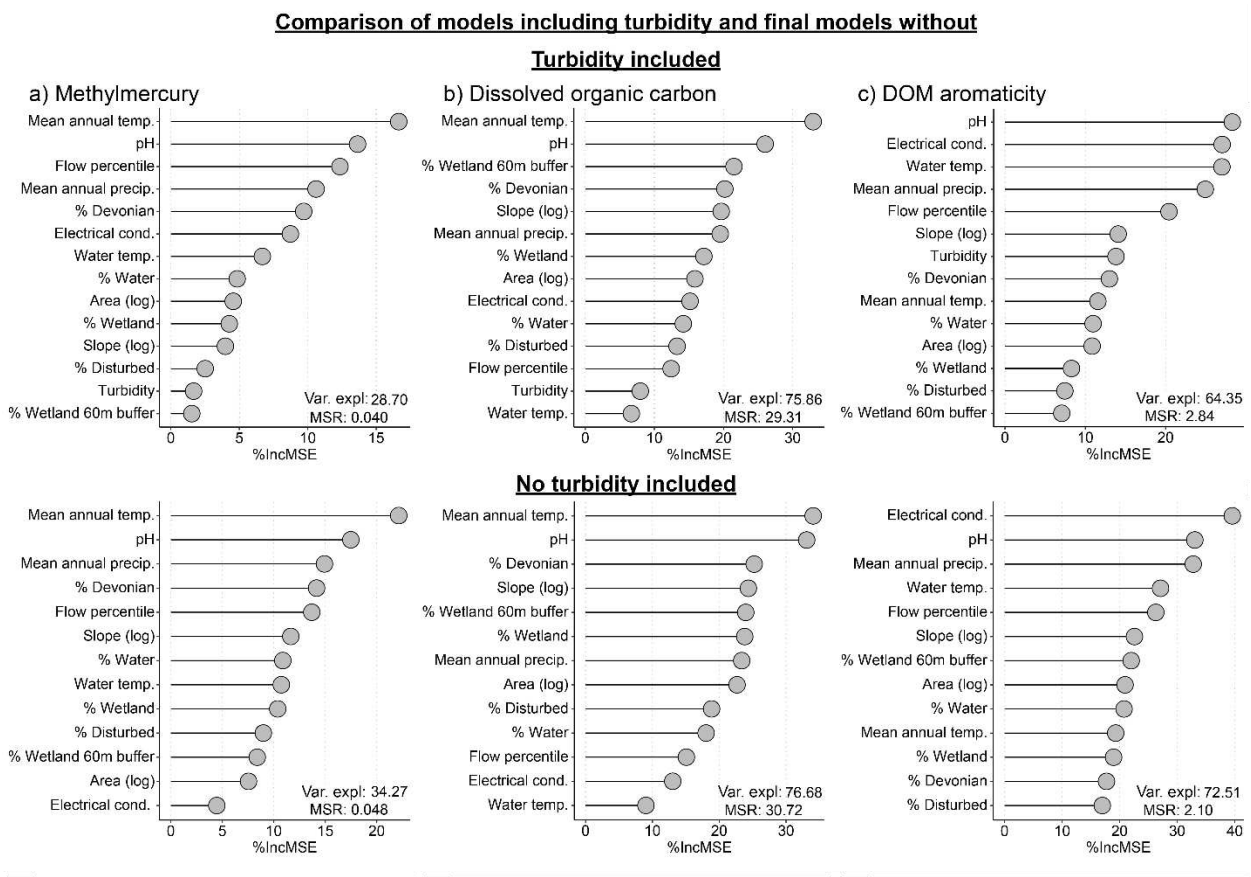

Figure A.2.1. Comparison between random forest model variable importance figures for models which included turbidity (June and August 2022 data) and which excluded turbidity (July 2021, June 2022, August 2022 data) for a) TMeHg, b) DOC, c) DOM aromaticity. The higher the variable on the y-axis the more important this variable is for predicting the concentrations of the parameter of interest. The x-axis shows the increase in mean squared error (MSE) of the model if that variable is removed from the model. Variance explained (Var. expl) and mean squared residuals (MSR) are based on predicting out of bag (OOB) samples. As turbidity was not a top predictor and model variance explained improved without it, turbidity was not used in final models.

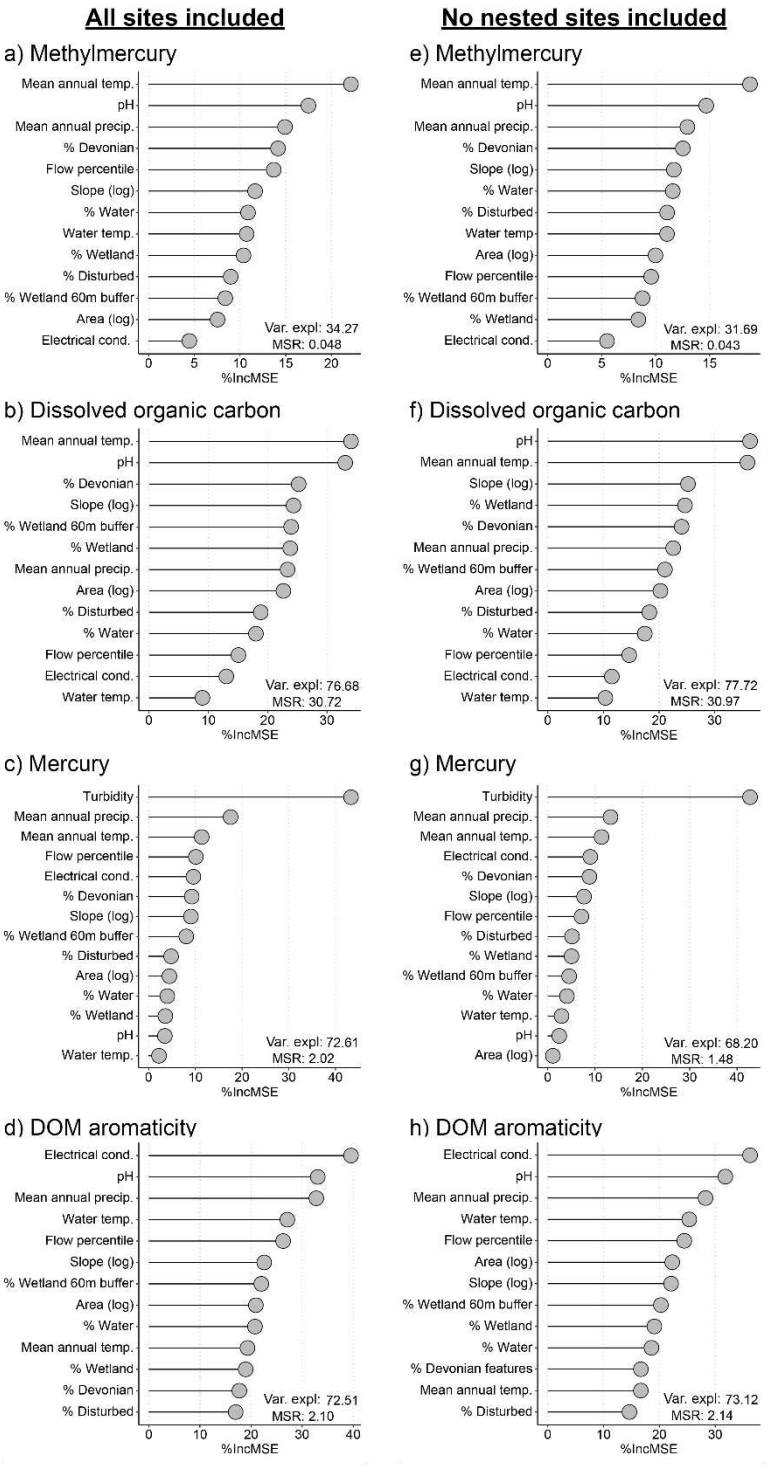

Figure A.2.2. Comparison between random forest model variable importance figures for models which included all catchment (a-d) and for models which excluded catchments which had other catchments nested within (e-h). The higher the variable on the y-axis the more important this variable is for predicting the concentrations of the parameter of interest. The x-axis shows the increase in mean squared error (MSE) of the model if that variable is removed from the model. The variance explained and mean squared residuals are based on predicting out of bag (OOB) samples.

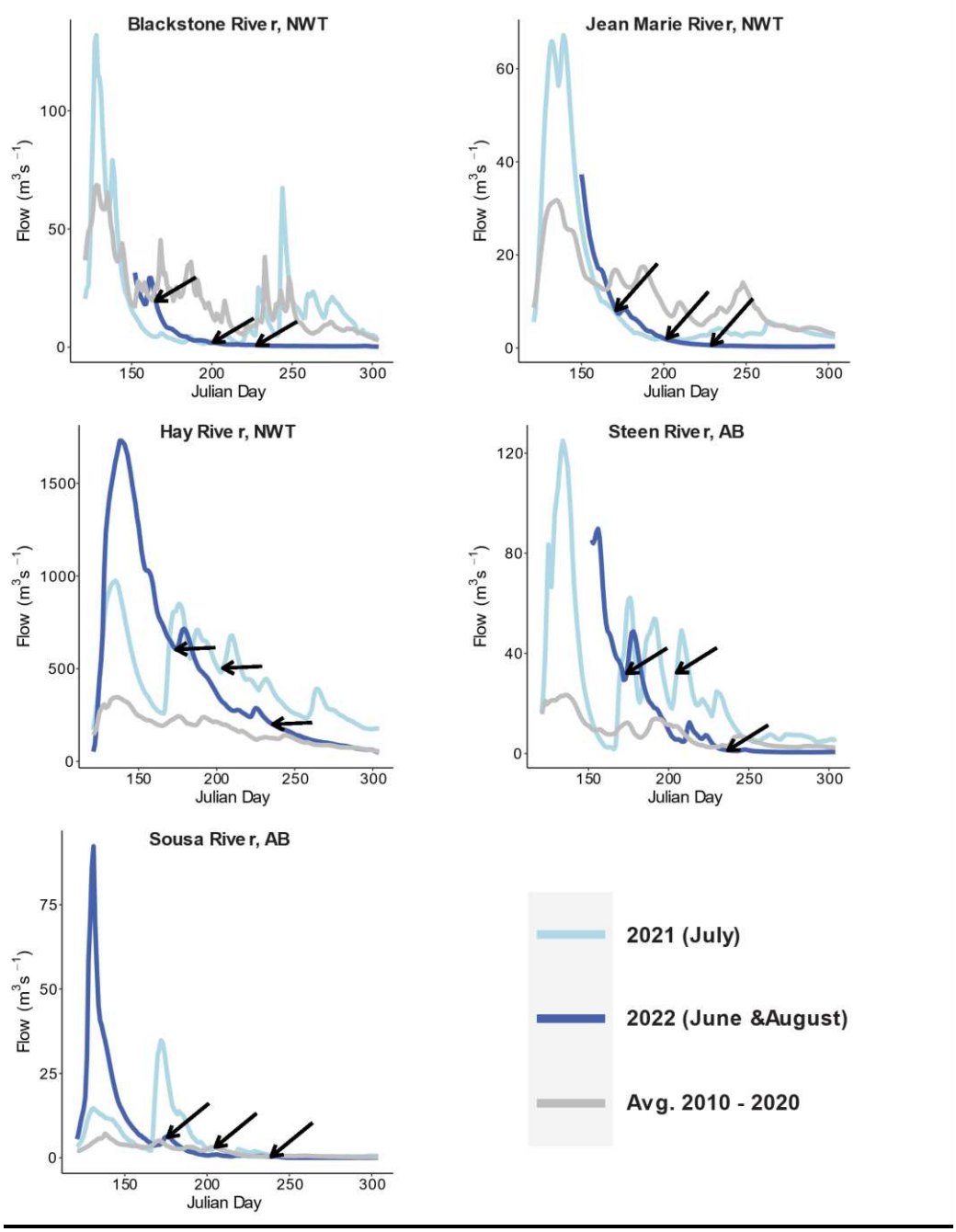

Figure A.2.3. Hydrographs of a subset of rivers that are monitored by Environment and Climate Change Canada from which we access flow data (ECCC, 2022). Black arrows represent the point on the hydrograph that was sampled for each of our sampling months. 2021 flow is represented in light blue and 2022 is represented in dark blue. An average of flow over the ten years before sampling is also included (grey) for comparison.

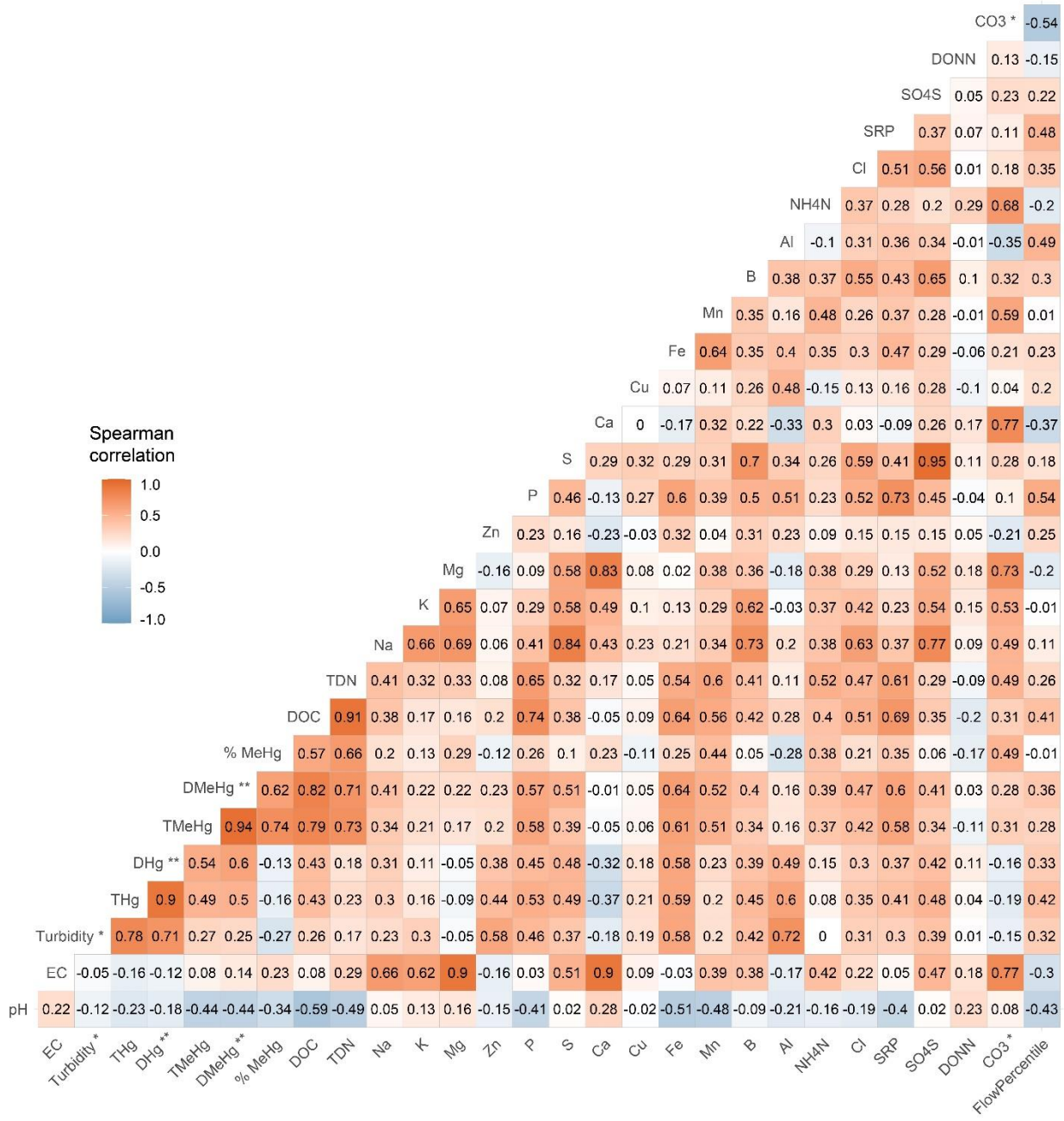

***** Data only present for June and August 2022.
** Data only present for July 2021 and June 2022.

Figure A.2.4. Spearman correlations for water chemistry relationships.

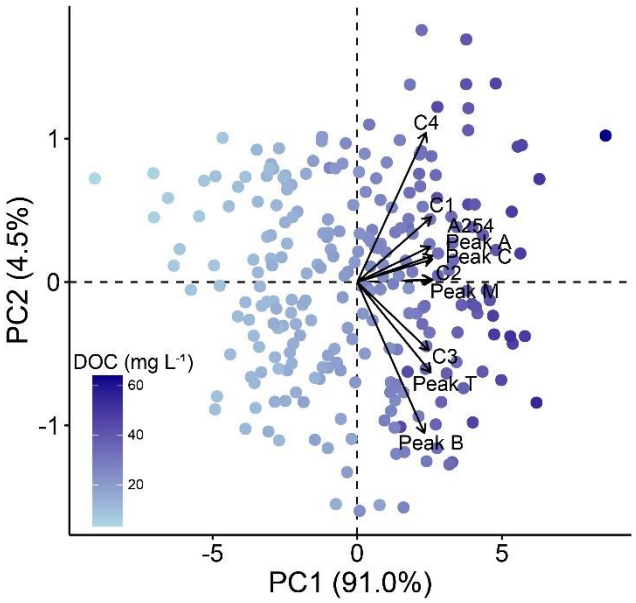

Figure A.2.5. PCA analysis for DOM composition using max fluorescence absolute values and peaks. Peak values were logged prior to the analysis.

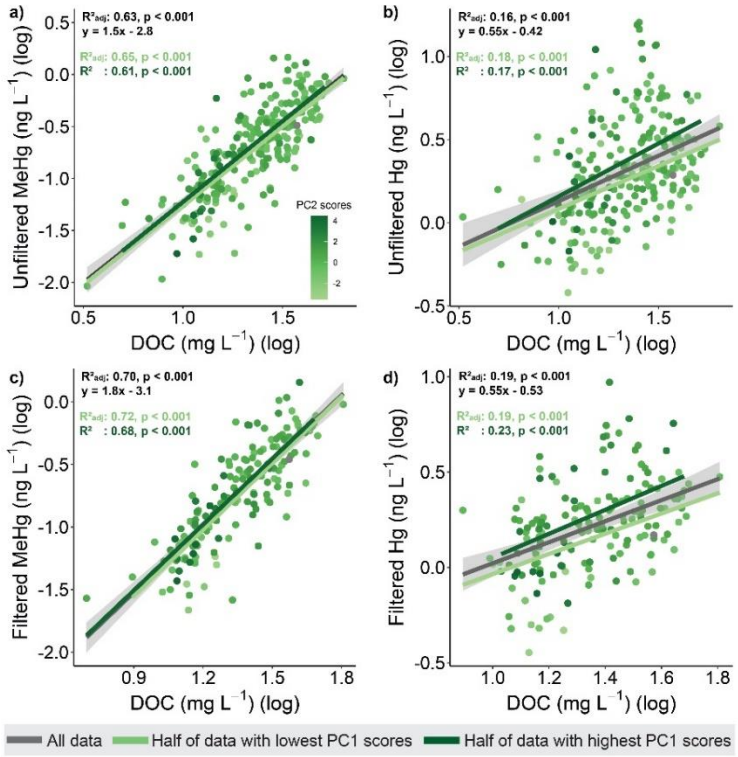

Figure A.2.6. Relationship between concentrations of DOC and a) unfiltered MeHg, b) unfiltered Hg, c) filtered MeHg, d) filtered Hg. Relationships were investigated for different groups of data including all data (grey/black), half of the data with the lowest PC2 scores (light green), half of the data with the highest PC2 scores (dark green) where scores are from a PCA of DOM composition (Figure 4.) and higher scores tend to represent a higher percent of component 4 and lower fluorescence index.

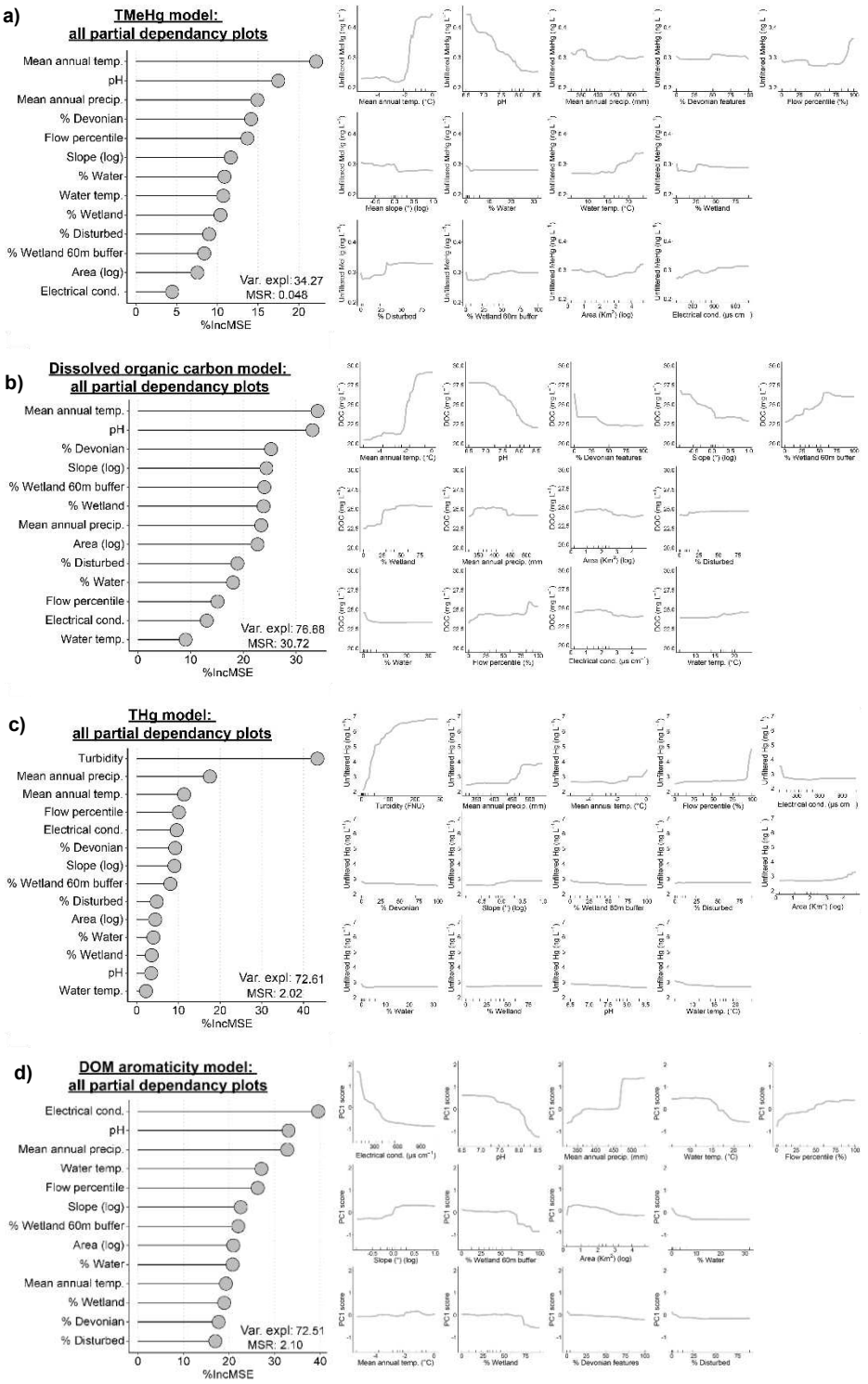

Figure A.2.7. Random Forest model variable importance plots for concentrations of a) TMeHg, b) DOC, c) THg, d) DOM aromaticity. The y-axis shows variable importance for predicting the concentrations of the parameter of interest. The x-axis shows the increase in mean squared error (MSE) of the model if that variable is removed from the model. Variance explained and mean squared residuals are based on predicting out of bag (OOB) samples. Partial dependency plots which show the marginal effect for each predictor variable are also shown. Rug lines show data min/max and deciles.

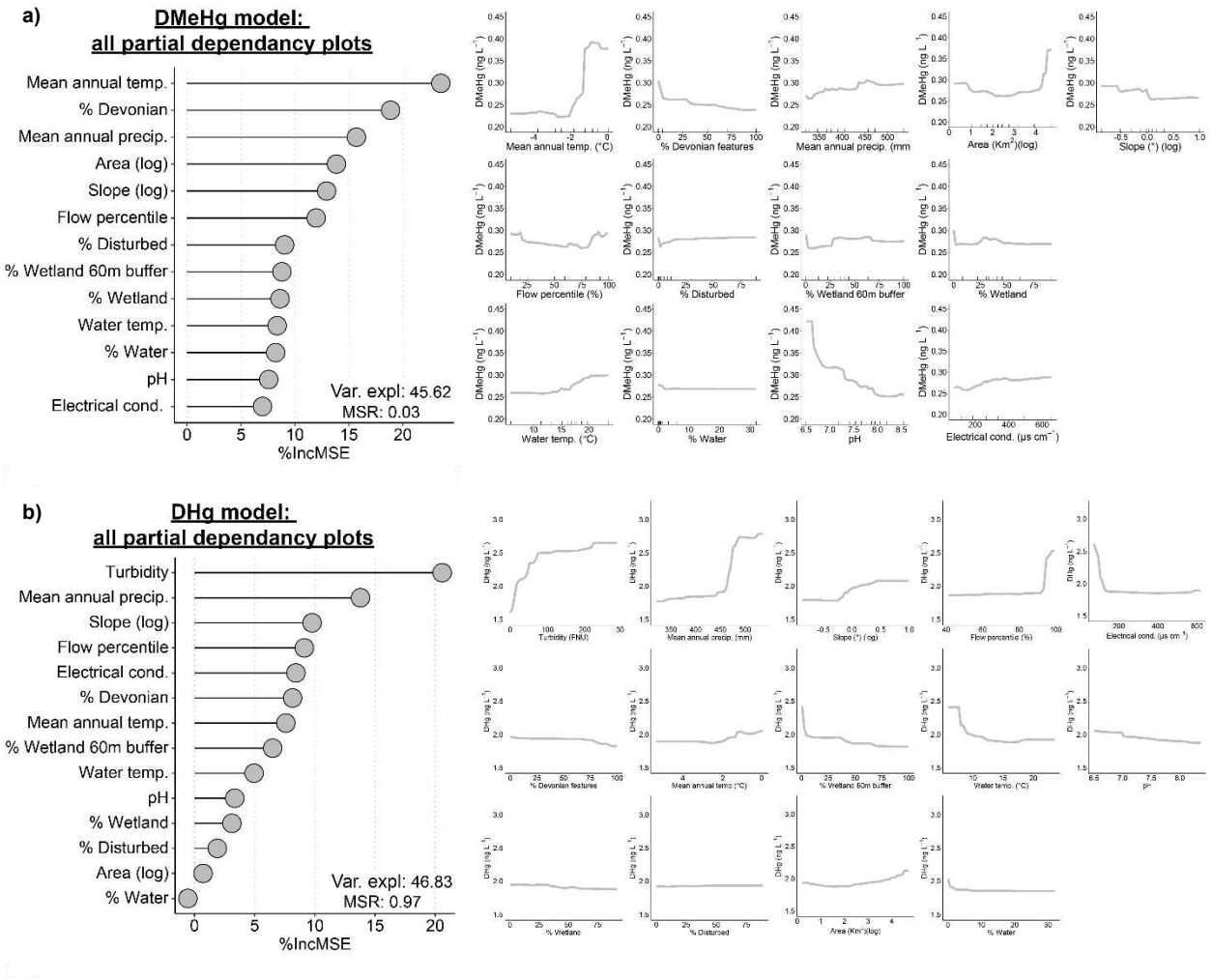

Figure A.2.8. Random Forest model variable importance figures for concentrations of a) DMeHg, b) DHg. The y-axis shows variable importance for predicting the concentrations of the parameter of interest. The x-axis shows the increase in mean squared error (MSE) of the model if that variable is removed from the model. The variance explained and mean squared residuals are based on predicting out of bag (OOB) samples. Partial dependency plots which show the marginal effect for each predictor variable are also shown. Rug lines at the bottom show data min/max and deciles.

.

a) **Random forest model for average TMeHg concentrations: All partial dependancy plots**

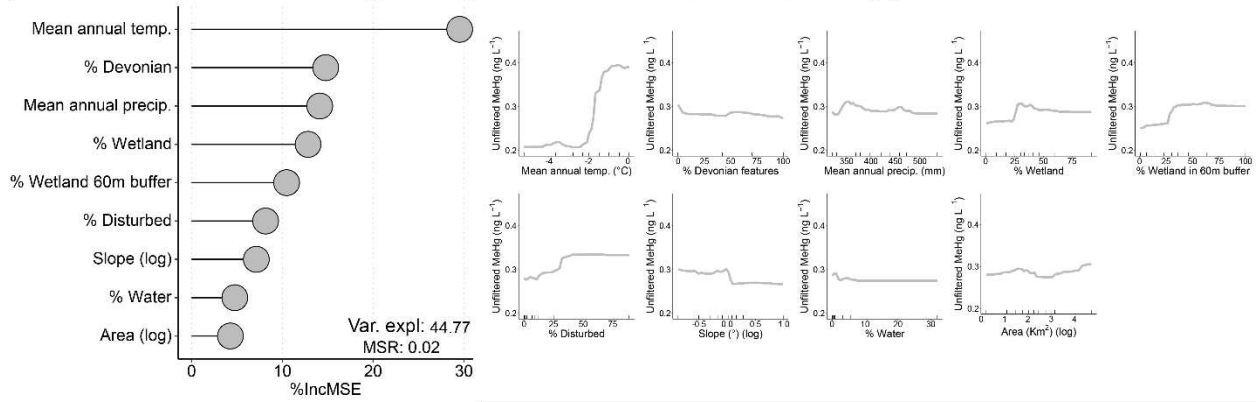

b) **Random forest model for average DOC concentrations: All partial dependancy plots**

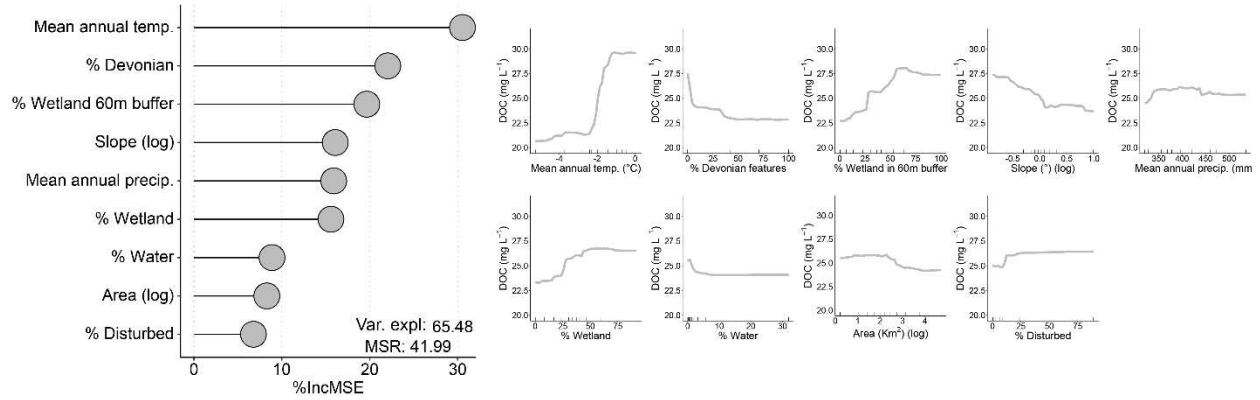

c) **Random forest model for average THg concentrations: All partial dependancy plots**

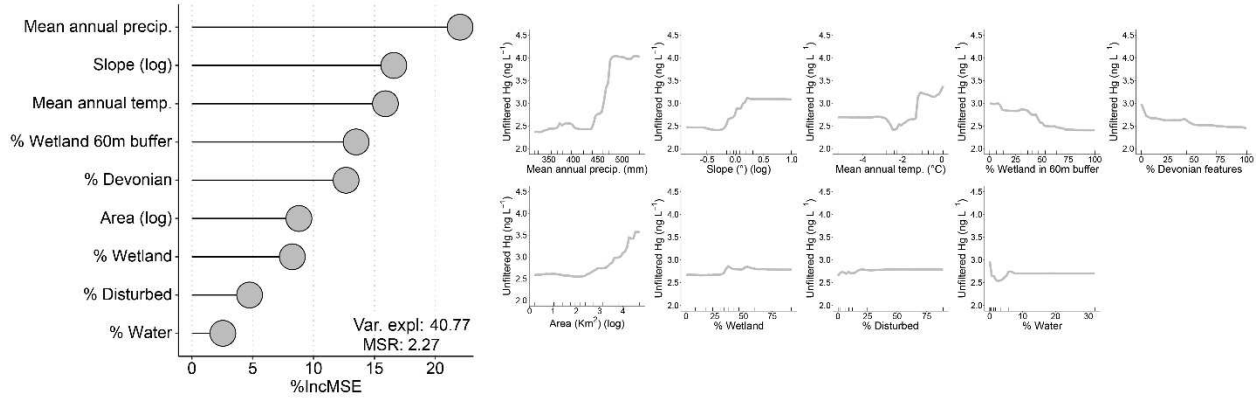

Figure A.2.9. Random Forest model variable importance figures for average concentrations of a) TMeHg, b) DOC, c) THg. The y-axis shows variable importance for predicting the concentrations of the parameter of interest. The x-axis shows the increase in mean squared error (MSE) of the model if that variable is removed from the model. The variance explained and mean squared residuals are based on predicting out of bag (OOB) samples. Partial dependency plots which show the marginal effect for each predictor variable are also shown. Rug lines at the bottom show data min/max and deciles.